Methods to extract maximum electrical energy from PV panels on the earth's surface

Bernard Bekker

Thesis presented in partial fulfilment of the requirements for the degree of Master of Engineering at the University of Stellenbosch

Supervisor: Dr. HJ Beukes

Declaration

I, the undersigned, hereby declare that the work contained in this thesis is my own original work, unless otherwise stated, and has not previously, in its entirety or in part, been submitted at any university for a degree.

Bernard Bekker
30 September 2004

Summary

This thesis investigates methods to extract the maximum amount of electrical energy from a PV panel. The thesis is divided into four parts, focussing on different aspects relating to this topic.

The first part will investigate the role that PV energy is likely to play in South Africa's future energy scenario, by looking at topics like the greenhouse effect and the economics of energy production.

Secondly the thesis will look at how to position PV panels optimally for maximum energy generation through the year. A software model of a PV panel is developed which can calculate available PV energy and energy generation costs for a given location, based on parameters like the positioning of the PV panel and historic weather data.

Thirdly the optimal design of a maximum power point tracker is investigated. The optimal design, based on a k-sweep voltage ratio maximum power point tracking algorithm, is implemented using a DSP controlled boost converter circuit.

Finally, the best methods to store energy generated using PV panels are explored. Energy storage technologies are compared for rural, off-grid applications in South Africa, and the design and implementation of a pulse-charging lead-acid battery charging strategy is explained.

Opsomming

Hierdie tesis ondersoek maniere waarop die maksimum hoeveelheid elektriese energie vanuit `n PV paneel onttrek kan word. Die tesis word in vier dele verdeel, wat elkeen fokus op `n ander aspek van die onderwerp.

Die eerste kyk na die rol wat PV energie potensieël kan speel in die toekomstige energie produksie binne Suid Afrika, deur te kyk na onderwerpe soos die kweekhuis effek, en die ekonomiese sy van energie produksie.

Tweedens kyk die tesis na metodes om `n PV paneel optimaal te posisioneer vir maksimum energie deur die jaar. `n Sagteware model van `n PV paneel word ontwikkel wat die hoeveelheid beskikbare energie, en die kostes daarvan, kan bereken vir `n spesifieke plek, gebaseer op PV paneel data en vorige jare se atmosferiese data.

Derdens word agtergrond oor maksimum drywingspunt volgers gegee, en die ontwerp en bou van `n k-variërende, spannings verhouding maksimum kragpunt volger verduidelik, geimplimenteer deur van `n DSP en `n opkapper baan gebruik te maak.

Laastens word die beste maniere om PV energie te stoor, vir landelike toepassings weg vanaf die Eskom netwerk, ondersoek. Alle beskikbare tegnologieë word eers vergelyk met mekaar, waarna die ontwerp en bou van `n puls-laai loodsuur batterylaaier verduidelik word.

Acknowledgements

I would like to acknowledge and thank the following people and institutions:

Dr Beukes, for inspiring and leading me through his knowledge and experience, and focusing my often-drifting attentions back to what I came to complete. Two of my most positive perception-changing trips, Hluleka and Gaborone, can also be blamed solely on him!

South African Weather Bureau, especially Coleen de Villiers for her patience and professional responses to my sometimes persistent and ridiculous requests, e.g. "Please send me complete five-minute irradiance and ambient temperature data sets for all the SAWB measurement locations in Southern Africa, preferably in an easy-to-work-with format, and as soon as possible. Oh yes, and can you email it to me using SAWB's ancient email system?"

Daleen Kleyn, for so effortlessly hiding all the bureaucratic nightmares behind bursaries, university administration and travel arrangements from me.

Petro Petzer and his staff in the workshop, for the high quality of their work, and the promptness and friendliness with which they completed my requests.

My friends, for the most necessary temptations they offered in order to pull me away from lifeless computer screens, oscilloscopes etc.

My family, for teaching me both the value and worthlessness of knowledge, and for supporting and loving me without interfering (too much!)

Table of Contents

List of Figures

List of Tables

List of Definitions and Abbreviations

Irradiance	The power from a radiant source falling on a unit area [6]
Irradiation	Irradiance integrated over a period of time [6]
G, D and B	Global, diffuse and beam (direct) irradiance components
SAWB	South African Weather Bureau
PV	Photovoltaic
LST	Local Apparent Solar Time
ST	Standard Time
MPPT	Maximum power point tracker
MPP	Maximum power point
D.O.D.	Depth of discharge
ES	Energy storage
V_{OC}	Open circuit voltage
V_{MPP}	Maximum power point voltage
I_{SC}	Short circuit current
I_{MPP}	Maximum power point current

Chapter 1 – Introduction

The society we live in is gradually beginning to favour renewable sources of electrical energy in comparison to fossil fuel-based energy generation. Especially factors like global warming and the depletion of the supply of fossil fuels has inspired this change in thinking.

Photovoltaic (PV) energy, i.e. solar radiation energy converted into electrical energy, is a well known source of this renewable electrical energy, and is well suited to South Africa, a country receiving high amounts of annual solar radiation.

One of the main obstacles in producing PV energy is the cost of the electricity compared to other methods of energy generation, like wind and nuclear power. This thesis looks at methods by which to extract as much electrical energy as possible from these PV panels, thereby bringing down the cost of PV energy, allowing more widespread implementation.

The thesis focuses on producing PV energy on the surface of the earth, especially in Southern Africa. This focus influences several design decisions made in the thesis.

Instead of following the traditional approach of focussing on one detailed topic, this thesis gives an overview of the wide field of PV, and focuses on four areas within this field.

The first area of focus is to investigate the future role that PV energy is likely to play, especially in Southern Africa. This investigation looks at topics like the greenhouse effect and the economics of energy production. It then attempts to predict a future energy scenario for South Africa, and the role PV can play in it.

Secondly the thesis focuses on how to position PV panels optimally for maximum energy generation through the year. A software model of a PV panel is developed which can calculate available PV energy and energy generation costs for a given location, based on parameters like the positioning of the PV panel and historic weather data near the location of interest.

Thirdly the development of a novel optimal maximum power point tracker algorithm is investigated. Once an optimal algorithm has been found, it is implemented using a DSP controlled power electronics circuit.

Finally, the thesis investigates optimal methods to store energy generated using PV panels, by first identifying the most suitable energy storage technology for South African implementation, and then developing and implementing an efficient battery charging strategy.

Chapter 2 – The future contribution of photovoltaic energy

2.1 Introduction

This chapter looks at the future role of photovoltaic (PV) energy in the electrical energy production scenario in South Africa, thereby justifying the aim of this thesis to investigate methods to produce PV energy as efficiently as possible.

Environmental concerns are at present one of the main reasons for the move towards energy from renewable sources. This chapter therefore firstly looks at how PV energy can help to address these environmental concerns, especially the problem of man-induced climate change.

The chapter then investigates the main obstacle hindering widespread deployment of PV technology, that of cost per unit energy. PV energy is compared with wind and coal/nuclear energy costs, and potential future reductions in cost discussed.

Finally a possible future South African energy scenario is presented, and the role that PV energy can play within this scenario discussed. This section also looks at legislation promoting renewable energy technologies.

In the conclusion of this chapter the question is answered on whether PV energy has a future contribution to make, and ideas offered on what this contribution will be.

2.2 *PV energy and the environment*

2.2.1 The greenhouse effect

To maintain a long-term stable temperature, the earth needs to radiate the energy it receives from the sun back into space. Solar energy arrives on the earth in the form of short-wave radiation. This radiation is converted into heat when it hits the earth's surface, from where it is then radiated back into the atmosphere as long-wave radiation.

While short-wave radiation can pass through the atmosphere relatively easily, long-wave radiation gets absorbed in the atmosphere by certain naturally occurring 'green-house' gases like water vapour, methane and carbon dioxide (CO_2). These gases prevent energy from the surface of the earth from being radiated back into space too quickly. The energy is instead slowly moved out into space by atmospheric processes, thereby regulating the earth's temperature within a range essential to maintaining life on the planet [2].

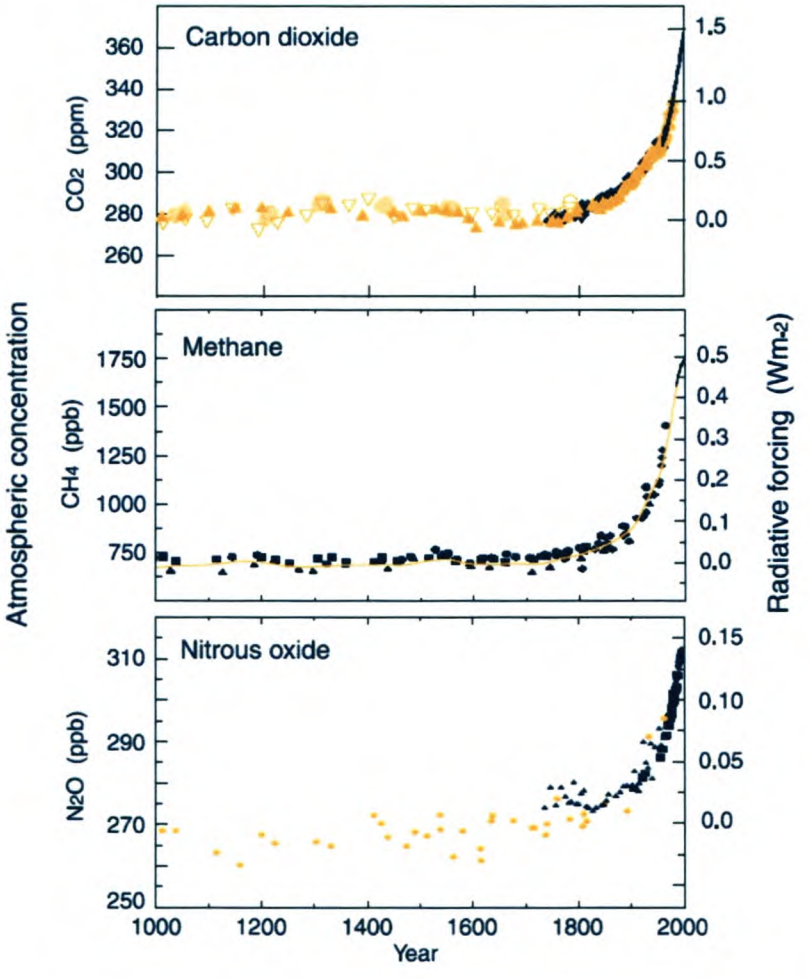

Figure 2-1: Global atmospheric concentrations over time of three greenhouse gases [1]

Human activity since the industrial revolution has increased the amount of greenhouse gases in the earth's atmosphere to such an extent that it is moving towards double its natural concentration, as shown in Figure 2-1. This increase in greenhouse gases reduces the flow of energy from the earth back into space. The extra energy has to go somewhere, however, forcing the earth's climate to change in order to maintain a balance between the energy arriving from the sun and the energy escaping back into space.

CO_2 emissions from the burning of fossil fuels to generate energy are the biggest source of greenhouse gas from human activities. CO_2 emissions are currently responsible for around 60% of the human-induced greenhouse effect [1].

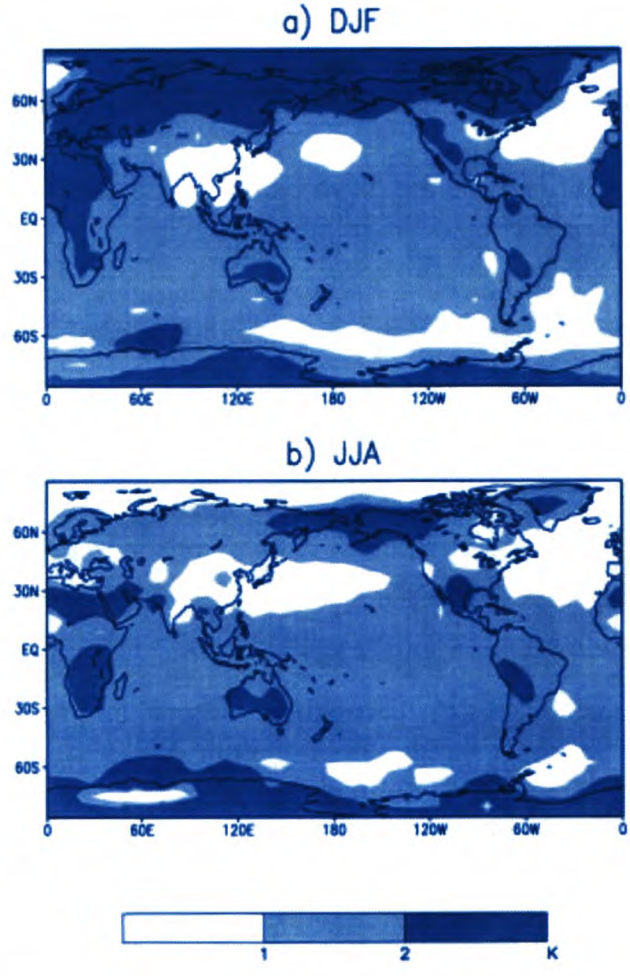

Figure 2-2: Predicted surface-temperature rise (in degrees Celsius) between the periods 1950-1979 and 2040-2049, for the months of a) December-January-February and b) June-July-August. The temperature K represents temperatures above 2 °C [origin in 5, reproduced in 1]

2.2.2 Predicted consequences of the greenhouse effect

The most direct consequence of the higher concentration of greenhouse gases is an increase in global temperatures, predicted to rise on average between 1.4 and 5.8 °C by 2100 [1].

Climatic models predict that inland temperatures in Southern Africa will rise by more than 2 °C by 2040-2049 compared to 1950-1979 as shown in Figure 2-2. The impact of such climate change on Southern African economies includes prolonged droughts, biome shifts (e.g. the projected complete loss or displacement of the succulent Karoo biome) and the southwards expansion of malaria risk areas [2].

The increase in average global temperature will lead to thermal expansion of the upper layers of the oceans, which, along with melting glaziers, leads scientists to predict a global rise in sea levels by between 9 cm and 88 cm by 2100 [1].

Global precipitation is predicted to increase, especially in the Northern mid- and high latitudes, while Australia, central America and Southern Africa shows consistently decreasing winter rainfall.

The change of climatic processes to compensate for the increased energy trapped within the atmosphere is furthermore predicted to lead to more frequent extreme climatic events like heat waves, tropical cyclones and flooding [1].

2.2.3 The response of the international community

The last decades of the 20th century saw a gradual increase in global awareness of the possibility of climate change. In 1979 a scientific gathering called the First World Climate Congress explored the influence of human activity on the earth's climate. As public awareness of environmental issues continued to increase during the 1980s, governments started to focus on climate issues. This led to 152 states signing the 1992 Framework Convention on Climate Change in Rio de Janeiro.

The Convention on Climate Change sets an ultimate objective of 'stabilizing greenhouse gas concentrations in the atmosphere at a level that would prevent dangerous human-induced interference with the climatic system.' In essence the convention recognised the existence of a climatic change problem, encouraged further research into climatic change, and laid the foundations for future action.

The convention also acknowledged the vulnerability of poorer nations to climatic change and their right to economic development, and placed most of the responsibility (and the bill) of

battling climate change with the rich nations. Rich nations in general are also the main polluters: the USA, as an example, contributed 24% to the total human-induced CO_2 emissions in 1998 [1].

The Kyoto protocol, opened for ratification in 1997, builds on the principles defined in the Climate Change Convention, adding much stronger and complex commitments. Where the convention only encouraged stabilization of greenhouse emissions, the Kyoto protocol sets legally binding targets and timetables for cutting developed country emissions. The target is set at 95% of 1990 emission levels by the years 2008-2012 [4].

Fifty-five countries, including developed countries accounting for at least 55% of developed countries' total 1990 CO_2 emissions, are required to sign the protocol in order to ratify it. Currently the protocol is not binding, as the USA and Russia, among the biggest contributors to greenhouse emissions (36.1% and 17.4% of total developed countries' 1990 CO_2 emissions [1]), are unwilling to sign due to economic and political reasons.

2.2.4 The environmental costs of PV energy

The costs of energy generation to the environment, in the context of climate change, are normally quantified as the amount of greenhouse gases, mainly CO_2, been released into the atmosphere per unit energy generated. A modern coal-fired power station, for example, produces around 1000 tonnes of CO_2 per GWh of electricity generated [6], while a nuclear plant emits around 9 tonnes of CO_2 per GWh. This figure, however, does not include the environmental effect of decommissioning and waste treatment [6].

Although renewable energy sources like wind and PV technologies do not produce any emissions during the generation process, some emissions are produced during the manufacturing, maintenance and decommissioning of the technologies. Energy from coal-fired power stations is for example utilized in the manufacturing of PV panels and wind generators, while CO_2 is also released during construction processes, e.g. when the cement foundation of a wind turbine is poured. The total CO_2 contribution of wind and PV energy can therefore not be ignored.

The environmental cost of wind energy, calculated in 1998 over the life cycle of three differently sized wind farms (1.2 MW, 25 MW and 107 MW), is given as between 9 and 20 tonnes of CO_2 per GWh [7]. This can be compared with PV energy, emitting between 2.7 and 45 tonnes of CO_2 per GWh during its life cycle [6]. The lowest emissions from PV technologies occur during the large-scale manufacture of thin-film polycrystalline panels, while the highest emissions occur during the small-scale manufacture of mono- or multi-crystalline silicon panels.

2.3 *The economics of PV energy production*

While the previous section clearly shows that PV energy is beneficial to the environment when compared to currently widespread energy generation methods such as coal-fired power stations, PV energy is still not an economically viable competitor in the energy market except in certain niche markets such as satellites. The following section will compare the current cost of PV with wind and coal-fired energy generation technologies. Two factors that can potentially lower PV energy costs in the future will then be investigated, namely advances in PV panel material and construction techniques, and emission trading schemes introduced by the Kyoto protocol.

2.3.1 Current energy generation cost comparison

2.3.1.1 Coal-fired/nuclear energy generation costs

Eskom, the South African electricity supplier, categorises commercial customers according to their maximum demand and energy usage per month into one of five tariff structures, as can be seen in Table 2-1.

Incentives are provided during off-peak hours (10 pm to 6 am during the week, and the full weekend) to encourage customers to use energy during these times. For Small Power Users cheaper energy rates apply during off-peak periods, while peak demand measurements are not done during off-peak periods for Large Power Users.

The cost of Eskom energy therefore varies between around R0.16 and R0.52 per kWh. Eskom energy is mostly generated using coal-fired (92.9%) and nuclear (6.4%) technologies [9].

	Small Power User (low consumption)	*Small Power User (high consumption)*	*Large Power User (low voltage*	*Large Power User (medium voltage)*	*Very Large Power User (medium voltage)*
Energy range (kWh per month)	<1000	>1000			
Demand range (kVA)	<500	<500	<1000		
Peak energy charge (Rand per kWh)	**0.5182**	0.3386	0.1676	0.1558	0.1450
Off-peak energy charge (Rand per kWh)	0.1676	0.1676	0.1676	**0.1558**	0.1450
Monthly demand charge (Rand per kVA)	0	0	49.88	46.38	21.12
Monthly service charge (Rand)	0	179.55	299.25	299.25	52326.00

Table 2-1: Eskom commercial customers electricity costs for different tariff structures

2.3.1.2 Wind energy generation costs

The Eskom Klipheuwel wind turbine test facility is at present the only grid-connected wind energy generation site in operation in South Africa, generating around 5.1 GWh of energy per year. A variety of other wind energy projects, e.g. the Darling national demonstration wind farm, are planned and in various stages of completion [9].

The cost of energy from wind generation in South Africa is therefore calculated using data from this facility, as shown in Table 2-2. The wind farm operates at around 20% conversion efficiency, so as best-case 23% efficiency was chosen, and as worst-case 15%. The energy costs were calculated based on best and worst-case costs as supplied by Eskom [8], assuming an excess inflation rate of 5% and a discount rate of 8% (life cycle costing is explained in detail in Section 3.4.2).

The cost of wind energy at the Klipheuwel facility is calculated as between R0.60 and R1.49 per kWh, representing best and worst-case scenarios. It is generally accepted that a number of factors, including the size of the wind farm, its distance from the grid and foreign exchange rates, influences the energy cost. The Eskom Klipheuwel site is experimental, and as such the costs calculated in Table 2-2 are higher than found in other sources of wind energy cost data, e.g. [16] which reports costs of between R0.28 and R0.42 per kWh for large-scale onshore wind generation in the USA.

	Best-case	*Worst-case*
Installation costs (Rand per kW peak)	8000	10000
Operation and maintenance costs, year 1 to 3 (% of installation costs)	1	2
Operation and maintenance costs, year 4 to 10 (% of installation costs)	3	5
Operation and maintenance costs, year 11 to 20 (% of installation costs)	10	15
Conversion efficiency (%)	23	15
Size of wind farm (MW peak)	2.5	3.9
Cost per unit electricity (Rand per kWh)	**0.60**	**1.49**

Table 2-2: Eskom Klipheuwel wind turbine test facility costs

2.3.1.3 PV generation costs

The SunSim simulation package (refer to Chapter 3) was used to obtain PV energy costs per kWh for South African conditions. Cost assumptions and parameters as given in Sections 3.4.2.2 and 3.4.2.3 were used to calculate these energy costs, using 20-year life cycle analysis.

As can be seen in Figure 2-3, the cheapest PV energy is produced at locations with high amounts of yearly irradiation, such as Upington in the Northern Cape province. At these locations, PV

energy costs of around R1.71 can be obtained. A location with lower yearly irradiation, such as Durban, is less suited for PV energy production, with PV energy costs of around R2.51.

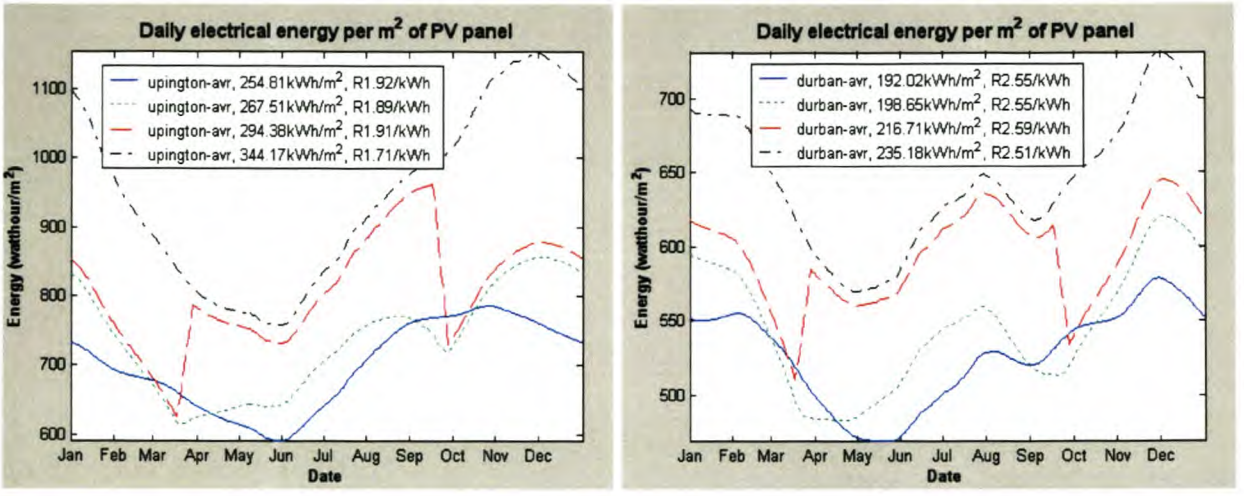

Figure 2-3: PV energy costs for Upington and Durban, calculated by SunSim using traditional silicon panels, for four different solar tracking configurations: 1) slope and azimuth angles fixed at the position of maximum total yearly energy 2) azimuth angle fixed, slope angle adjusted twice yearly 3) full azimuth angle solar tracking, slope angle adjusted twice yearly 4) full azimuth and slope angle solar tracking

2.3.2 Future PV energy generation cost reductions

2.3.2.1 Advances in PV panel material and construction techniques

A wide variety of PV panel materials exist, with applications ranging from energy production in satellites to battery charging in third world countries.

Mono- and polycrystalline silicon PV cells are currently the most widely used building blocks for PV panels, due to their relatively cheap cost of manufacture. New, so-called thin-film PV cell technologies are however beginning to provide competition to traditional silicon in the PV panel market. Thin-film technologies offer cost benefits, as less PV material is necessary for the same amount of generated power, and cheaper substrates can be used [6].

This movement towards thin-film technologies is illustrated by a recent development at the physics department of RAU in South Africa. A process was developed here for producing copper-indium-gallium-diselenide (CIGS) thin-film PV panels at one quarter of the cost of equivalent silicon panels. Commercial development of this process is at present receiving backing from the South African government, in the form of a R13 million grant from the Innovation Fund. Large-scale production of these thin-film PV panels is planned for the beginning of 2005 [10 and 11].

If the new thin-film panels mentioned above are used instead of traditional silicon panels, the PV energy generation costs fall to between R1.04 and R1.38 per kWh of generated electricity, as calculated in Figure 2-4. Even though the thin-film PV panels are a quarter of the price of traditional silicon PV panels, additional costs like the tracking frame and power electronics does not change, leading to a reduction in cost of only 40-45% (see Section 2.3.1.3).

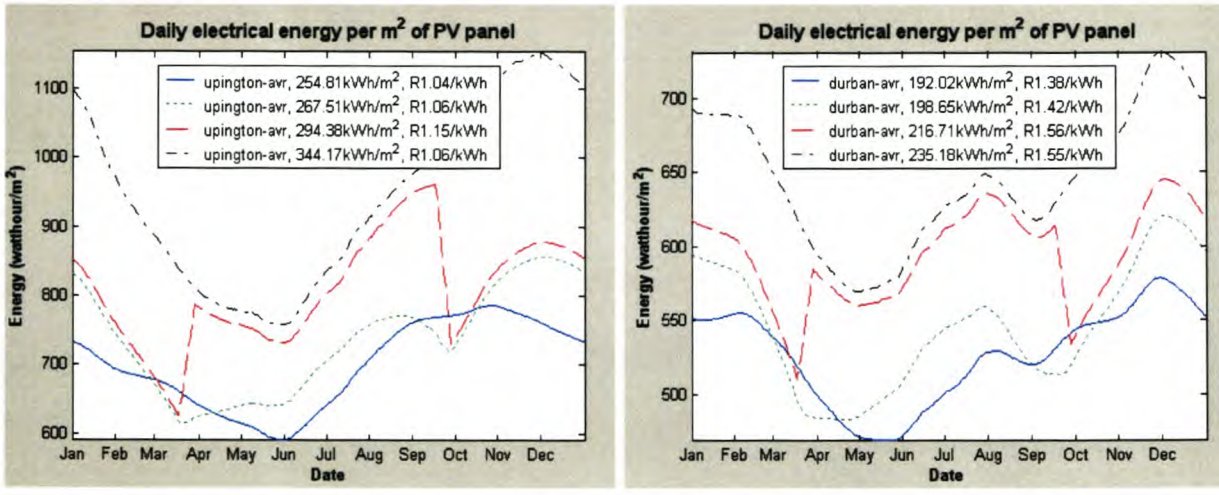

Figure 2-4: PV energy costs for Upington and Durban, calculated by SunSim using thin-film CIGS panels, for four different solar tracking configurations: 1) slope and azimuth angles fixed at the position of maximum total yearly energy 2) azimuth angle fixed, slope angle adjusted twice yearly 3) full azimuth angle solar tracking, slope angle adjusted twice yearly 4) full azimuth and slope angle solar tracking

2.3.2.2 The Clean Development Mechanism and emission-trading

The Kyoto protocol, described in Section 2.2.3, was put in place to force countries to lower their greenhouse gas emissions. However, the cost of cutting emissions varies between countries, depending on factors like the efficiency at which energy is already being produced. Furthermore, the location of emission reduction is of little importance, as long as the reduction is made. The protocol takes these facts into account, and offers several mechanisms through which developed countries can gain emission 'credits' by reducing emissions in other countries where emission-reduction costs are lower. Two of these mechanisms are relevant to South Africa as a developing country [11].

Firstly the Clean Development Mechanism will generate credits to developed nations for financing emission reducing or emission avoiding projects in developing countries. A pre-requisite for this mechanism is that the project should contribute to sustainable development in the host country.

Secondly a voluntary emission-trading scheme was put in place offering a marketplace for countries to buy and sell emission credits, e.g. 'I saved 2000 tonnes of CO_2 by generating energy using wind instead of coal, so if you give me R50 per tonne, you can get the credit for the emission saving'. As South Africa is classed as a developing country, it is currently not bound by the Kyoto protocol to lower its emissions, thereby making all local emission savings available for sale through emission trading.

Current market rates fluctuate around R35 per ton of CO_2 [13], but are expected to increase significantly in the next few years, as the governments of developed countries increase pressure on polluters to reach their 2008-2012 emission reduction targets.

Table 2-3 calculates the economic benefits of replacing coal-fired energy with renewable energy under the Kyoto protocol emission-trading scheme. The calculations assume that only 85% of the energy generated at the coal-fired power station reaches the consumer due to transmission inefficiencies. This means that 1177 tonnes, and not 1000 tonnes, of CO_2 will be produced for every GWh of electricity delivered to the consumer.

In the best-case scenario, where CO_2 emissions from renewable energy technologies are very low, and the emission trading prices very high, PV energy generation costs will benefit by around R0.15 per kWh, or 14% of the thin-film PV panel best-case energy generation cost.

	Best-case	*Worst-case*
Coal-fired energy CO_2 emissions with transmission efficiency included (ton per GWh)	1177	1177
PV energy CO_2 emissions (ton per GWh)	2.7	45
Wind energy CO_2 emissions (ton per GWh)	9	20
Emission trading benefit (Rand per ton of CO_2)	140	35
Coal-fired energy as percentage of total Eskom energy	92.9	92.9
CO_2 reduction using PV energy (ton per GWh)	1090	1040
CO_2 reduction using wind energy (ton per GWh)	1082	1069
Benefit per unit energy using PV instead of coal (Rand per kWh)	**0.15**	**0.04**
Benefit per unit energy using wind instead of coal (Rand per kWh)	**0.15**	**0.04**

Table 2-3: Emission trading benefits when replacing coal-fired with renewable energy generation.

2.4 Future South African energy scenario

Now that the environmental and economic costs and benefits of PV energy have been discussed, one final topic must be looked at before a conclusion can be reached on the future contribution of PV energy in South Africa. This section attempts to predict the future South African energy scenario, by looking at future electricity demand and supply and its influence on future electricity prices, and finally the role of government legislation in establishing renewable energy technologies in South Africa.

2.4.1 Electricity demand, supply and cost predictions

The growth in South African yearly energy demand between 2004 and 2013 is predicted to be 60000 GWh, which translates into an increase of 34% from the 2001 total energy demand of 177300 GWh. In 2003 the total South African electricity generation capacity was around 37 GW, with peak demand around 31.5 GW. Typical winter peak demand is predicted to rise to 34 GW by 2005, and 44 GW by 2015. This rise in energy and peak demand leads to a predicted shortage in generation capacity by 2005 – 2007 [14].

This predicted shortage means that South Africa will either have to enlarge its current capacity by installing additional generation capacity or importing electricity from its Southern African neighbours, or by implementing demand side management measures.

All these solutions will cost money, leading to a statement by Eskom's executive manager, Thulani Gcabashe, in the beginning of 2004, warning that South African electricity prices will be 'significantly higher' in the future [17].

Another indication of future trends in South African electricity costs is the recent disagreement between Eskom and the National Electricity Regulator, where Eskom requested a cost increase of 8.5% in July 2003 to finance new generation capacity, and the National Electricity Regulator only approved a 2.5% increase.

2.4.2 The contribution of renewable energy

How much of this new generation capacity will be supplied by renewable energy technologies? The 2003 South African renewable energy white paper states that the government's medium term target is '10 000 GWh renewable energy contribution to final energy consumption by 2013, to be produced mainly from biomass, wind, solar and small-scale hydro.'[15] Given the

predicted growth in demand by 2013 to 60 000 GWh, around 12% of new energy generation capacity will therefore need to come from renewable energy technologies.

A study by the Department of Minerals and Energy on the renewable energy white paper, with regards to strategy formulation, concluded that only around 4 400 GWh of energy from renewable energy technologies will be financially viable. The additional 5 600 GWh necessary to fulfil the 2013 renewable energy target will need a subsidy of R225 million from the government or electricity end-users [14]. This calculation again indicates that electricity prices will have to increase in the future.

2.5 Conclusion

This chapter set out to investigate the future role of PV energy in the electrical energy production scenario in South Africa.

The investigation started by looking at how the use of PV energy could help solve a serious environmental problem facing our civilizations; that of climate change. PV energy offers definite environmental benefits, producing between 2.7 and 40 tonnes of CO_2 per GWh, compared to the 1000 tonnes of CO_2 per GWh produced by coal-fired power stations.

Environmental benefits are unfortunately not enough reason to implement PV technology. PV energy costs per kWh were therefore compared with that of coal-fired power stations and wind generation. Over a 20-year life cycle, using best-case scenarios, it was found that a well-positioned PV array generates energy that is ten times more expensive than coal-fired energy, and almost three times as expensive as wind energy. Technological developments in the near future are predicted, however, to almost half the cost per unit PV energy generated. Emission trading, introduced by the Kyoto protocol, is predicted to lower the cost of PV energy by another 15% in a best-case scenario.

The future energy scenario of South Africa favours renewable energy, with the government's renewable energy white paper requiring 10000 GWh of final energy consumption to come from renewable sources. Rising electricity prices due to rising demand and limited supply will also mean that renewable energy technologies will become more economically viable in the future compared to coal-fired power.

Wind energy is cheaper than PV energy, and as such will probably be the main renewable energy technology used for grid-connected generation in the near future. Large-scale wind generation is however limited mostly to the west coast of South Africa due to the available wind resource [9], while the solar resource in South Africa favours PV energy generation through most of South Africa, as the SunSim results in Chapter 3 show. This fact, combined with the advantages of modularity, reliability and ease of installation, will continue to ensure a place for PV energy generation within South Africa's energy landscape, mostly for off-grid, rural applications. Only if the price of PV energy drops significantly will grid-connected PV generation become a reality.

Now that the future contribution of PV energy has been verified, this thesis continues to investigate methods to produce PV energy as efficiently, and therefore as cheaply as possible.

Chapter 3 - Optimal positioning of the PV panel

3.1 Introduction

To extract the highest amount of electrical energy from a PV panel, the surface of the panel should always face the sun. This means the PV panel should track the position of the sun through the day and year. But how should a PV panel be positioned if solar tracking is not possible, i.e. the panel is fixed at a certain tilt angle throughout the year? Or will the PV panel always supply maximum electrical energy if it faces the sun, even on a cloudy day when the atmosphere contains almost no direct irradiance, but a lot of diffuse irradiance? And by how much will the amount of electrical energy generated by a PV panel installed in Durban differ from one installed in Upington?

This chapter explains the development of a computer model, called SunSim, that is used to address the above and other issues in designing a PV system. This computer model takes as input atmosphere data from previous years, as well as the location, positioning and characteristics of the PV panel, and predicts as output the amount of electrical energy available from the PV panel. The model can also predict the position at which the PV panel should be installed to satisfy certain criteria, e.g. maximum total energy through the year. Finally the model is able to estimate the cost of PV energy generation for a set of given parameters.

The chapter starts by looking at the journey of solar irradiance from the sun, through the atmosphere, to the PV panel on the surface of a spinning earth. Factors that influence the efficiency at which the PV panel converts solar energy to electricity are then investigated.

With this background knowledge, the chapter then continues to discuss how the SunSim model was developed, and compares its simulation results to real-life measurements.

Finally the results and conclusions from the computer simulations are presented.

3.2 Irradiance on a tilted plane on the surface of the earth

3.2.1 Radiation in the earth's atmosphere

3.2.1.1 The sun as source of radiation

Most of the energy available on earth originates as nuclear reactions in the interior of the sun. These huge amounts of energy would long ago have caused the sun to explode, were it not radiated out to the sun's surface, at a rate of around 3.9×10^{26} W [22].

From here the radiation travels around 150 million kilometres through the vacuum of space, before reaching the outside of the earth's atmosphere. This journey from the sun's surface to the earth does not have much effect on the shape of the solar radiation spectrum. Figure 3-1 shows the similarity between the solar radiation spectrum measured near the earth and the predicted shape of the same spectrum at the surface of the sun, that of a Planck blackbody in equilibrium with a temperature of 5762°K [22].

The differences between the two spectrums are mainly caused by variations in temperature on the outside sphere of the sun from around 8000°K to a minimum of 4300°K, as well as by absorption of certain wavelengths of the spectrum by components of the sun's 'atmosphere'. This absorption process will be explained in more detail later in this chapter.

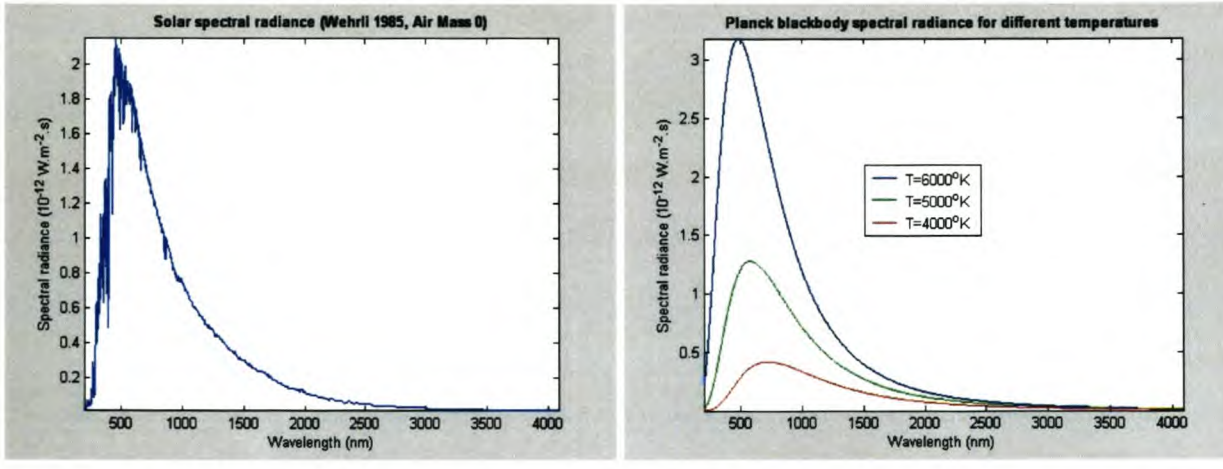

Figure 3-1: The solar radiation spectrum measured outside the atmosphere of the earth [20], and a Planck blackbody's radiation spectrum for different temperatures

The last few kilometres of solar radiation's journey to the earth's surface, as it enters the collection of gases surrounding planet Earth, has the most pronounced effect on its spectral shape, as shown in Figure 3-2. Certain regions of the incoming radiation spectrum are absorbed by atmospheric components, while other wavelengths are scattered or reflected by the

atmosphere. The three atmospheric processes that influence the amount of irradiance that reaches an object on earth's surface, being absorption, scattering and reflection, will now be discussed.

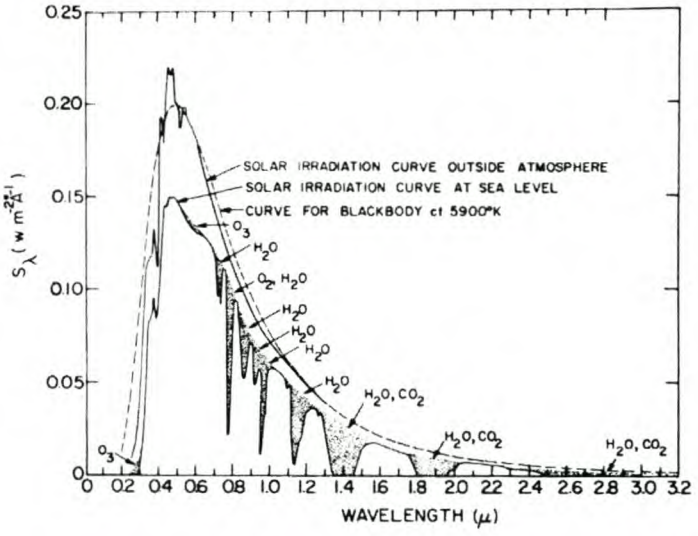

Figure 3-2: The effect of the atmosphere on the spectral distribution of solar energy [24]

3.2.1.2 Atmospheric absorption

Around 99 percent of the atmosphere consists of nitrogen and oxygen. It is, however, the insignificant components such as ozone, carbon dioxide and water vapour that contributes most to the absorption of certain regions of the incoming solar radiation spectrum. The physics behind why only certain wavelengths are absorbed by certain components are beyond the scope of this text, but is developed in many of the references e.g. [24].

The absorption effect of different components in the earth's atmosphere is shown in Figure 3-3. From this figure it is clear, for example, that biological destructive UV-C radiation is totally absorbed by ozone and oxygen in the upper atmosphere. UV-B radiation, which has less energy than UV-C, but is still harmful to the biosphere, is almost completely absorbed by these same molecules. However, as the stratospheric ozone layer becomes thinner, environmental damage from UV-B radiation becomes more pronounced.

The UV-A, visible, and near infrared wavelength spectrums are only absorbed in small amounts by the atmosphere. Long wave thermal radiation, radiated by the earth (a Planck blackbody with a temperature of 250°K), is almost completely absorbed by water vapour and carbon dioxide.

A wide variety of other factors such as the path length of the sun's radiation through the atmosphere and natural and man-made atmospheric pollution (dust and smog) also influences the intensity of absorption in the atmosphere.

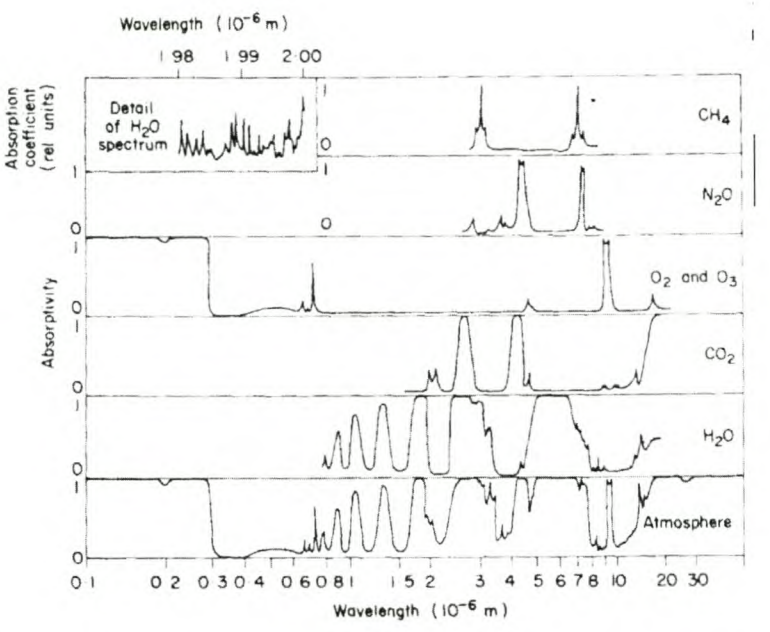

Figure 3-3: The spectral absorption efficiency of different components in the earth's atmosphere, and the atmosphere as a whole [22]

3.2.1.3 Atmospheric scattering

Scattering of incoming solar radiation is mainly caused by density fluctuations in the earth's atmosphere. This scattered irradiance is also known as diffuse irradiance.

It can be shown [24] that the intensity of scattering significantly depends upon wavelength, mostly increasing with the decrease in wavelength (see Figure 3-4). This explains why the sky is blue: blue has the lowest wavelength within the visible spectrum, and is therefore scattered most in a clear atmosphere. Clouds, on the other hand, scatter and reflect a wide spectrum of wavelengths, and therefore appear white. Clouds cause intensive solar radiation scattering, varying in scattering intensity with the type of cloud cover (Figure 3-5).

Other influences on the intensity of diffuse radiation include the position of the sun in the sky (the closer to the horizon, the greater the scattering), the atmospheric transparency and turbulence conditions, and the albedo (explained in the next section) of the underlying surface.

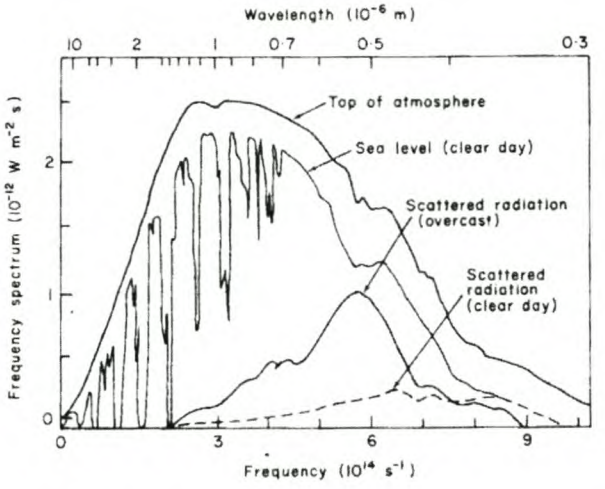

Figure 3-4: Typical spectra of diffuse (scattered) irradiance for the two extremes of cloudless and overcast days, as compared with the complete solar radiation spectrum. Note that the x-axis is opposite to the direction of most other solar spectrums given in this chapter [22]

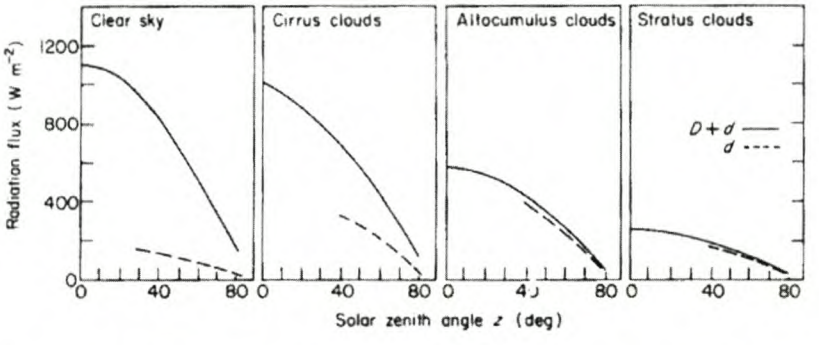

Figure 3-5: The influence of different types of clouds on the global (D+d) and diffuse (d) irradiance components that reaches a horizontal plane [22]

3.2.1.4 Reflection from clouds and the underlying surface

A percentage of the direct and diffuse solar radiation reaching the earth's surface is reflected from it. Clouds also reflect incoming solar radiation towards the upper atmosphere, as well as diffuse and reflected irradiance towards the earth's surface.

The ratio of the amount of reflected irradiance to the amount of incident irradiance on a surface is called the surface's albedo. As an example, the spectral albedo of surfaces covered with various plants is shown in Figure 3-6. Typical mean albedo values for different ground types vary from 30-40% for desert sand, to 10% for dry black earth [24]. As can be seen in Figure 3-6, the height of the sun above the horizon sometimes has an influence on the albedo value of a surface, in this case water. The glass that covers a PV panel will have a similar albedo effect.

Spectrally clouds have theoretically calculated mean albedo values of around 45% in the infrared regions and up to 85% in the visible and UV regions [24]. The mean albedo of clouds is furthermore a function of cloud thickness, as shown in Figure 3-7.

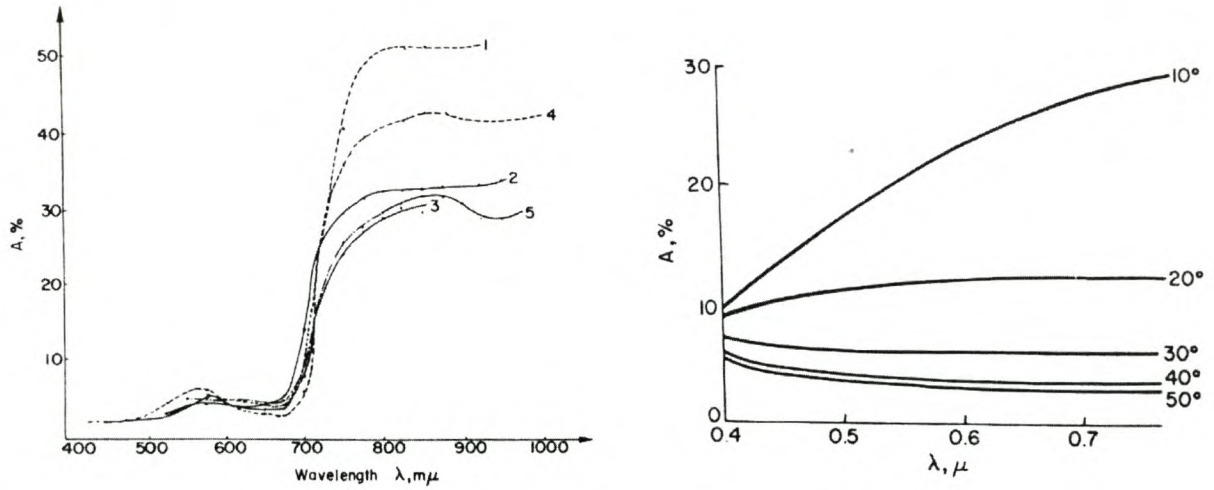

Figure 3-6: The spectral albedo for different plants. 1) Sudan grass, 2) maize, 3) clover, 4) Lucerne in June and 5) Lucerne in July [24,p414], and the dependence of the spectral albedo of water upon solar height for global irradiance in a cloudless sky [24]

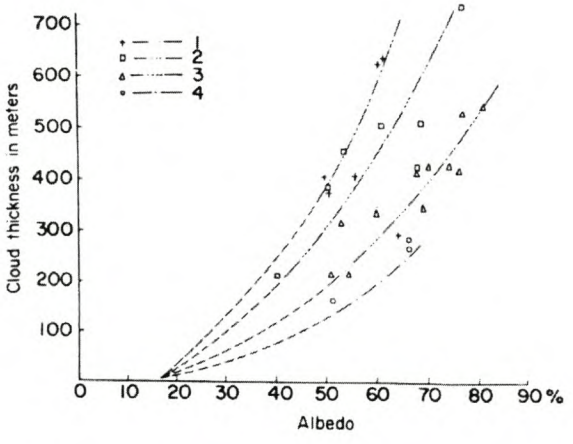

Figure 3-7: Dependence of cloud albedo upon vertical cloud thickness, for four measurement sets done on different fully overcast days [24]

3.2.2 Position of the sun relative to the earth

3.2.2.1 The earth's movement around the sun

In the previous section it became clear that the position of the sun relative to the measurement location (solar height, and therefore atmospheric path length) influences the intensity of atmospheric absorption, scattering and reflection. What influence does this position of the sun have on direct solar radiation (i.e. parallel beams that have not been deflected during the journey from the sun) reaching the surface of the earth?

Some astronomical background of the earth is required to answer this question. Observations confirm that the earth follows an elliptical orbit around the sun, with a complete orbit taking 365.25 days. The earth is closest to the sun near 1 January, and furthest away near 1 July, causing the total solar energy that reaches the earth's outer atmosphere to vary by about 7% during the year (see Figure 3-8).

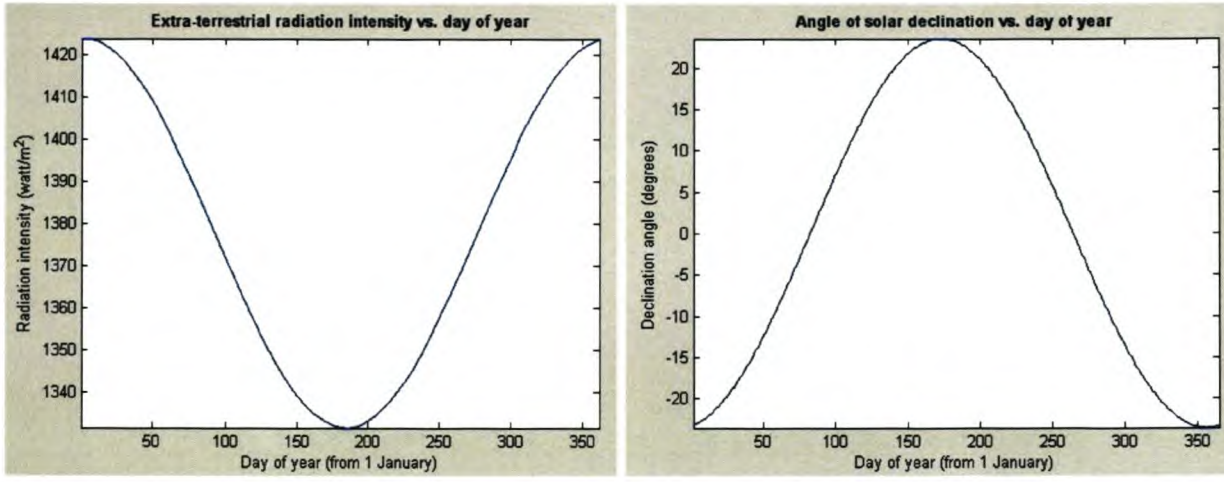

Figure 3-8: Total solar radiation at the outside of the earth's atmosphere as a function of the time of year, and solar declination as a function of time of year

The rotation axis of the earth is also tilted 23.45° with respect to its orbit plane around the sun. Because of this, the position of the sun, as observed from the earth, moves north or south by up to 23.45°, depending on the day of the year. The angle between the direction of the solar rays and straight up, at noon on the equator, is called the solar declination angle. This declination (Figure 3-8) causes the seasons on earth, with June 21 and December 21 being the days when the axis is tilted exactly towards or away from the sun.

3.2.2.2 Solar time vs. standard time

Because of the movement of the sun relative to the equator, as well as the elliptical orbit of the earth around the sun, differences through the year exist between the apparent solar time (noon occurs when the sun is directly above) and the time indicated by normal clocks.

These differences led to the development of a time system called mean time. In the mean time system the sun moves with uniform speed along the equator, and maintains a constant motion calculated as the average over the year of the true sun's angular motion along the ecliptic.

The differences through the year between the apparent solar time and mean time is contained in the equation of time (see Figure 3-9), and can be expressed mathematically as follows [6]:

$$EoT = 2.292(0.0075 + 0.1868\cos\beta - 3.2077\sin\beta - 1.4615\cos 2\beta - 4.089\sin 2\beta) \quad 3\text{-}1$$

where $\beta = \frac{2\pi}{265}(n-1)$ and n the day of the year.

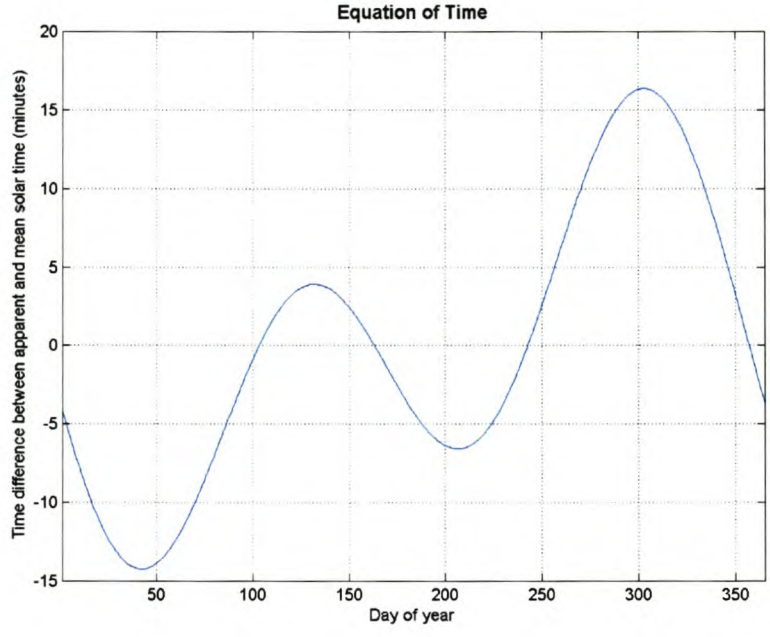

Figure 3-9: The equation of time – the different between apparent solar time and mean solar time

Mean time, like local apparent solar time, is still based on longitude. For this reason mean time was adapted to zone time, or standard time, in which the earth is divided into 24 time zones. Standard time is the time displayed on conventional watches and clocks. The equation below is used to convert between local apparent solar time (LST) and standard time (ST):

$$LST = 4\times(L_{st} - L_{loc}) + EoT - ST \quad 3\text{-}2$$

where L_{st} is the standard meridian for the local time zone, and L_{loc} is the longitude of the location.

All the time quantities in this chapter and the SunSim computer model, described later in this chapter, refer to local apparent solar time.

3.2.2.3 Calculating irradiance on a tilted surface

With the astronomical knowledge given above, a formula can now be derived to calculate the amount of direct irradiance from the sun incident upon a tilted surface located at any latitude on the surface of the earth.

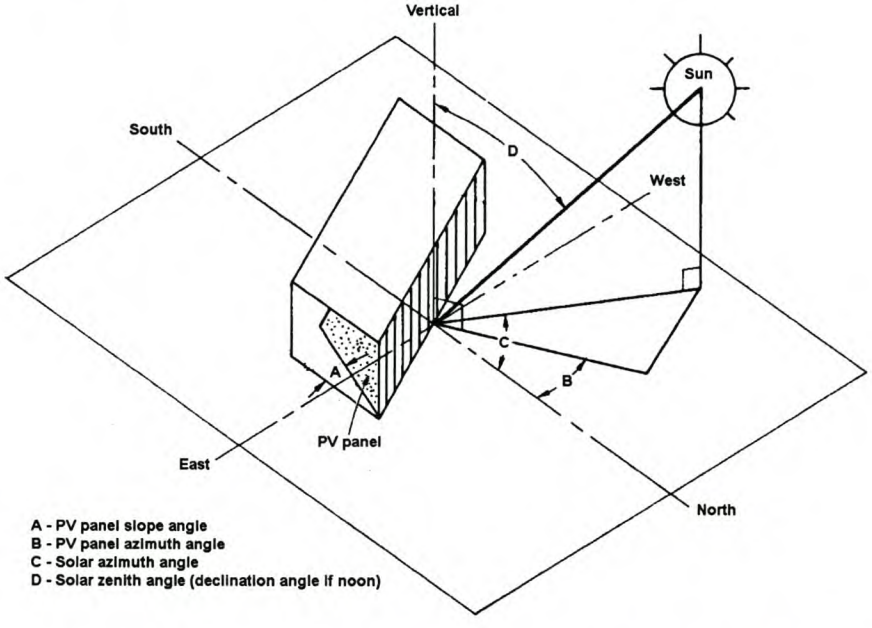

Figure 3-10: The position of a tilted surface relative to the sun (adapted from [21])

The positioning of this tilted surface can be described using two parameters. The first is the angle at which the surface is tilted from its horizontal position, called the *slope angle*. This slope angle is zero for a horizontal surface and 90° for a vertical surface facing north, and is represented in Figure 3-10 as angle A.

The second angle is the *azimuth angle* that the surface makes with the north-south plane, represented as angle B in Figure 3-10. If the tilted surface faces towards the north the azimuth angle is 0°, while if it faces towards the east, the angle is -90°.

The positioning of the sun in the sky can also be described using two angles. The first angle is the *solar azimuth angle*, which is the angle the position of the sun makes with the north-south plane, represented as angle C in Figure 3-10. The value of this angle at any given time of the year can be calculated using the following equation,

$$solar\_azimuth = \tan^{-1}[\frac{\cos(decl)\times\sin(hourangle)}{(\sin(lat)\times\cos(decl)\times\cos(hourangle)-\cos(lat)\times\sin(decl))}] \quad 3\text{-}3$$

where *decl* represents the solar declination, *lat* the latitude of the observer on the earth, and $hourangle = \frac{((time-12)\times 15\times\pi)}{180}$, with *time* in LST format (see section 3.2.2.2).

The second angle describing the position of the sun is the *solar zenith angle*, the angle the position of the sun makes with straight up, represented as angle D in Figure 3-10. The value of this angle at any given time of the day is given by the following equation:

$$solar\_zenith = \cos^{-1}[\sin(lat)\times\sin(decl)+\cos(lat)\times\cos(decl)\times\cos(hourangle)] \quad 3\text{-}4$$

Now that the positioning of both the tilted surface and the sun can be described, the direct irradiance on the tilted surface can be calculated using the following equation,

$$B_{tilted} = B_{normal}\times[\cos(slope)\times\cos(solar\_zenith)+ \sin(slope)\times\sin(solar\_zenith)\times\cos(solar\_azimuth-azimuth)] \quad 3\text{-}5$$

where B_{tilted} is the direct irradiance on the tilted surface and B_{normal} the direct irradiance on a surface normal to the sun at the equator.

The derivation of the above equations can be found in most solar energy texts, e.g. [43], and is therefore presented only in their final forms.

As with direct irradiance, the amount of diffuse irradiance on a surface is also subject to the angle at which the surface is tilted. If it is assumed that the diffuse irradiance is distributed isotropically across the sky dome, the diffuse radiation on the tilted surface can be calculated as follows,

$$D_{tilted} = D_{normal}\times 0.5(1+\cos(slope)) \quad 3\text{-}6$$

where D_{normal} is the diffuse irradiance on a surface normal to the sun at the equator.

3.2.3 Measuring irradiance

3.2.3.1 Measurement devices

It is important to understand how irradiance data is measured, as this measured data will be used in SunSim. Usually only the global and diffuse irradiance components are measured, as the direct irradiance can be calculated as the difference between these two data sets.

A typical irradiance measurement device, or pyranometer, similar to those used by the South African Weather Bureau (SAWB) is shown in Figure 3-11. This device is designed to measure global irradiance with an accuracy of within 1% for solar altitudes higher than 20°, and is sensitive to wavelengths between 0.3 and 3 micrometers. The diffuse component of global irradiance is measured by placing the pyranometer on a shadow-band stand that block any direct irradiance from the sun.

Figure 3-11: The Kipp & Zonen CM11 pyranometer

For measurements relating to the sensitivity of photovoltaic cells, a mono-crystalline silicon-based irradiance sensor, the Mencke & Tegtmeyer Si-01TC, is used. This sensor, shown on the left in Figure 3-12, was used for all non-SAWB supplied irradiance measurements presented in this text. The tiltable platforms shown on the right in Figure 3-12 allows irradiance measurements on tilted surfaces to be made, while the shadow band platform makes diffuse irradiance measurements possible. The measured diffuse values are increased by 5% to take the loss in irradiance caused by the shadow band into account. This adjustment is approximate, developed for an 'average partly cloudy sky' [25].

A study was done in 1996 comparing the measurements of a selection of silicon-based irradiance sensors to those of a Kipp & Zonen CM11 pyranometer [26]. The M & T Si-01TC sensor was one of the instruments tested, and had a global irradiance measurement deviation from the pyranometer of –1.4% for clear and partly cloudy skies, and 8.3% for cloudy skies.

Figure 3-12: The M & T Si-01TC irradiance sensor is shown on the left, while the shadow band platform and tilt angle adjustable platforms with mounted sensors are shown on the right.

Irradiance over extended periods of time was recorded using a Tektronix oscilloscope connected via a serial cable to a computer. A MATLAB program called Seriallog was developed to record the daily measurements to files (see Figure 3-13). The program automatically creates new data files daily, and offers additional functionality like oscilloscope screen capturing, used for most of the oscilloscope results shown in this text. The source code of Seriallog is available on the CD distributed with this thesis.

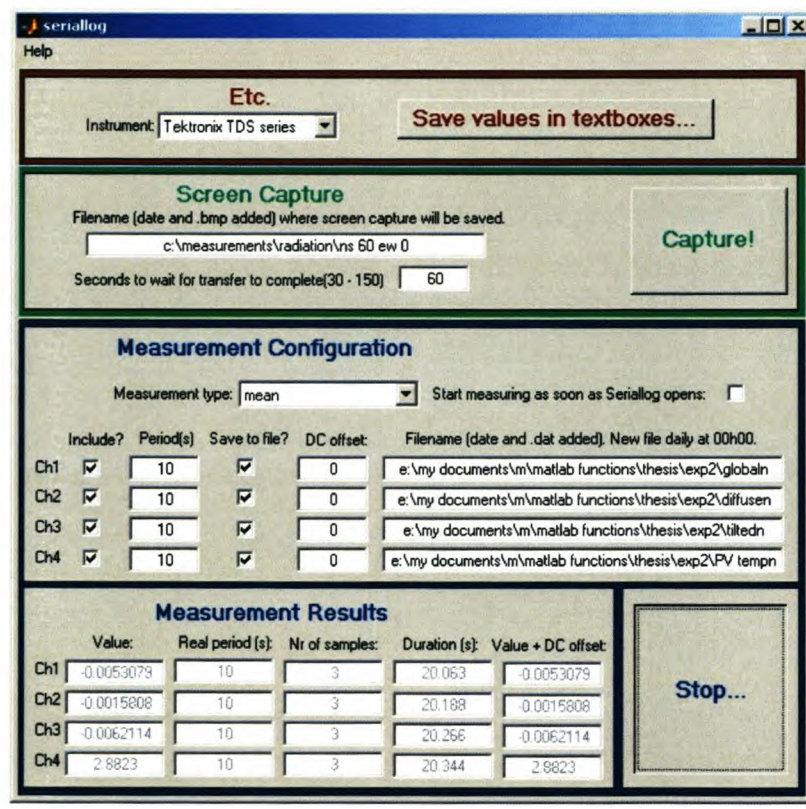

Figure 3-13: The Seriallog oscilloscope data capturing program

3.2.3.2 Typical irradiance measurements

This section will attempt to give the reader a better understanding of the interaction between atmospheric conditions and the global and diffuse irradiance measurements obtained. The accuracy of using SAWB irradiance data to model irradiation at a location some distance away from the SAWB weather station is also investigated.

Measurements done by the SAWB pyranometer at Cape Town airport and by the M & T irradiance sensors at Stellenbosch for a variety of atmospheric conditions are shown in Figure 3-15 and Figure 3-16, along with photos of the atmospheres on those days. The distance between the M & T solar irradiance sensors and the SAWB pyranometer is around 30 km. As can be seen from the Boland map presented in Figure 3-14, the SAWB pyranometer is closer to the sea, which explains the higher diffuse radiation measurements obtained.

From the two sets of measurements it is clear that the correlation between the SAWB data and data at the PV panel site is greater than 80% for cloudless days. The important conclusion that can be reached is that SAWB irradiation data for a location near to the PV panels gives a reasonably accurate indication of the irradiance on the PV panels, especially on cloudless days, when most irradiance is also available. This is obviously dependant on how similar the SAWB and PV panel environments are to each other, in terms of geography, proximity to the sea etc.

Figure 3-14: Map showing the locations of the SAWB pyranometer at CPT international airport, and the M & T irradiance sensors at Stellenbosch. Map courtesy of the SA Department of Survey and Mapping.

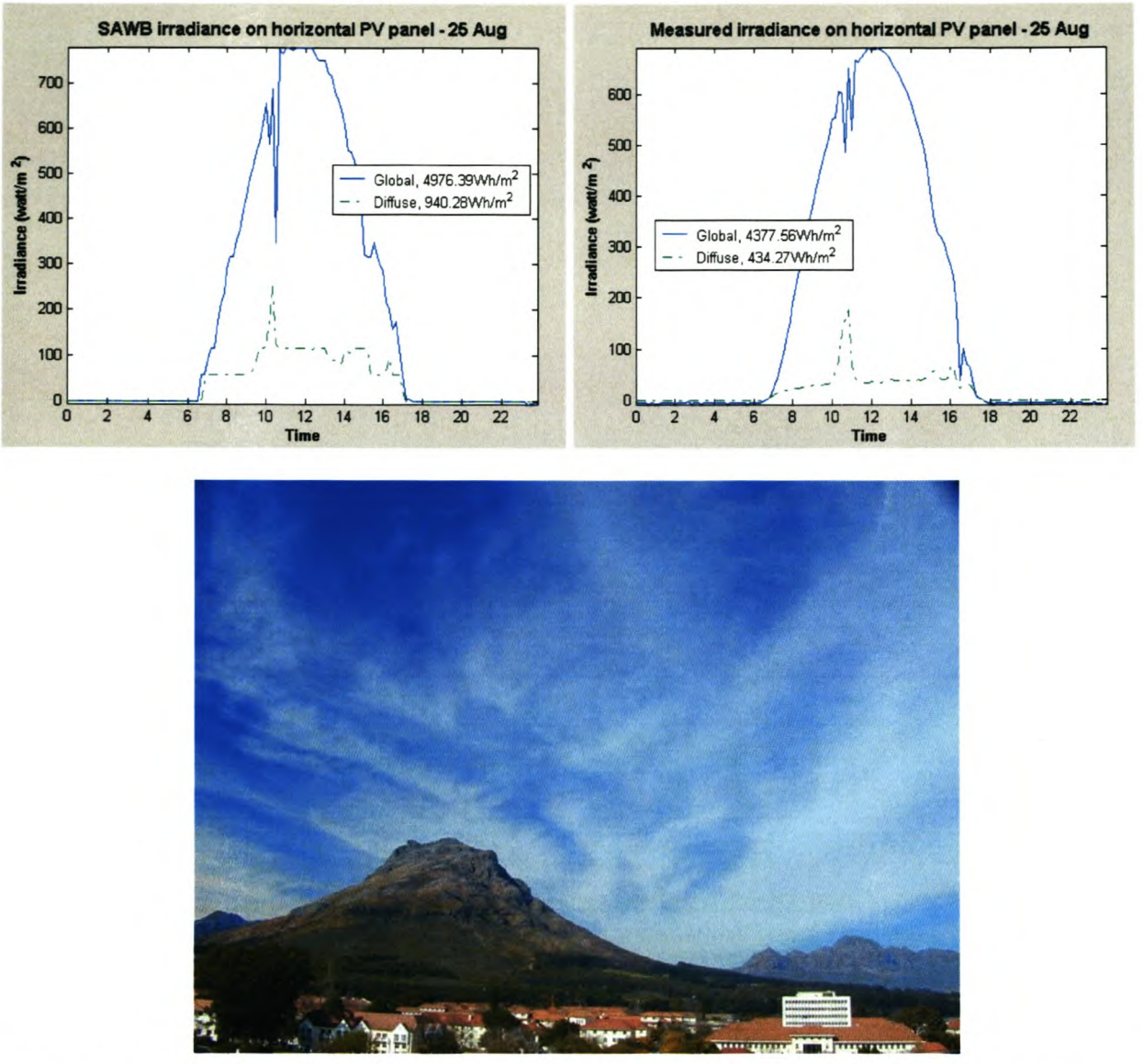

Figure 3-15: Irradiation data for 25 August, a day with mostly clear skies, scattered cloud for a period during the morning, and high clouds moving in during the afternoon as shown, with high visibility during most of the day. Global and diffuse irradiance as measured by the SAWB at CPT airport are shown in the top left figure, and measured using M & T irradiance sensors at Stellenbosch in the top right figure.

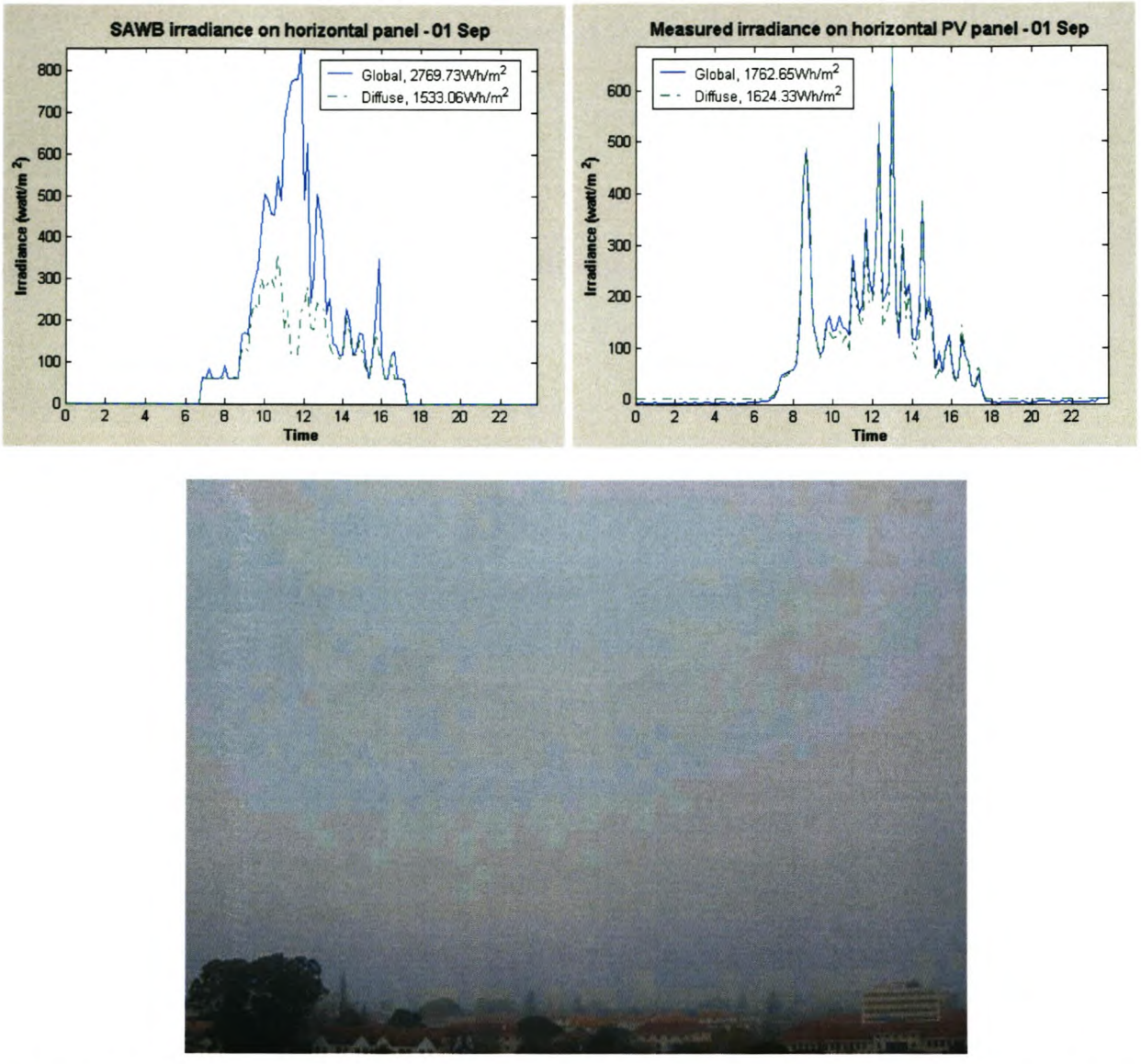

Figure 3-16: Irradiation data for 1 September, a day with periodic soft rain, low clouds and low visibility during most of the day. Global and diffuse irradiance as measured by the SAWB at CPT airport are shown in the top left figure, and measured using M & T irradiance sensors at Stellenbosch in the top right figure.

3.2.4 Predicting irradiance

The most accurate method to predict future irradiance at a location is to use irradiance from previous years measured at or near the location. The need sometimes arises, however, to predict irradiance at a location where measured irradiance data from previous years are not available.

As has been shown in the preceding text, irradiance is influenced by the atmosphere of the earth, which in turn is immensely complex to model mathematically beyond general trends. Therefore the prediction of irradiance for a specific location on the earth's surface through mathematical modelling of the atmosphere is not feasible.

Fortunately the need for exact prediction of irradiance seldom exists. A typical problem would rather be to predict the variations in irradiation over a period of a year. Typically other data would be available for the location, or a location nearby, like the total hours of sunshine, percentage cloud cover, humidity, atmospheric turbulence and even UV-B exposure. From these data sets global irradiation data sets can be constructed with accuracies of up to 90% [25]. Details on the methods used to construct this irradiation data are beyond the scope of this text, as measured irradiance data from previous years do exist for most large cities in South Africa.

3.3 Efficiency of PV panel energy conversion

3.3.1 Introduction to photovoltaic energy conversion

PV cells are the fundamental units from which PV panels are manufactured. These cells directly convert sunlight into electricity. A material that absorbs light falling on it typically converts the energy of the incident photon into heat. However, some semi-conducting materials are able to convert a percentage of this energy into electricity – these materials are used in PV cells. On a particle level, the incoming photon transfers its energy to an electron in the absorbing material, raising the energy state of the electron within the atom, or freeing the electron, allowing it to move through the material, resulting in a rise in temperature and/or an electric field.

Various materials are used to manufacture PV cells. The most widely used material is crystalline silicon, as it is relatively easy and cheap to manufacture. Thin-film cells using amorphous silicon or a wide variety of other semi-conducting materials are steadily improving in efficiency and decreasing in cost, and are predicted to compete with crystalline silicon cells in the near future, as mentioned in Chapter 2.

3.3.2 Factors influencing PV panel efficiency

3.3.2.1 PV cell manufacturing

Why do PV cells on average convert less than 15% of the energy available in sunlight into electricity? A large percentage of the energy generated in freeing the electrons in a PV cell is dissipated as heat. Additionally, a percentage of the incident solar radiation spectrum is not utilised, as the semiconductors used in the PV cells have relatively limited energy absorption bandwidths (compare Figure 3-17 with the solar radiation spectrum shown in Figure 3-2).

One way in which scientists are trying to overcome this limited spectrum problem is by manufacturing tandem cells, where materials with different spectrum sensitivities are layered on top of each other. Frequencies not absorbed by upper cells are transmitted to lower cells, thereby increasing the efficiency of the conversion process between solar and electrical energy.

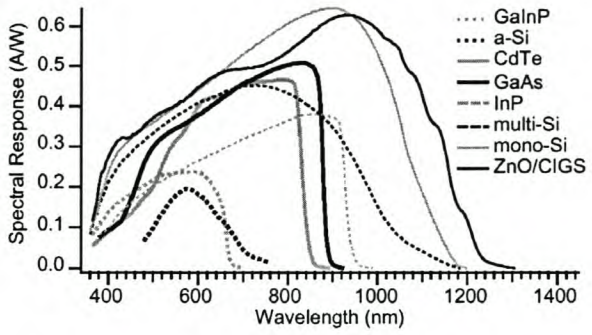

Figure 3-17: Spectral sensitivity for a selection of photovoltaic materials [27]

Potential energy is also lost by light reflection on the surface of the cell. For this reason most PV cells are treated with an anti-reflective coating. Another technique is surface texturing, where the top surface of the cell consists of small pyramids, which creates another chance for reflected light particles to be absorbed. If in addition the back panel of the PV cell is made optically reflective, light is in effect trapped in the cell, presenting the PV cell material with more exposure time to absorb the solar energy.

3.3.2.2 PV panel construction

A PV panel consists of a number of PV cells, which are usually electrically connected together in series to result in a useable output voltage. By connecting these PV cells in series, the efficiency of all the PV cells are lowered to that of the least efficient cell in the group, which is why cell efficiencies are measured during the manufacturing process, allowing cells of similar efficiencies to be grouped together on a PV panel.

A more serious negative effect of constructing PV panels out of series connected PV cells occurs when a PV panel is partly shaded, e.g. by bird droppings or tree branches. This scenario, and a solution in the form of a maximum power point tracker, is discussed in detail in Chapter 4.

Other ways to gain higher conversion efficiencies for PV panels include solar concentrators and PV panels with transparent back plates, allowing conversion of irradiance reflected off the ground.

3.3.2.3 Cell temperature and irradiance

PV cell efficiency is a function of the cell temperature as well as the irradiance on the cell. The cell temperature can easily be calculated as follows,

$$T_{cell} = T_{ambient} + \frac{(NOCT - 20)}{800} G \qquad 3\text{-}7$$

where $NOCT$ is the nominal operating cell temperature parameter for the specific PV panel, $T_{ambient}$ the ambient temperature and G the irradiance on the cell in Watts per square meter.

The temperature coefficient value of each PV panel is usually available as a percentage decrease in power per °C increase in cell temperature, allowing calculation of the effects of temperature and irradiance on the PV panel efficiency.

3.4 PV array financial cost considerations

A background on irradiance on a tilted surface on the earth, as well as on PV panel efficiency, has been presented in the previous sections. One last subject needs to be discussed in preparation for a discussion on the development of SunSim: the way in which PV array financial costs are calculated.

3.4.1 Introduction

The need often exists to compare electricity-generation technologies, e.g. PV and wind, with each other to find the most economical solution for a specific site. An accurate financial cost calculation method is required for this comparison, taking a wide range of factors into account. When comparing diesel generation with PV, for example, initial capital costs will definitely favour diesel. Only by also taking fuel, maintenance, and reliability costs into account will a more balanced perspective be obtained. Life cycle cost analysis calculates the cost per unit of electricity over the lifetime of the technology, and is ideal for the comparisons mentioned above.

This section will explain life cycle cost analysis, and show how the cost per unit of PV-generated electricity can be calculated.

3.4.2 Calculation of PV array life cycle cost

3.4.2.1 The cost of money over time

Some of the costs over a life cycle will be incurred at the beginning of the life cycle, for example capital costs to buy equipment, while other costs will happen yearly, like fuel costs. Costs can also occur only once at a date some time into the life cycle, for example equipment replacement costs. To accurately compare these three types of costs, all future costs are converted into the equivalent costs at the beginning of the cycle, taking the cost of money over time into account.

This beginning-of-cycle cost, called the present worth value, can be calculated using equation 3-8 for annual recurring costs, and equation 3-9 for a once-off future cost.

$$PW_{recurring} = Cost_{recurring} \times P_a \qquad 3\text{-}8$$

$$PW_{once-off} = Cost_{future} \times \left(\frac{1+i}{1+d}\right)^N \qquad 3\text{-}9$$

where i represents inflation, a measure of the decline in buying power of money over time, and d the discount rate, which is the amount of interest that would be earned if money were invested over time. N represents the amount of years over which the annual cost occurs, or the amount of years from the present before the cost will be incurred.

The annualisation factor P_a can be calculated as

$$P_a = (\frac{1+i}{1+d})(\left|\frac{1+i}{1+d}\right|^N - 1)(\frac{1+i}{1+d} - 1)^{-1} \quad \text{3-10}$$

Once the present worth of all the costs during the life cycle are known, the life cycle cost LCC can be found by summating all these costs.

The end value of interest is the cost per unit of electricity, which can be found using the following equation,

$$Cost_{electricity\_unit} = \frac{ALCC}{Energy_{yearly}} = \frac{LCC}{P_a \times Energy_{yearly}} \quad \text{3-11}$$

where $ALCC$ represents the annualised life cycle cost, found by dividing LCC by the annualisation factor, and $Energy_{yearly}$ the yearly average electrical energy supplied over the life cycle period.

3.4.2.2 Assumptions

The following assumptions are made during PV array life cycle costs calculations:

- The generated electricity will be fed into the national grid, i.e. 220 V, 50 Hz AC power.
- No energy storage costs will be taken into account.
- A MPPT will be connected to every PV panel.
- A period of 20 years will be taken as the life cycle. This is the average period for which PV panel output power is guaranteed (Shell and BP guarantees their PV panels for between 20 and 25 years).
- Excess inflation is taken as 5%, while a discount rate of 8% is used, as recommended by the World Bank for South African economic conditions [44].
- The cost is calculated for a PV array of 10 kW_{peak}, to ensure a reasonable economy-of-scale benefit.

3.4.2.3 PV array cost parameters

The following parameters are considered when calculating the life cycle cost:

- *PV panel costs.* Typical prices for mono-crystalline PV panels in South Africa is taken as R38 500 per kW_{peak}, based on two quotes, one from Liselo Solar (R5800 for a 150W PV panel), and one from Energy Efficient Options (R2800 for a Shell SP70 70 Watt panel). Prices on the Internet average around R26 700 per kW_{peak} (assuming a relatively constant exchange rate of R6.50 to USD1), while new CIGS PV panel-manufacturing technology promises prices of around R7000 per kW_{peak} in the near future [11].
- *Structural support and wiring costs.* These costs take into account the different types of structures necessary for the different solar tracking options. For no tracking, i.e. mounting a fixed panel, Energy Efficient Options quoted R4000 per kW_{peak}. Prices for azimuth angle one-axis trackers on the internet varied between R7300 and R8800 per kW_{peak}, while a two-axis full solar tracker is priced at around R12300 per kW_{peak}.
- *Operation and maintenance costs.* These costs are low for PV arrays, as normal maintenance involve mainly keeping the panels clean, except in the case of solar tracking structural mounts, which might need lubrication and periodical parts replacement. Yearly costs are assumed to be between R200 and R500 per kW_{peak}.
- *MPPT costs.* Prices of MPPTs on the Internet vary from R2600 to R5000 per kW_{peak}. The MPPTs are assumed to have a 10-year life cycle, after which they will be replaced.
- *DC to AC inverter costs.* Liselo Solar quotes around R2900 per kW_{peak} for an inverter. The inverters are assumed to have a 10-year life cycle, after which they will be replaced.
- *Installation costs.* This includes all labour, transport etc. necessary to install the PV array. Installation costs are usually taken as between 10 and 20% of the capital cost.
- *Government subsidies.* Any contributions to installing a PV array by the government or non-governmental organizations are taken into account by using this parameter. For the calculations presented in this text, no such contributions were included.

3.4.2.4 PV energy cost calculations: an example

An example will now be given showing how the cost of PV energy per kWh is calculated. The PV system used for the example is located at Upington, and makes use of PV panels that fully tracks the sun through the day and year.

The PV system costs are as follows:

PV panels	R38500 per kW_{peak}
Full solar tracking structure	R12300 per kW_{peak}
Operation and maintenance	R500 per kW_{peak} per year
Installation costs:	R7000 per kW_{peak}
MPPT cost:	R2600 per kW_{peak} (replaced every 10 years)
Inverter cost:	R2900 kW_{peak} (replaced every 10 years)

Once-off capital costs at present worth include the PV panels, tracking structure, installation costs and the initial MPPT and inverter, with a total cost of R63300. Future once-off costs (the replacement of the MPPT and inverter after 10 years) can be calculated using equation 3-9 as an additional R4150.

The annualisation factor P_a can be calculated using equation 3-10, with excess inflation of 5% and a discount rate of 8%, as 15.0759. The recurring costs (operation and maintenance) at present worth can now be calculated using equation 3-8, as R7538.

The life cycle cost over 20 years can now be found by summing all these present worth values, for a total present worth of R74988.

The amount of electrical energy available at Upington per year for a fully tracking system is 344.17 kWh per m^2 of PV panel per year, according to SunSim. As a 75 W PV panel has an area exposed to the sun of 0.6324 m^2, an PV array of one kW_{peak} will expose an area of 8.432 m^2 to solar radiation. A one kW_{peak} fully tracking PV array will therefore produce 2902 kWh of energy at Upington per year.

Finally the cost per unit energy can be calculated, using equation 3-11, as R1.71 per kWh.

3.5 Development of the SunSim computer model

3.5.1 Background to SunSim's development

3.5.1.1 Introduction

No freely available software model existed by 2003 that could predict the optimal positioning of, and energy from PV panels used in Southern Africa. Knowledge during the design phase of a PV array installation, on how much energy the array will deliver and the optimal positioning of the panels, is important. With this knowledge, for example, the amount of PV panels required to satisfy a site's energy needs can be more accurately calculated, offering financial benefits.

3.5.1.2 Specifications of SunSim

The SunSim computer model simulates the conversion from solar energy into electrical energy by a PV panel. The model takes the influence of the atmosphere, the location and positioning of the PV panels, and PV panel characteristics into account. SunSim offers the following functionality:

- Predicts a PV panel's energy output and generation costs through the year, given a nearby site's historic atmosphere data, info on the PV panel's position relative to the sun and the PV panel characteristics like efficiency, temperature sensitivity and cost.
- Calculates the PV panel's optimal position relative to the sun for highest total energy output through the year, or for highest minimum daily energy through the year.
- Displays graphically how different factors like the atmosphere and PV panel positioning and characteristics can influence the generation of PV electricity.

3.5.1.3 Assumptions

The following assumptions were made while developing SunSim:

- Albedo radiation is not taken into account in SunSim calculations, as it is assumed that the PV panels are not bifacial (i.e. only the front of the panel is sensitive to solar irradiance), and the contribution from the albedo component is therefore minimal.
- Accurate measured irradiance data are available at or near all locations within South Africa, making additional functionality within SunSim to predict irradiance from other data sets (e.g. sun hours or cloud cover) unnecessary.

- The PV panel modelled in SunSim operates at its maximum power point (MPP) at all times, and is not shaded or defective in any manner.
- Array mismatch losses, caused by mismatches in PV panel operating voltages when connected together in a PV array, are not taken into account in SunSim.
- Energy storage losses during the charge/discharge cycle of the energy storage device are also not taken into account.
- All data presented in SunSim are in Local Apparent Solar Time, which differs slightly from Standard Time, as explained in section 3.2.2.2.
- During leap years, data from the 29th of February is ignored, i.e. SunSim always works with a 365-day year.

3.5.2 SAWB atmospheric data

3.5.2.1 Importing and verifying the data

Global and diffuse irradiance, and ambient temperature data for as many locations as possible within Southern Africa was requested from the South African Weather Bureau (SAWB). Two types of data sets were made available and were processed separately:

1) Data averaged over a number of years, in the format of hourly values for each month of the year. This data is used in SunSim for predicting future energy from, and optimal positioning of the PV panel.

   SunSim uses 10-minute data for 365 days of the year for its calculations. The averaged data from SAWB therefore had to be interpolated, first by creating 10-minute data from 1-hour data, and then by creating daily data from monthly data. During this last conversion it is assumed that each month is 365/12 days long to simplify the interpolation calculations – the error introduced by this assumption is acceptably small.

   The sets of averaged data were complete, and the SAWB confirmed its accuracy, so no additional processing was required.

2) Data in 5-minute intervals for one complete year. This data is used in SunSim to give an accurate display of the interaction between the different irradiance components and ambient temperature through the day, and their influence on the efficiency and energy production of the PV panels.

The accuracy of the data sets between 1999 and 2002 could not be confirmed by the SAWB, as the pyranometers were not calibrated during this period. The data sets also included days during which no measurements were done, or where the measurements were clearly incorrect. The data on these days were replaced with data from adjacent days, as indicated in Table 3-1.

To ensure the accuracy of the data, these now complete data sets were normalised against 'expected average maxima per day' benchmark data that has been verified as correct by the SAWB. Data that deviated dramatically from the benchmark data, e.g. Upington 1999 to 2001, was not included in SunSim.

Data set	Days of the year with non-existent or error data	Day used as replacement
Cape Town 2001	17 42 124 149-150 214 305 364	16 41 123 148 213 304 363
De Aar 2002	43 362-365	42 360
Durban 2002	44 57-65 184	45 355 183
Port Elizabeth 2002	84 216 225 310-311	83 215 224 309
Springbok 2002	45 281-282 365	46 284 363

Table 3-1: Days where non-existent or error data was replaced with data from adjacent days

3.5.2.2 SAWB irradiation and temperature data displayed

The sets of averaged data available within SunSim will now be displayed to give the reader an overview of the irradiation available within Southern Africa. A map with the locations where the data is available is shown in Figure 3-18. The irradiance data presented in Figure 3-19 to Figure 3-28 represent irradiance on a horizontal PV panel (i.e. a slope angle of 0°) located at the given location.

Figure 3-18: Locations for which global, diffuse and temperature data are available within SunSim. This data is available either averaged over a number of years, or measured over a one-year period, or both.

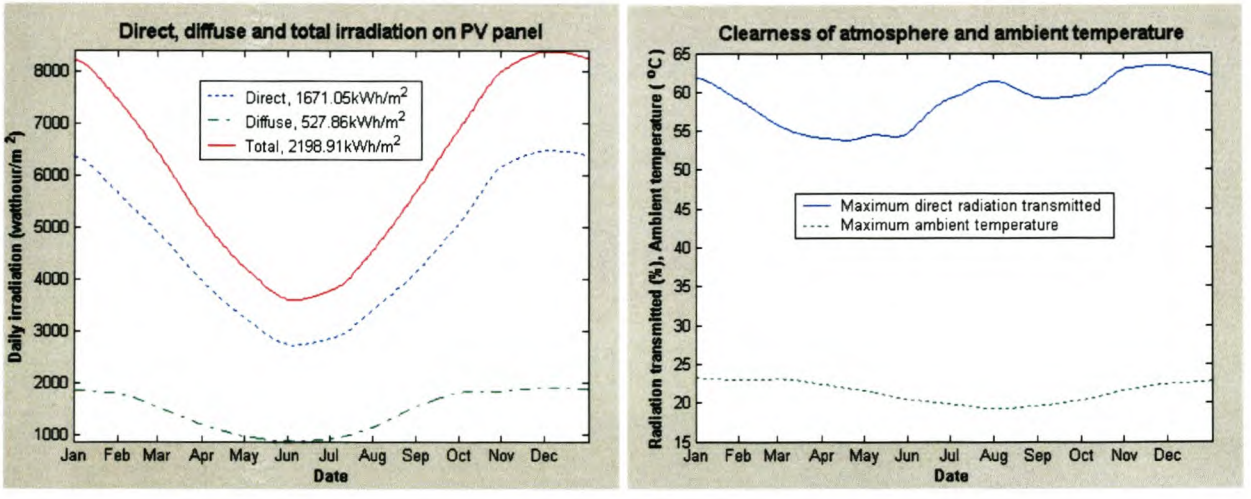

Figure 3-19: Alexander bay 1957-1984

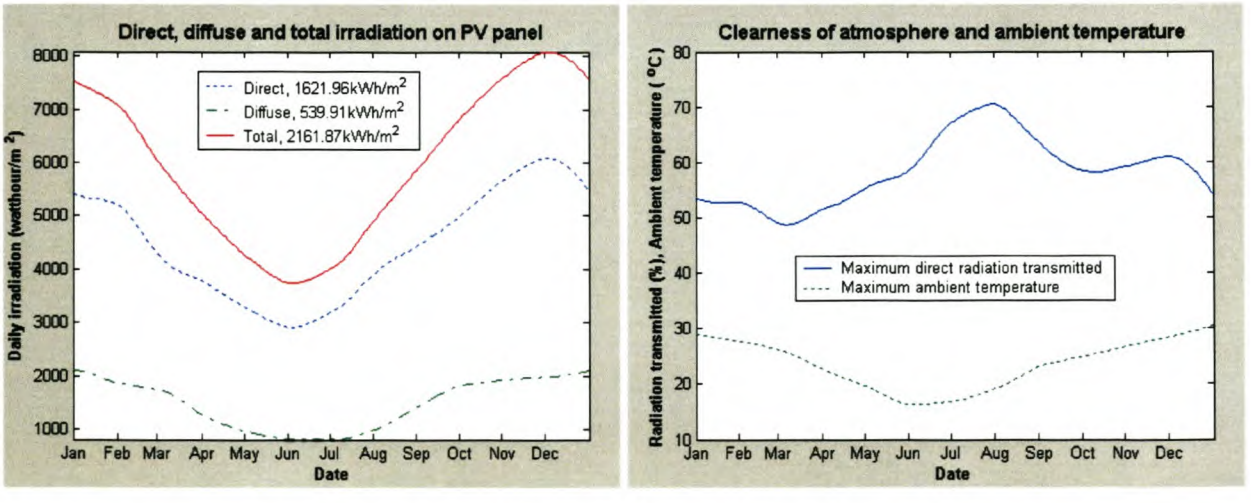

Figure 3-20: Bloemfontein 1957-1987

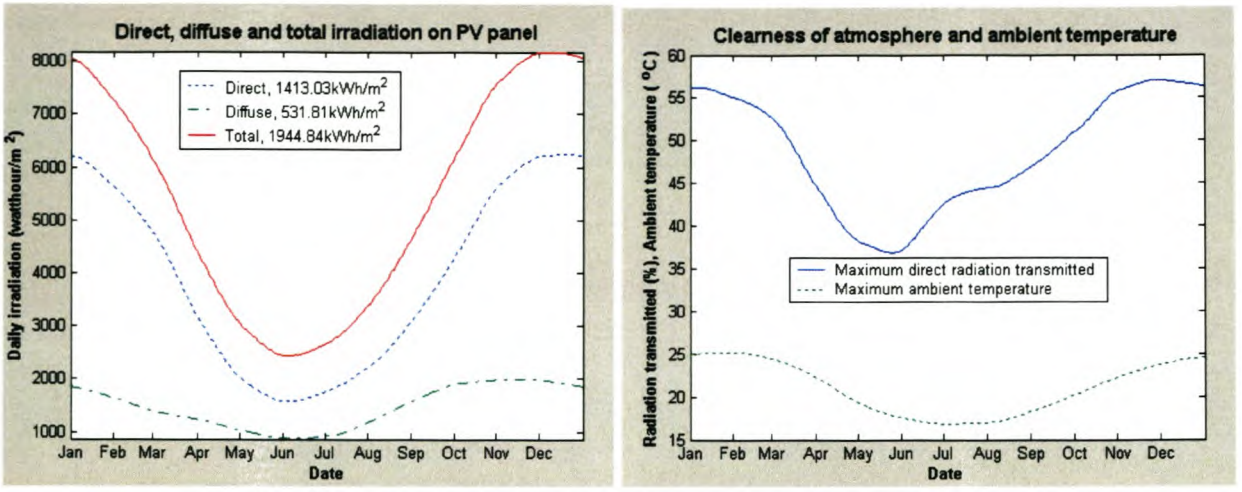

Figure 3-21: Cape Town 1957-1986

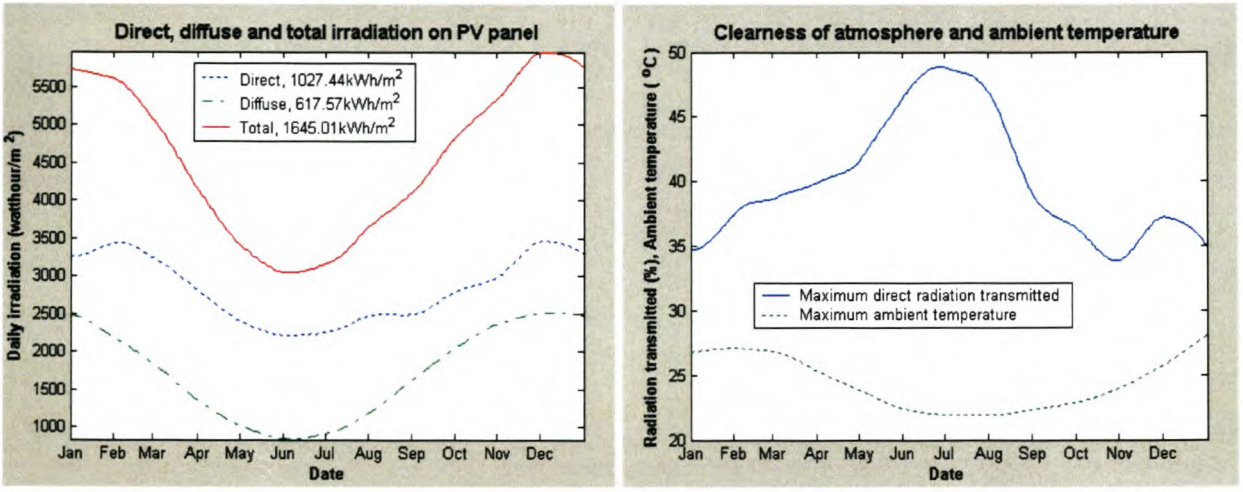

Figure 3-22: Durban 1957-1987

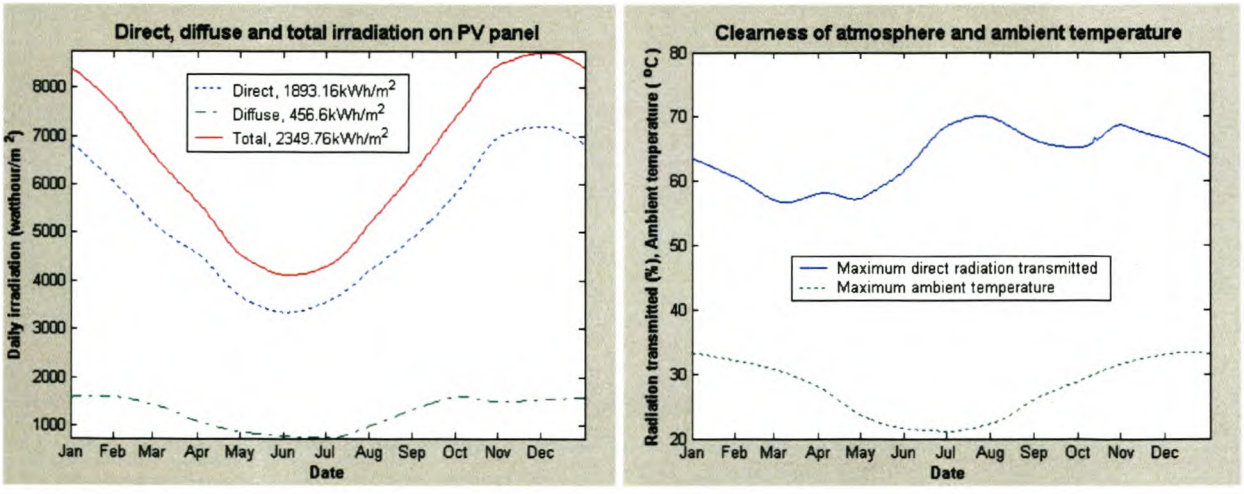

Figure 3-23: Keepmanshoop 1957-1985

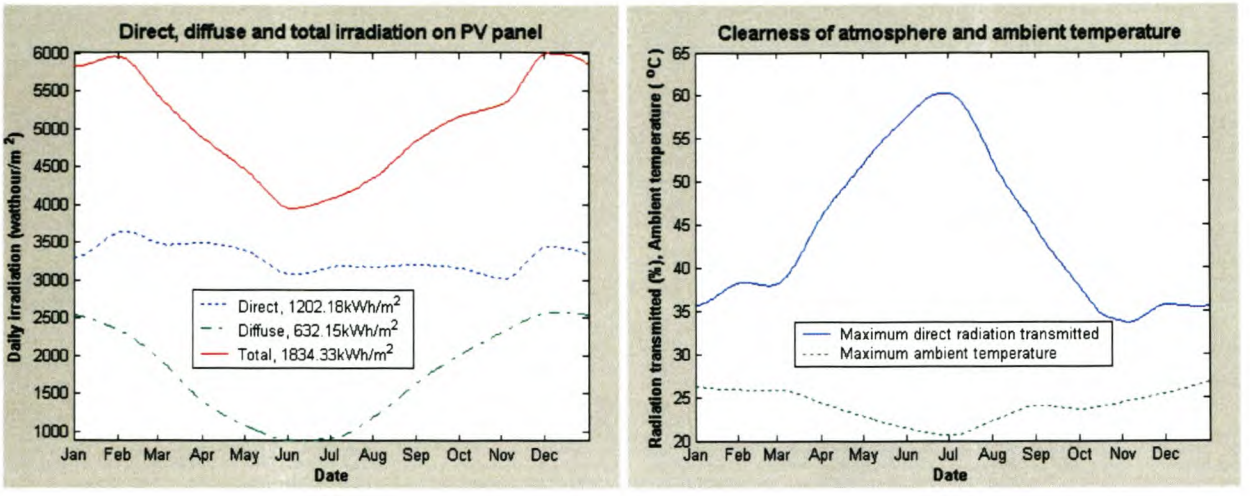

Figure 3-24: Nelspruit 1973-1983 for irradiation data, 1994-2003 for temperature data

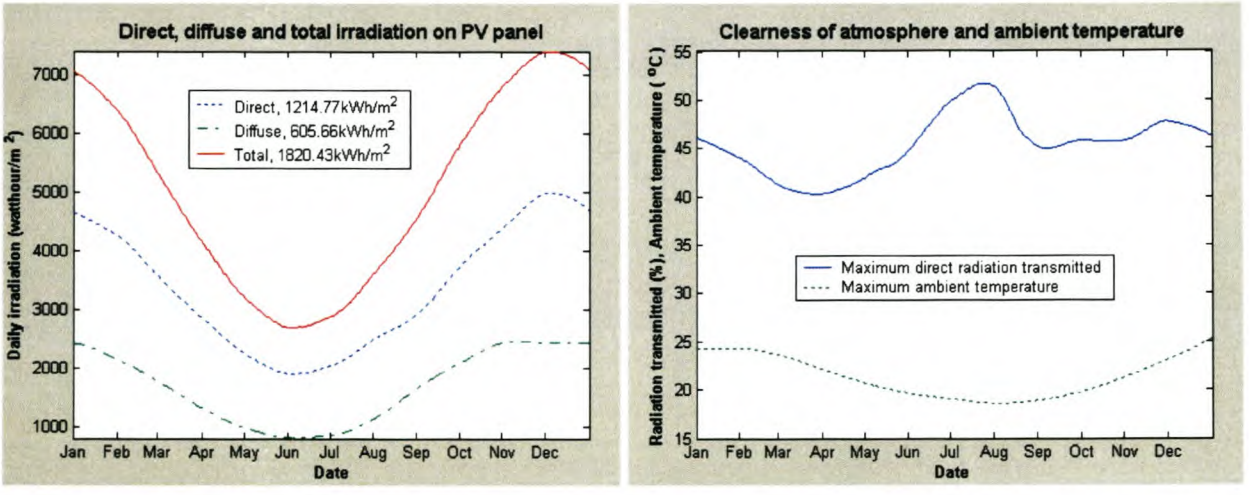

Figure 3-25: Port Elizabeth 1957-1987

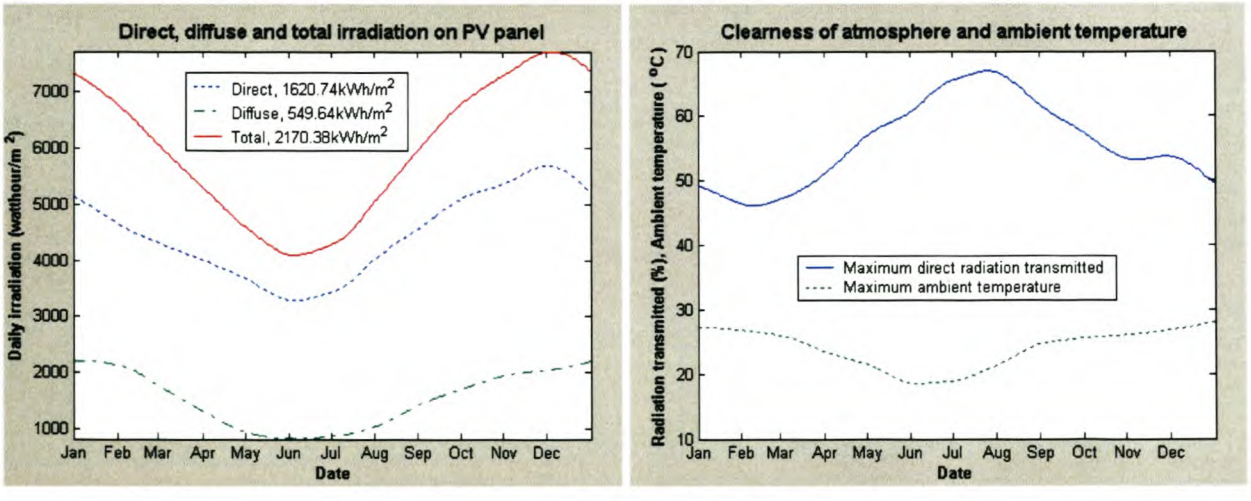

Figure 3-26: Pretoria 1957-1987

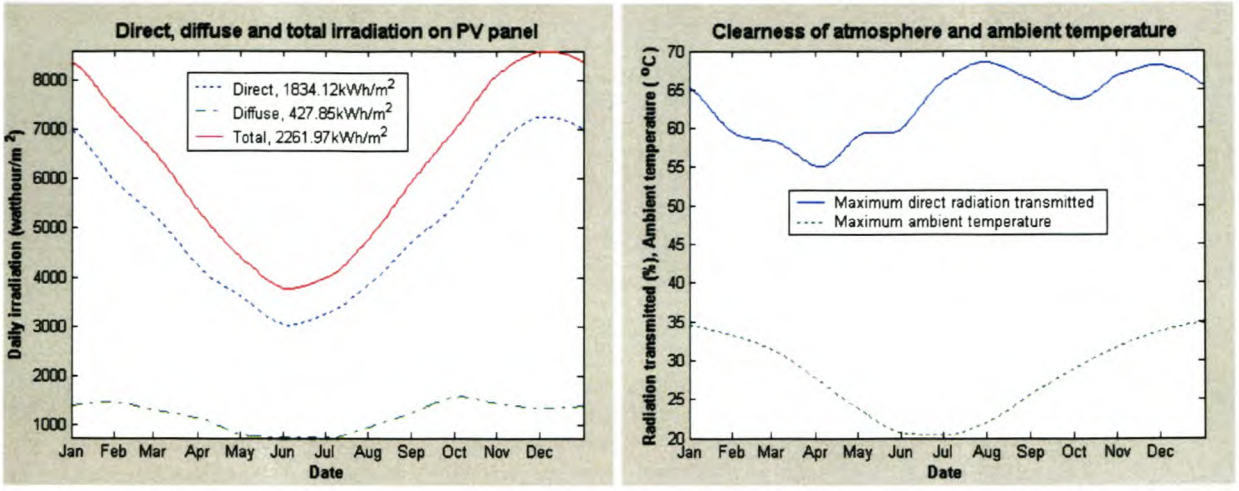

Figure 3-27: Upington 1966-1987

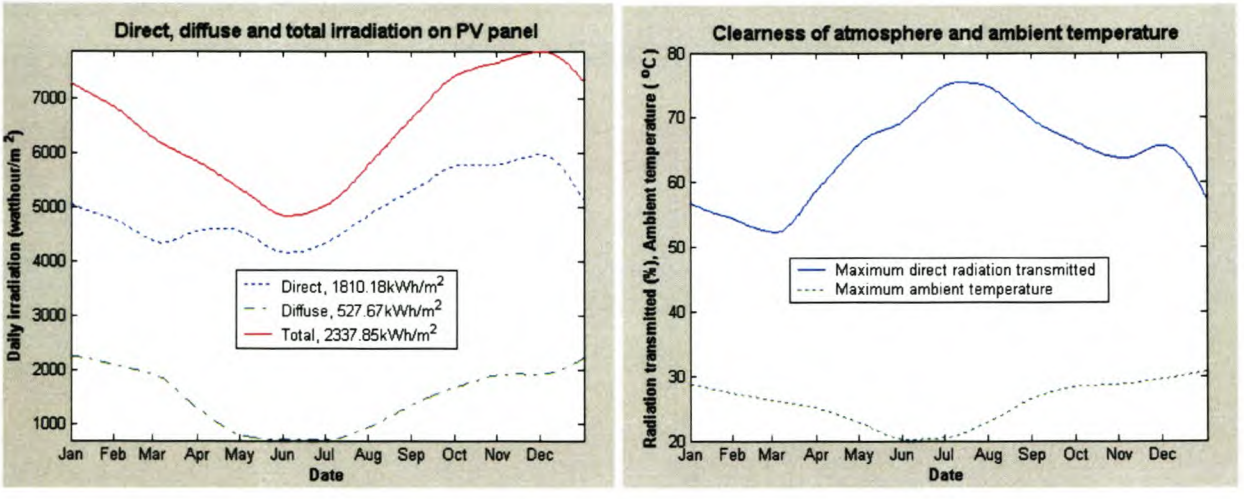

Figure 3-28: Windhoek 1957-1983

3.5.3 Structure of program

3.5.3.1 Design philosophy

SunSim was designed to be as easy to use and understand as possible. For this reason all of the parameters often accessed during different simulations were placed within one window, in which the results are also displayed. This placing makes it easy for the user to change the parameters without having to access submenus, open new windows etc. Parameters that would seldom change for the duration of the simulation, and that needs to be grouped together, i.e. PV panel characteristics and atmospheric data, were placed in files that could be edited outside SunSim, and easily loaded.

Placing most of the parameters, as well as the results within one window has the risk of confusing the user. For this reason popup menus and text boxes that are not relevant, e.g. the date

if a period of one year is selected, or the azimuth angle, if azimuth angle solar tracking is enabled, are hidden until they become relevant.

A detailed help file, 'SunSim explained.pdf', is distributed with the program to ensure ease of use (see Appendix A – SunSim explained).

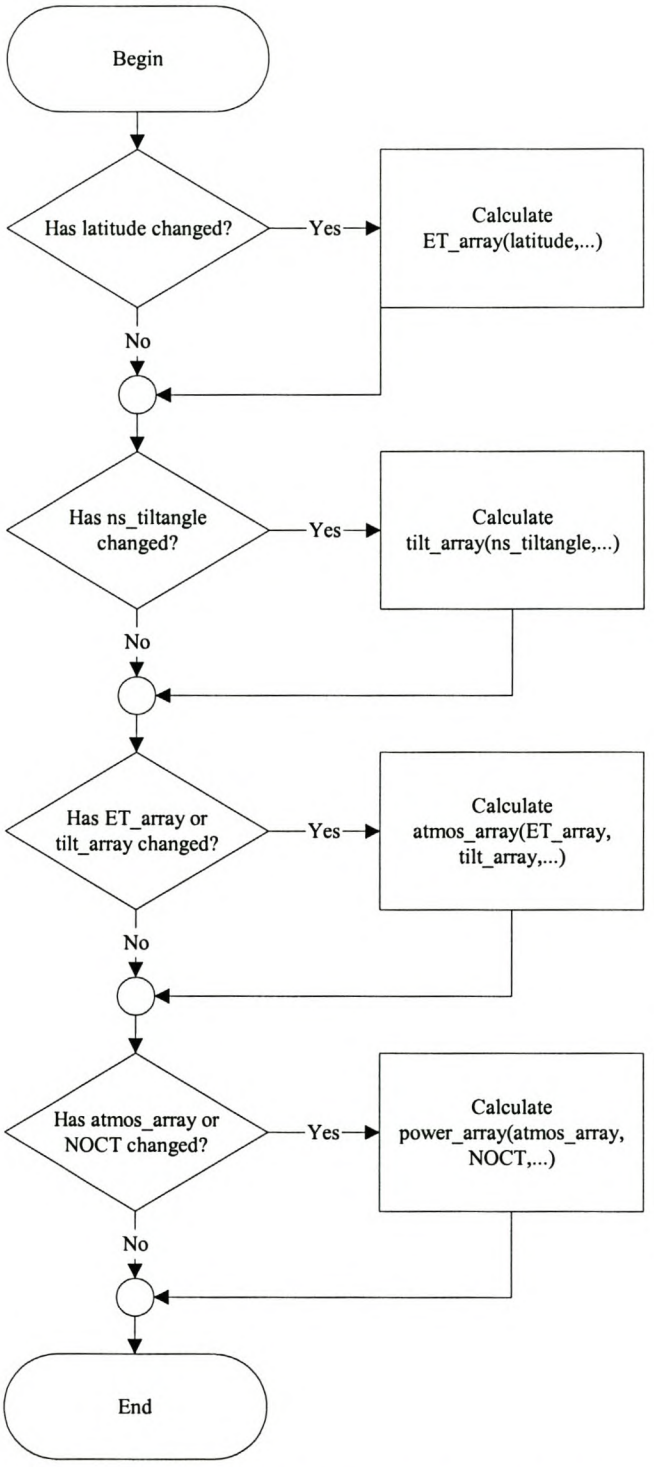

Figure 3-29: Flowchart indicating speed optimisation during the calculation of the SunSim power array

Speed of execution was another design criteria. To ensure the fastest possible calculations, the calculation process was broken down into smaller calculation functions, which would only be executed if their individual result has changed since the previous time they were executed. The calculation to find the array containing the power values from a PV panel, for example, is broken into four smaller calculation functions shown in Figure 3-29. The first time the power array needs to be calculated, all four functions will execute. If the power array needs to be found again, and for example all the positioning and atmospheric parameters are still the same, with only the normal operating conditions temperature (NOCT) PV panel parameter changed, only the power_array function will execute, instead of all four functions. This allows faster program execution.

3.5.3.2 Optimisation algorithms used

A calculation-intensive iterative process is required to find the optimal azimuth and slope angles for the highest total energy per year, and for the highest minimum daily energy per year. Two methods are used to speed up this optimisation process:

1) Firstly the user has the option to specify how much accuracy should be traded for speed of execution. The user has a choice of three CPU speeds: for computers with slow CPUs, the optimisation angle results can be specified to be within two degrees of the correct angle, medium CPUs one degree, and with fast CPUs within a half degree of the correct angle, with the associated differences in processing time required for each option.

2) Secondly, for the calculation of the optimal slope angle, an optimisation algorithm is used that first roughly finds the region within which the correct angle lies, before searching this region with higher resolution to find the answer. This method potentially saves much iteration. The algorithm will now be explained for finding the slope angle for highest total energy per year. This algorithm is similar to the one used for the highest minimum daily energy per year.

   Figure 3-30 shows a flowchart for the algorithm to be described. The slope angle at which the highest total energy per year can be found will always lie within ±23.5° (the declination angle of the sun) of the negative latitude of the location.

   The total yearly energy values within this 47° region will have only one maximum, so a hill-climbing algorithm can be used to find this maximum point. The total yearly energy at a slope angle of –latitude+18.5° is found, and compared with the energy at a slope angle of 9°

less. Within a maximum of five iterations the region is found where the maximum power occurs.

The algorithm now increments the tilt angle by the resolution specified by the user (1,2 or 3° accuracy), and calculates the power. If the energy value increases, the slope angle increments are continued until the optimal is found. If the energy value is the same, this slope angle is the optimal. If the energy value is smaller, the slope angle is decremented until the answer is found. A maximum of another 8 iterations will find the optimal.

This algorithm therefore finds an optimal slope angle within a maximum of 13 iterations, compared to a maximum of 48 iterations if the calculations were to be done sequentially.

As more than one maximum value might exist for the optimal azimuth angle, the hill climbing algorithm cannot be used. To find this value, the azimuth angle is incremented sequentially from –12° to 12° in accuracy steps defined by the user. The assumption is made that the optimal azimuth angle will lie in this region, based on experience gained with the South African atmospheric data sets.

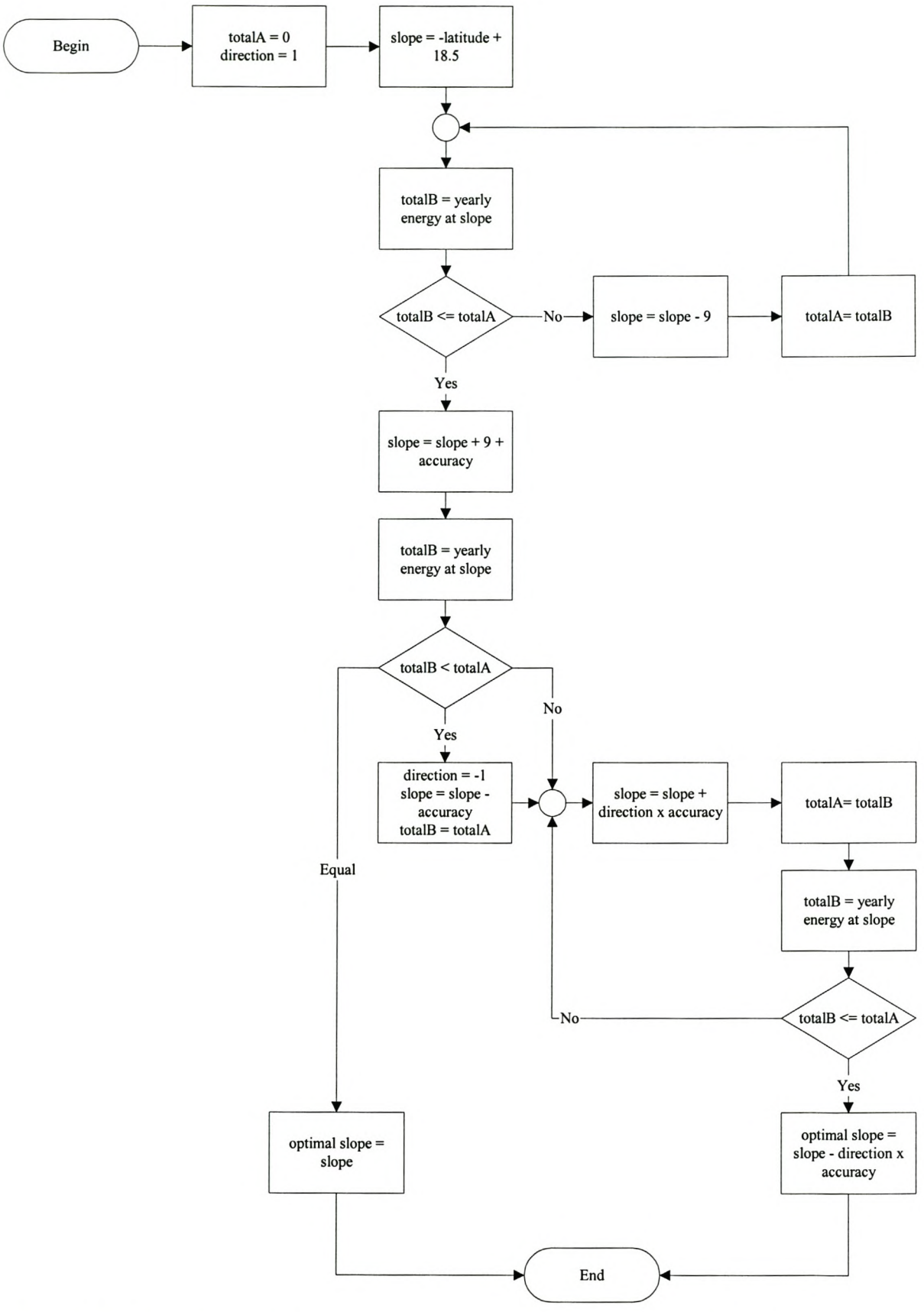

Figure 3-30: Flowchart illustrating the algorithm used to find the slope angle that would result in the highest total energy per year

3.6 *Results from SunSim simulations*

3.6.1 Accuracy of SunSim simulations

Before any results from SunSim simulations can be presented, the accuracy of these simulations must be verified. The principle behind verifying SunSim's accuracy is to give exactly the same input parameters (PV panel characteristics, positioning details and atmospheric data) to SunSim as in a physical world experiment, and then comparing the simulation results to the physical world measurements.

Two practical configurations were used to verify SunSim's accuracy. With the first, the correlation between the horizontal irradiance and irradiance on a tilted surface is verified, while with the second the predicted PV panel temperature and power output are confirmed.

3.6.1.1 Verifying horizontal vs. tilted surface irradiance calculations

In the first practical configuration three M & T irradiance sensors were used to verify the accuracy of the correlation between horizontal global and diffuse irradiance data (the format of the irradiation data as supplied by SAWB) and the calculated total irradiance on a tilted surface. The output of the M & T sensors were logged using a Tektronix oscilloscope connected to a computer running Seriallog.

To ensure accurate measurements from the three M & T sensors, they were placed horizontally next to each other, and their measurements for a cloudy day compared. The results, shown in Figure 3-31, confirm that the deviation between the measurements returned by the three M & T sensors is on average less than 5 W/m^2.

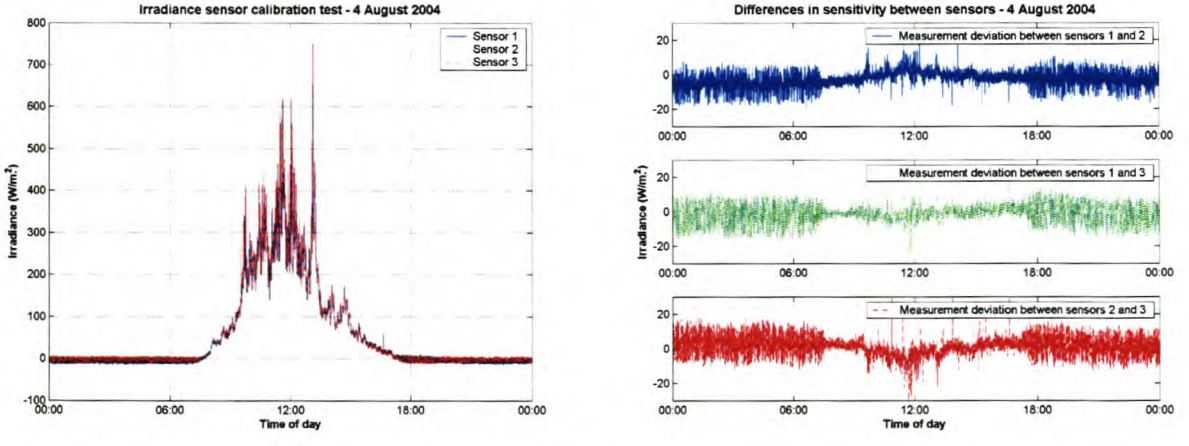

Figure 3-31: Comparison between irradiance sensitivity of the three M & S irradiance sensors used in the experiment, all three positioned horizontally next to each other.

The first M & T sensor was positioned horizontally to measure global irradiance on a horizontal surface. The second M & T sensor, also positioned horizontally, was covered with a shadow band to measure diffuse radiation. These measurements were used as global and diffuse horizontal irradiance inputs into SunSim. Measurements were done on two days with different atmospheric conditions, 22 and 26 August 2004. 22 August had high cirrus clouds in the morning, and lower, denser clouds by the afternoon, compared to 26 August's cloudless, clear conditions. Figure 3-32 shows the direct (global - diffuse) and diffuse irradiance measurements.

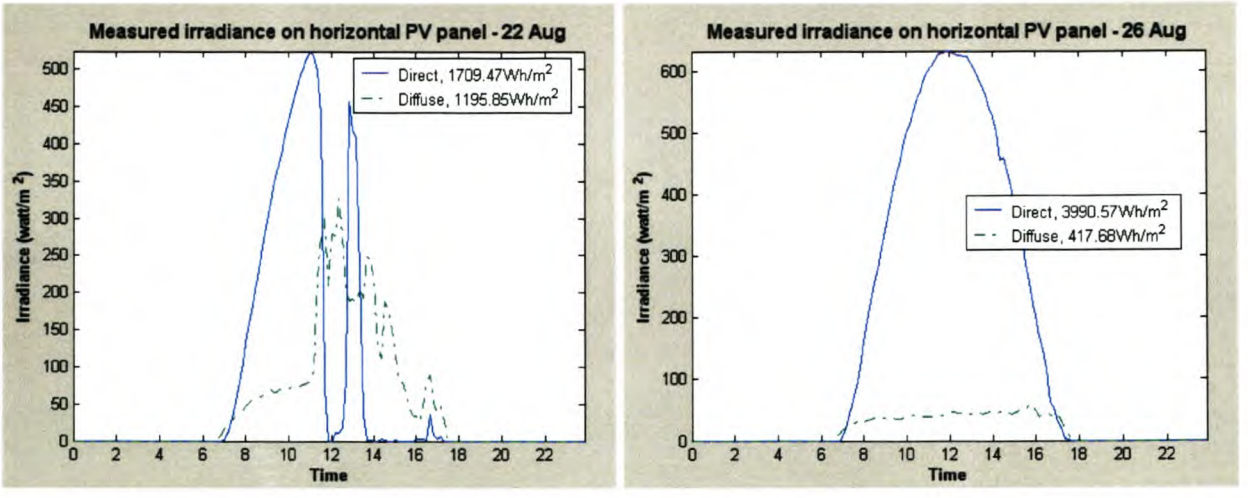

Figure 3-32: Measured direct and diffuse irradiance on a horizontal plane, 22 and 26 August 2004

The predicted total radiation (direct + diffuse) on a tilted surface was then calculated with SunSim, and compared with the measured radiation from the third M & T sensor, tilted at –90° azimuth angle, 30° slope angle on 22 August and -50° azimuth angle, 50° slope angle on 26 August. The calculated irradiance of the surface tilted as described is shown in Figure 3-33.

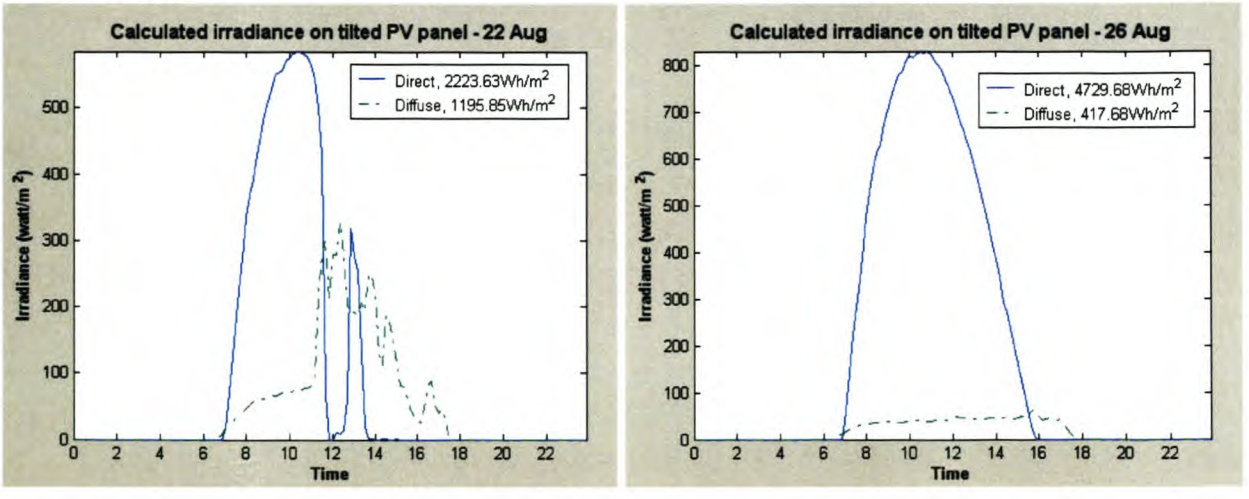

Figure 3-33: SunSim calculated direct and diffuse irradiance on a plane tilted at –90° azimuth angle, 30° slope angle on 22 August and -50° azimuth angle, 50° slope angle on 26 August.

The total irradiance on the tilted plane as calculated by SunSim can now be compared with the measured irradiance, as shown in Figure 3-34.

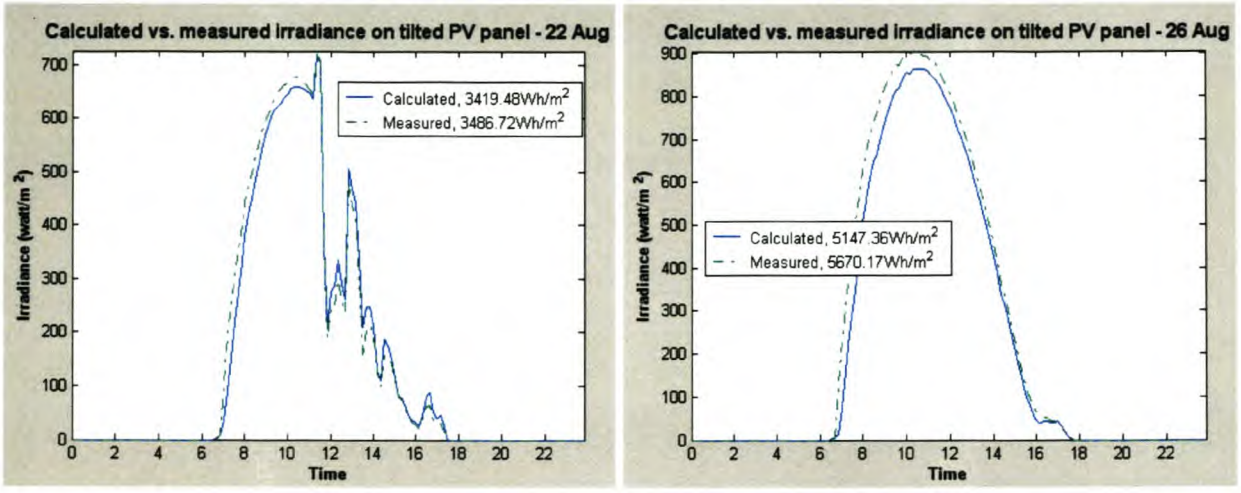

Figure 3-34: Comparison between total irradiance measured on a tilted surface, and total irradiance predicted by SunSim for the same tilted surface, given the same global and diffuse horizontal irradiance data.

From Figure 3-34 it is clear that the measured and calculated irradiance values disagree by up to 5%. During periods of low diffuse irradiation, the measured irradiance tends to be higher than the calculated irradiance, while the opposite is true during periods with high diffuse irradiance.

The mathematics used to find direct radiation on a tilted surface has been verified as correct by a variety of sources, e.g. [43]. The disagreement between the measured and calculated values is therefore caused either by incorrect diffuse irradiance measurement, or inaccurate calculation of the contribution of diffuse radiation to total irradiance, or both. Measurements done by the M & T irradiance sensors deviates from pyranometers by between –1.4% and 8.3% depending on the atmospheric conditions (see section 3.2.3.2), while diffuse irradiance on a tilted surface is very difficult to predict due to the many influencing factors like atmospheric conditions and surface albedo [43].

Given these problems regarding the measurement and calculation of diffuse radiation, the accuracy of SunSim's calculation of irradiance on a tilted surface is acceptable, and will potentially be higher if measurements done using pyranometers are used as measured data.

3.6.1.2 Verifying PV panel temperature calculations

The second practical configuration consisted of a north-facing (i.e. azimuth angle of 0°) Shell SP75 mono-crystalline PV panel with a slope angle of 50°. A maximum power point tracker (MPPT) connected this PV panel to a battery. The PV panel's voltage and current were

measured, as well as its temperature and the ambient temperature (using LM335 temperature sensors). Irradiance on a surface tilted in the same way as the PV panel, as well as global and diffuse irradiance, was measured using M & T irradiance sensors. Measurements were logged using a Tektronix oscilloscope connected to a computer running Seriallog.

The measured ambient temperature, as well as the irradiance measured by the tilted M & T sensor was used as input to SunSim. The PV panel temperature calculated by SunSim using this data is compared to the measured temperature in Figure 3-35. The differences between the calculated and measured results is on average never more than 10%, which is acceptable given the relatively uncontrolled environment in which the measurements were made, e.g. the specific location of the temperature sensor on the PV panel was not taken into account, nor the effect of air movement over the panel.

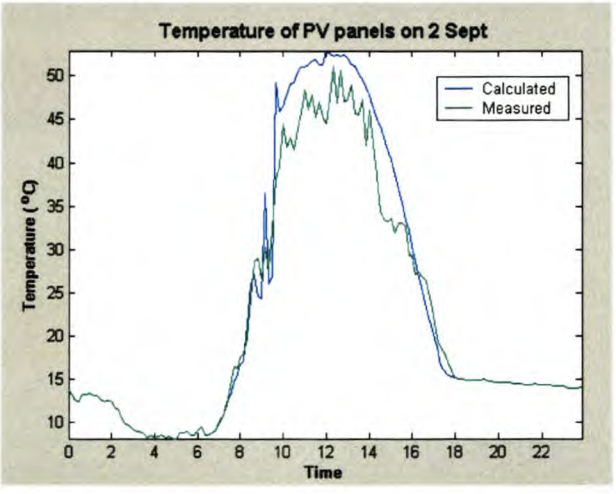

Figure 3-35: Comparison between the SunSim calculated and measured PV panel temperature.

3.6.1.3 Verifying PV power calculations as a function of irradiance and PV panel temperature

The next part of experiment two was to verify the accuracy of SunSim's PV power calculations. The program was given as inputs the measured PV panel temperature and the global irradiance measured by a M & T irradiance sensor positioned at the same slope as the PV panel (as shown in Figure 3-36). These input parameters override any inaccuracies that would have entered the experiment if SunSim had to calculate the PV panel temperature and tilted surface irradiance from ambient temperature and global and diffuse irradiance data.

Figure 3-37 compares the calculated PV panel power to the measured power, taking power losses, mostly due to the 1.3 Ω impedance of the cable connecting the PV panels on the roof to the MPPT on the ground floor, into account. From this figure it is clear that SunSim's PV power

calculations are accurate – discrepancies are small, and can mostly be attributed to measuring inaccuracies.

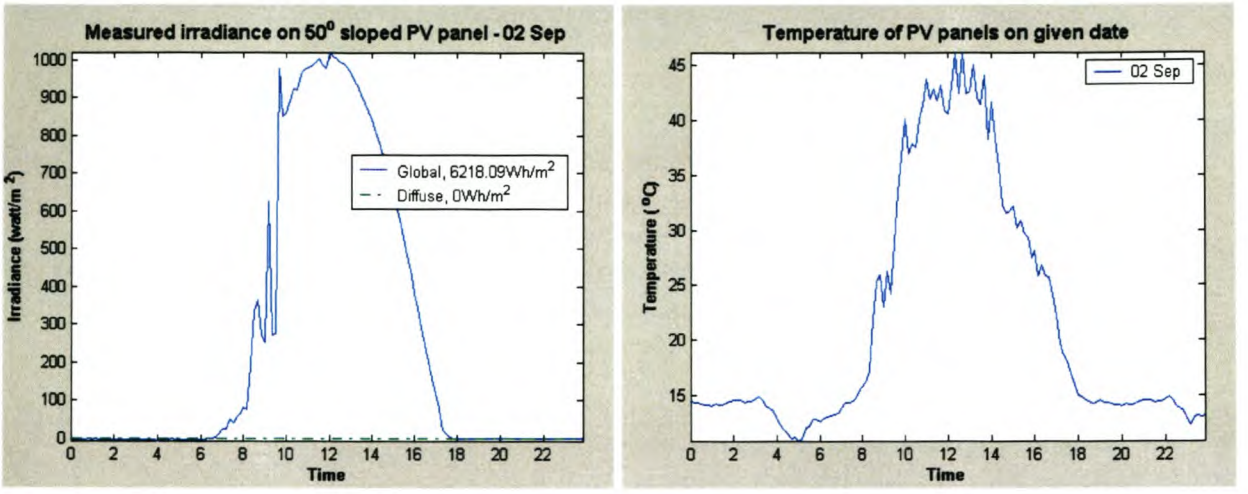

Figure 3-36: The global irradiance measured by a M & T irradiance sensor sloped at 50°, and the measured PV panel temperature. This data was used directly in calculating the PV power output, instead of calculating the power output from ambient temperature, and global and diffuse horizontal data sets.

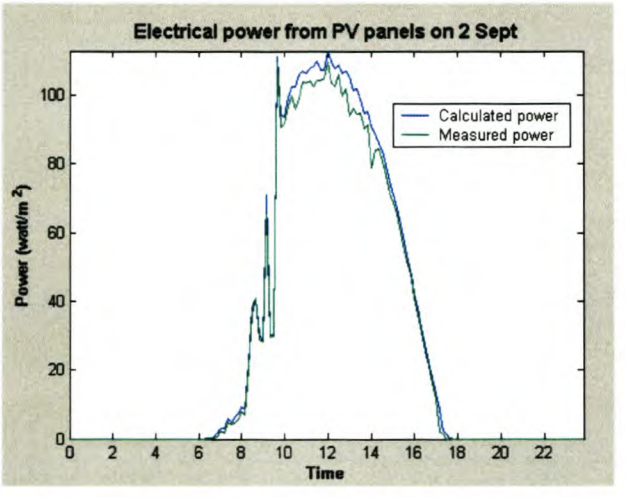

Figure 3-37: Calculated vs. measured PV panel power output

3.6.1.4 Verifying a complete SunSim power calculation vs. measurement

Now that the individual calculations within SunSim has been verified, a comparison of a complete SunSim PV power calculation and power results from measurements using experiment two's pratical setup will be presented.

As input SunSim was given the global and diffuse irradiance on a horizontal surface and the ambient temperature, as shown in Figure 3-38. This same data is given in the SAWB data sets. SunSim now calculates the PV power for a PV panel tilted in the same way as the PV panel in the practical setup. The comparison between the measured and calculated results are shown in

Figure 3-39, indicating an accuracy of 94% between the SunSim calculated and measured results.

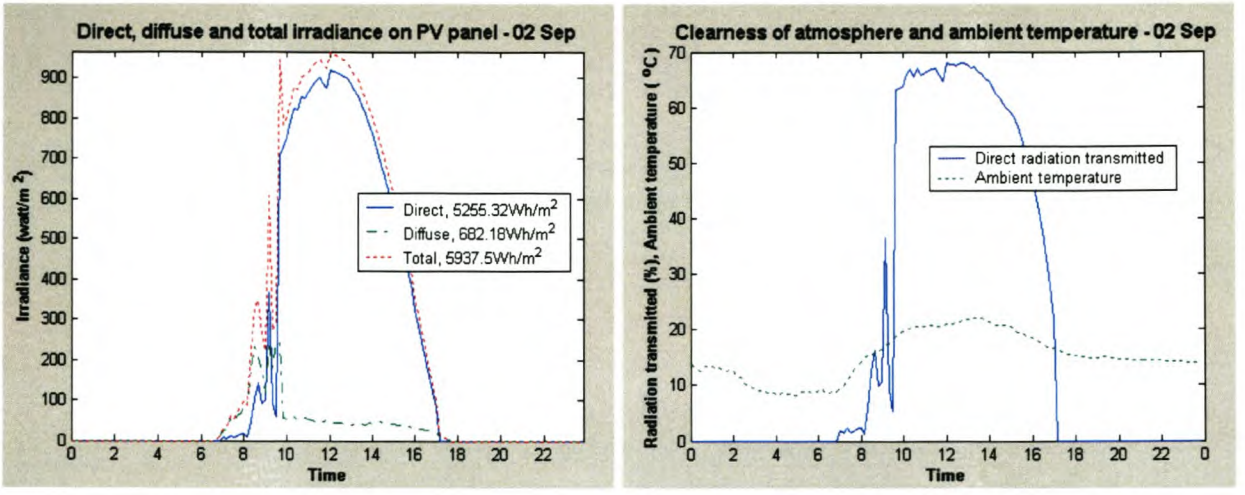

Figure 3-38: Atmospheric conditions given to SunSim as input data. A clear spring day was chosen with thick morning mist

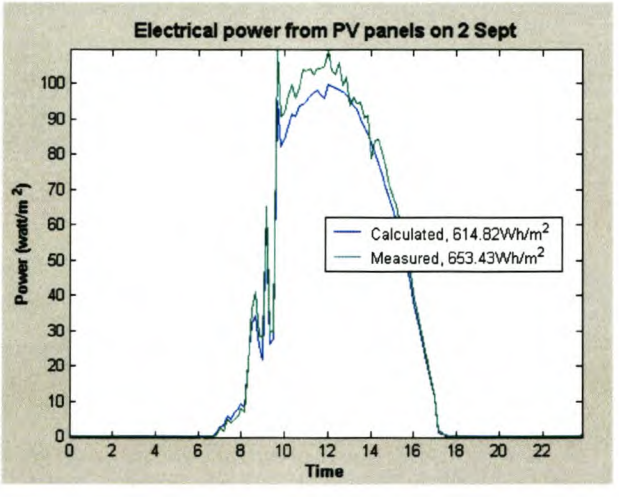

Figure 3-39: Calculated vs. measured PV panel power output

3.6.2 Simulation of the influence of the atmosphere on PV power generation

To illustrate the results obtained from SunSim simulations, three dates at different locations were chosen that represents typical atmosphere conditions:

7 April 2002, Durban – a overcast day with large amounts of moisture in the atmosphere,

5 October 2001, Cape Town - a spring day with broken cloud cover, and

2 December 2002, Springbok - a warm, clear summer day.

The clearness of the atmosphere and ambient temperature, as well as the predicted direct and diffuse radiation components on these days, falling on a PV panel that fully tracks the sun through the day, are shown in Figure 3-40 to Figure 3-42.

SunSim was now used to calculate the PV panel temperatures and efficiencies on these days, as shown in Figure 3-43 and Figure 3-44. The inverse relationship between PV panel temperature and efficiency are clearly illustrated in these figures.

Lastly SunSim was used to predict the amount of electrical power from the PV panel on the three given days. The results are shown in figure Figure 3-45.

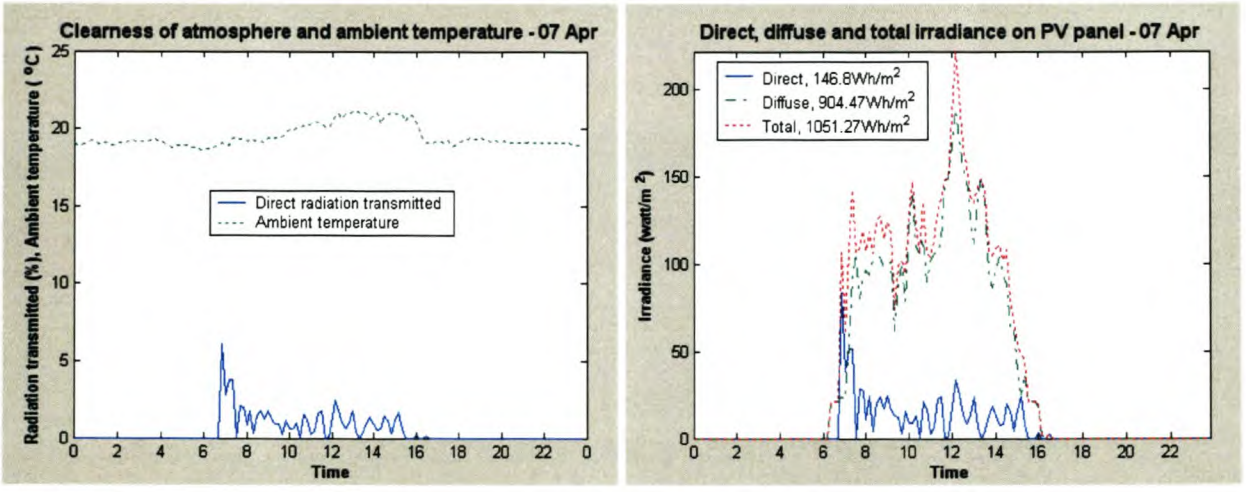

Figure 3-40: Durban 7 April 2002 - Atmospheric conditions and radiation falling on a tracking PV panel

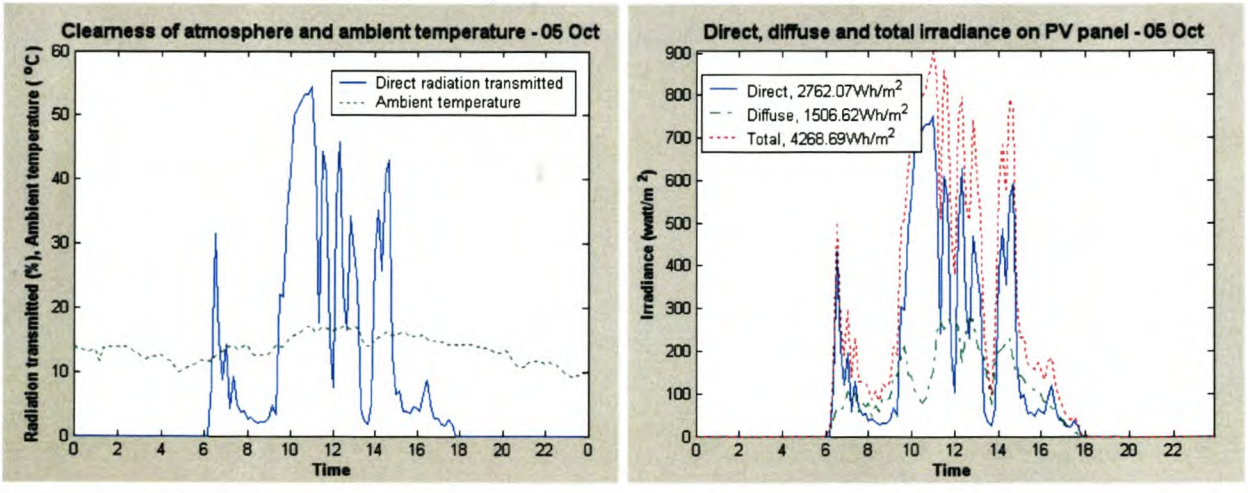

Figure 3-41: Cape Town 5 October 2001 - Atmospheric conditions and radiation falling on a tracking PV panel

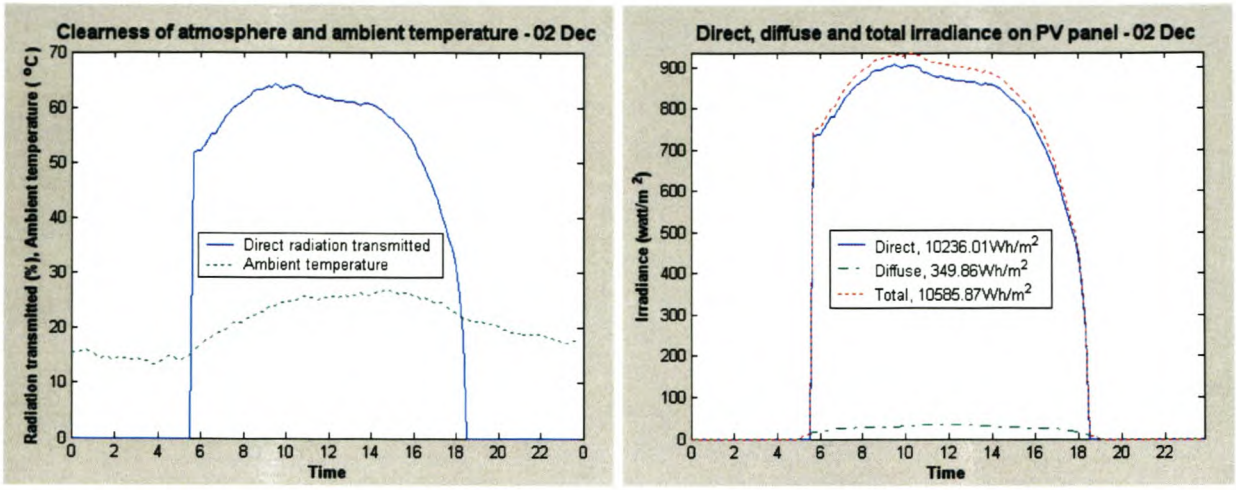

Figure 3-42: Springbok 2 December 2002 - Atmospheric conditions and radiation falling on a tracking PV panel

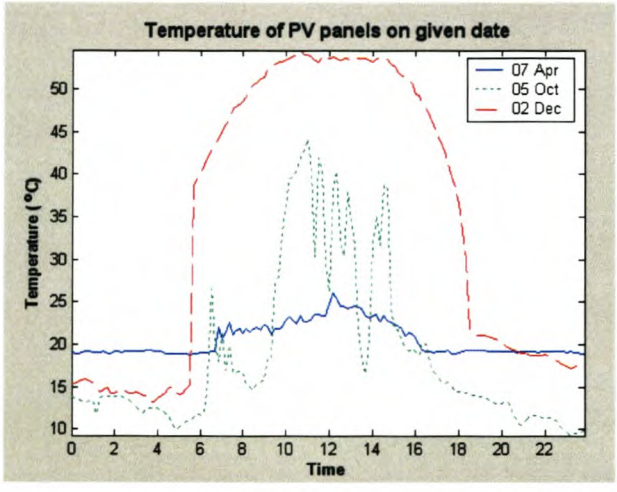

Figure 3-43: The PV panel temperatures predicted by SunSim on the three selected days

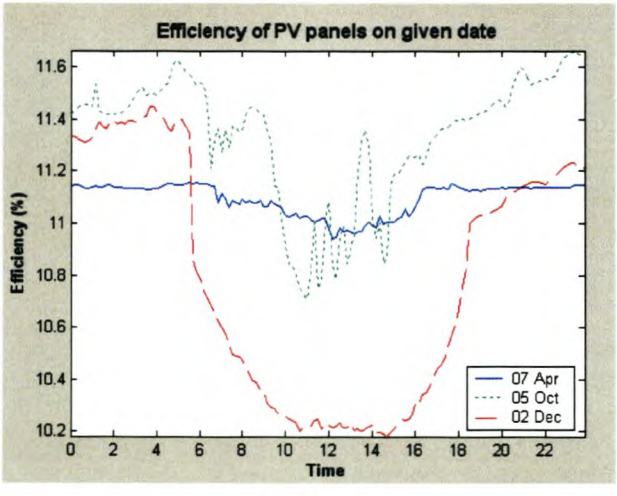

Figure 3-44: The PV panel efficiency predicted by SunSim on the three selected days

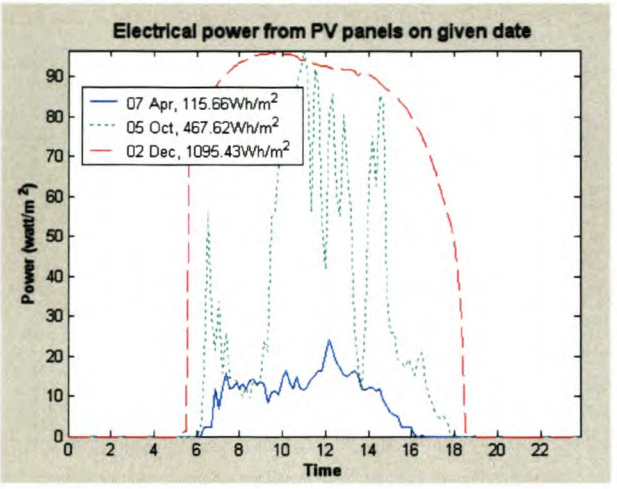

Figure 3-45: The PV panel power output predicted by SunSim on the three selected days

3.6.3 Optimal positioning of the PV panel

In order to investigate the optimal positioning of PV panels for the highest total energy generation per year, four solar tracking configurations were simulated in SunSim:

1) The PV panels are fixed facing north (i.e. the azimuth angle is 0°), and fixed at a given slope angle, for the whole year.

2) The PV panels are again fixed facing north, but the azimuth angle is adjusted twice yearly (on days 82 and 265, with +23° and –23°) to better follow the solar declination.

3) The PV panels are fixed facing north, but the slope angle tracks the solar declination angle (i.e. the solar zenith angle at noon) throughout the year.

4) The panels fully track the sun, both in the azimuth and slope angles (i.e. the PV panel azimuth and slope angles are equal to the solar azimuth and zenith angles at all times).

Two locations with very different atmospheric characteristics, Nelspruit and Upington, were used, and the optimal angles for highest total energy per year for the four tracking configurations calculated. The results are shown in Figure 3-46, with the legend giving the total yearly energy values for each of the four tracking configurations. Table 3-2 indicates the percentage of energy increase associated with each more advanced solar tracking method.

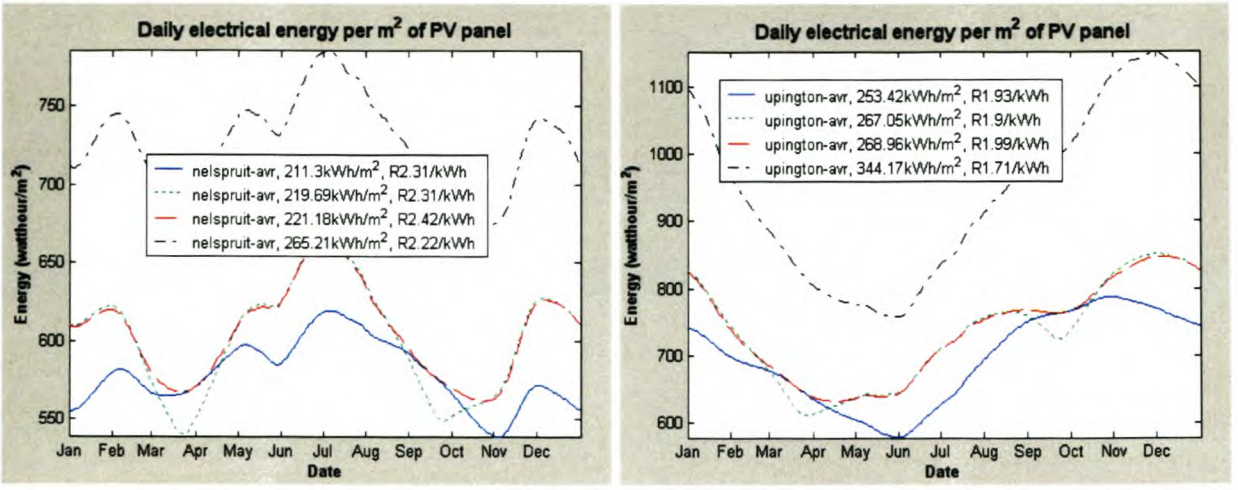

Figure 3-46: Yearly highest total energy from PV panels for the four tracking configurations described, with 0° azimuth angle, for Nelspruit and Upington

	Nelspruit			Upington		
Tracking method Azimuth, Slope	**Optimal azimuth, slope angles (°)**	**Yearly total energy with 0° azimuth (kWh/m²)**	**Energy increase (%)**	**Optimal azimuth, slope angles (°)**	**Yearly total energy with 0° azimuth (kWh/m²)**	**Energy increase (%)**
Fixed, Fixed	*-11, 29*	*211.3*	-	*-17, 26*	*253.42*	-
Fixed, Adjusted	*-7, 25±23*	*219.69*	*4*	*-8, 28±23*	*267.05*	5.4
Fixed, Tracking	*-7, declination*	*221.18*	*0.7*	*-10, declination*	*268.96*	0.7
Tracking, Tracking	*Azimuth, zenith*	*265.21*	*19.9*	*Azimuth, zenith*	*344.17*	28

Table 3-2: The percentage increase in energy associated with each more advanced solar tracking method, with 0° azimuth angle, for Nelspruit and Upington

The effect of adjusting the azimuth angle is investigated in Figure 3-47. The PV panel was again optimised for the highest total yearly energy, but the predictions now included an azimuth angle adjustment of 5° for Nelspruit, and 8° for Upington. The benefits of adjusting not only the slope angle, but also the azimuth angle, are demonstrated in Table 3-3.

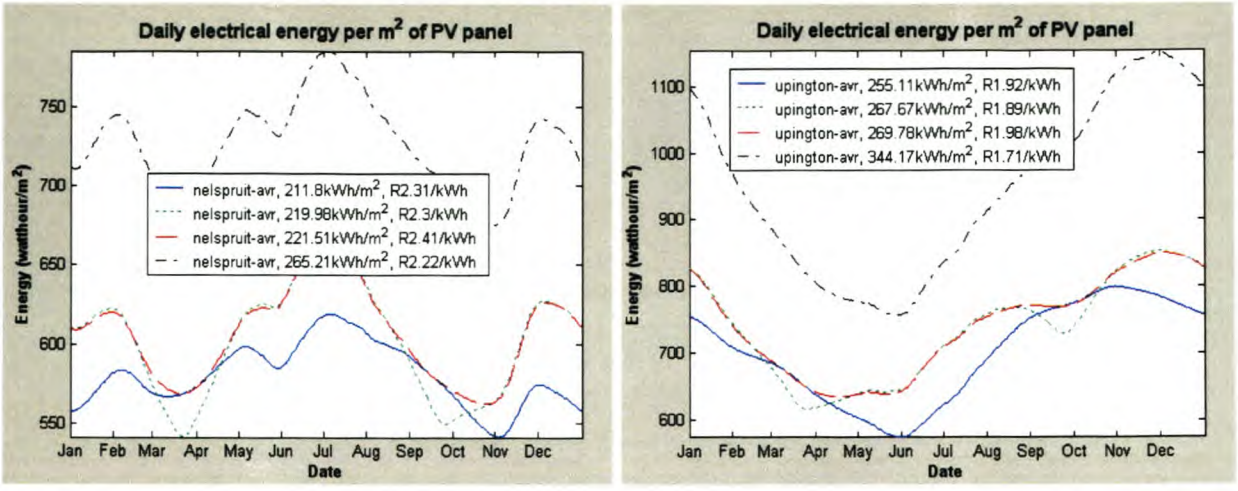

Figure 3-47: Yearly highest total energy from PV panels for the four tracking configurations described, with the azimuth angle adjusted for maximum energy, for Nelspruit and Upington

	Nelspruit			Upington		
Tracking method Azimuth, Slope	**0° azimuth Yearly total energy (kWh/m²)**	**Optimal azimuth Yearly total energy (kWh/m²)**	**Energy increase (%)**	**0° azimuth Yearly total energy (kWh/m²)**	**Optimal azimuth Yearly total energy (kWh/m²)**	**Energy increase (%)**
Fixed, Fixed	*211.3*	*211.8*	*0.2*	*253.42*	*255.11*	0.7
Fixed, Adjusted twice	*219.69*	*219.98*	*0.1*	*267.05*	*267.67*	0.2
Fixed, Tracking	*221.18*	*221.51*	*0.1*	*268.96*	*269.78*	0.3
Tracking, Tracking	*265.21*	*265.21*	*0*	*344.17*	*344.17*	0

Table 3-3: The percentage increase in energy associated with adjustment of the azimuth angle, for Nelspruit and Upington

Fixed PV panels most clearly illustrate the effects of optimising for yearly highest minimum daily energy instead of yearly highest total energy, when comparing Figure 3-48 to Figure 3-47.

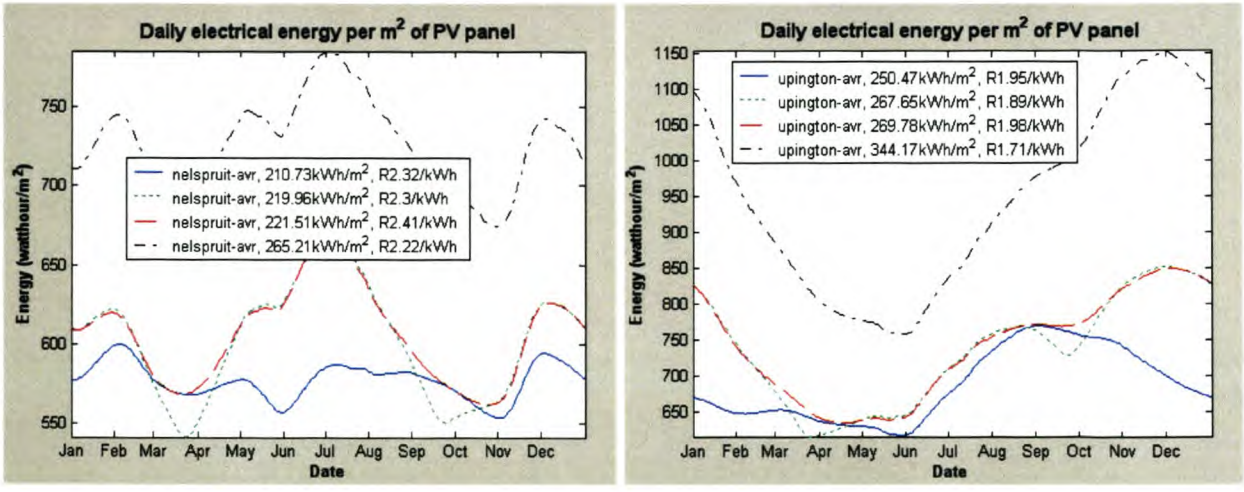

Figure 3-48: Yearly highest minimum daily energy from PV panels for the four tracking configurations described, with the azimuth angle adjusted for maximum energy, for Nelspruit and Upington

3.6.4 Effects of PV panel cooling

The rise in PV panel efficiency due to panel cooling can be simulated in SunSim. The optimal tilt angles for yearly highest energy, along with the four tracking options, were once again used, but in this simulation the PV panel temperature was kept at a constant 15°C. The resulting predictions are shown in Figure 3-49. Note that the energy costs are inaccurate in this case, as SunSim does not take the cost of cooling the panel into consideration when calculating the energy cost values.

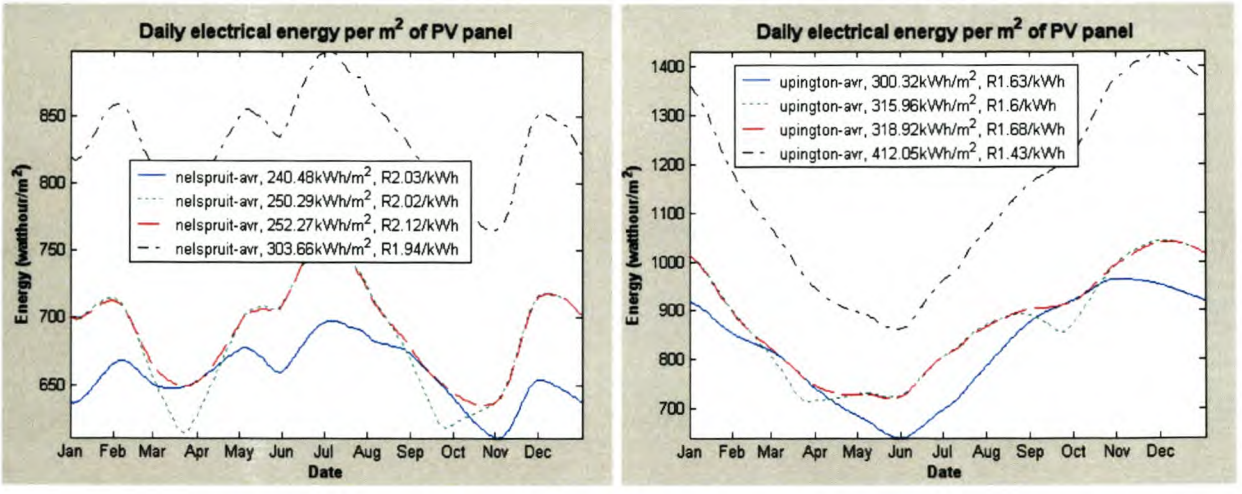

Figure 3-49: Yearly highest total energy from PV panels for the four tracking configurations described, with the azimuth angle adjusted for maximum energy and the panel temperature kept constant at 15°C, for Nelspruit and Upington

	Nelspruit			Upington		
Tracking method Azimuth, Slope	**Non-cooled PV panel Yearly total energy (kWh/m²)**	**Cooled PV panel Yearly total energy (kWh/m²)**	**Energy increase (%)**	**Non-cooled PV panel Yearly total energy (kWh/m²)**	**Cooled PV panel Yearly total energy (kWh/m²)**	**Energy increase (%)**
Fixed, Fixed	*211.8*	*240.48*	*14.1*	*255.11*	*300.32*	19.9
Fixed, Adjusted twice	*219.98*	*250.29*	*13.8*	*267.67*	*315.96*	18
Fixed, Tracking	*221.51*	*252.27*	*13.9*	*269.78*	*318.92*	18.2
Tracking, Tracking	*265.21*	*303.66*	*14.5*	*344.17*	*412.05*	19.7

Table 3-4: The percentage increase in energy associated with PV panel cooling, for Nelspruit and Upington

3.7 Conclusion

This chapter described the development and results of the SunSim computer model that takes as input atmosphere data from previous years, as well as the location, positioning and characteristics of the PV panel, and predicts as output the amount of electrical energy from, and energy generation costs associated with the PV panel.

Firstly the validity of using atmospheric data from previous years at a location near the PV panel was confirmed.

The chapter then continued to describe the development of the SunSim model, and successfully verified its accuracy through extensive measurements.

In the introduction to this chapter questions were asked on how to optimally position PV panels. The SunSim computer model answered these questions by simulating different tracking configurations.

The simulations showed that fully tracking the sun in both the azimuth and slope angles return the maximum yearly energy. Even though full solar tracking is associated with higher maintenance (more moving parts) and higher installation costs, the energy cost over a 20-year life cycle is the lowest of all the tracking options considered, due to the increase in energy production obtained from the tracking panels.

Only tracking the declination of the sun returns around 20% less yearly energy, and offers worse energy costs than the full solar tracking configuration.

An interesting result is that there is little difference in yearly electrical energy output (only 0.7%) between manually adjusting the slope angle twice yearly, and constantly tracking the declination of the sun.

Fixing both the azimuth and slope angles returns between 25-30% less yearly energy than tracking the sun in both planes.

Further simulation results shows that using the optimal azimuth angle of fixed PV panels instead of a 0° azimuth angle does not really offer much benefits, with at most 0.7% increase in yearly energy.

Cooling PV panels, however, are shown to be beneficial, as between 14% and 20% more energy per year can be obtained in this manner.

3.8 Future work

The following functionality will make SunSim more useful and/or accurate:

- The effect that a solar concentrator will have on a PV panel's power output can easily be added to the existing functionality.
- SunSim can be modified to design the optimal size for a lead-acid battery array connected to a PV array, given certain parameters like the energy storage requirements and battery parameters.
- Diffuse radiation is at present modelled very simply in SunSim, leading to some inaccuracy as was shown in section 3.6.1.1. More accurate modelling will increase SunSim's accuracy.
- Due to lack of data on the costs involved with cooling PV panels, no cooling cost parameter was included in the cost calculations. If cost data on this can be found, the resulting energy cost comparisons can lead to interesting conclusions.
- Currently, when the optimal slope and azimuth angles are calculated, first the optimal slope angle, and then the optimal azimuth angle as a function of this slope angle is calculated. The results are then returned. These results are however not totally accurate, as the slope angle is again a function of the azimuth angle, and an iterative calculation process will therefore be needed to calculate these optimal values with higher accuracy. The assumption was made in the current version of SunSim that the additional accuracy obtained by this iteration process (around 10% of the slope angle value, leading to a smaller than 1% variation in yearly total energy predictions) is not worth the additional calculation time required.

Chapter 4 - Optimal MPPT algorithms

4.1 Introduction

The previous chapter briefly mentioned the use of maximum power point tracking (MPPT) to extract the maximum amount of power from a PV panel. This chapter discusses MPPT devices in detail, explaining the development and implementation of a PV panel MPPT algorithm that periodically sweeps the voltage-power curve for the maximum power point (MPP), and then uses voltage control to keep the system at this MPP.

The chapter starts by giving the reader a background into the need for MPPT in a PV system, and analyses a variety of existing MPPT algorithms.

The best characteristics of these existing MPPT algorithms are then used as a foundation for the development of a new optimal MPPT algorithm.

Once this optimal MPPT algorithm has been developed, it is implemented using a boost converter circuit controlled by a DSP. The design process of this implementation is briefly presented, the problems experienced highlighted, and solutions to these problems explained.

Finally measurements are shown demonstrating the usefulness of MPPT, and the successful operation of the MPPT implementation.

Note that a Shell SP75 mono-crystalline PV panel was used for all measurements in this chapter (refer to Appendix B – Shell SP75 PV panel specifications).

4.2 The need for MPPT in a PV system

4.2.1 The effects of solar irradiation and panel temperature variations

The relationship between the output voltage and current of a typical PV panel for a variety of irradiance and cell temperatures is shown in Figure 4-1. Note that the short-circuit current is influenced mostly by the irradiance reaching the panel (higher irradiance, higher current), while the open-circuit voltage is influenced mostly by the temperature of the panel (higher PV cell temperature, lower voltage).

The power vs. voltage relationship for the same measurements can also be seen in Figure 4-1, from which it is clear that the maximum output power (MPP) of a PV panel is found at an operating voltage that varies with irradiance and panel temperature.

Due to this variation, the maximum power cannot be extracted from a PV panel just by connecting it directly to a battery. Some form of tracking of the MPP is required to extract the maximum possible power from the PV panel.

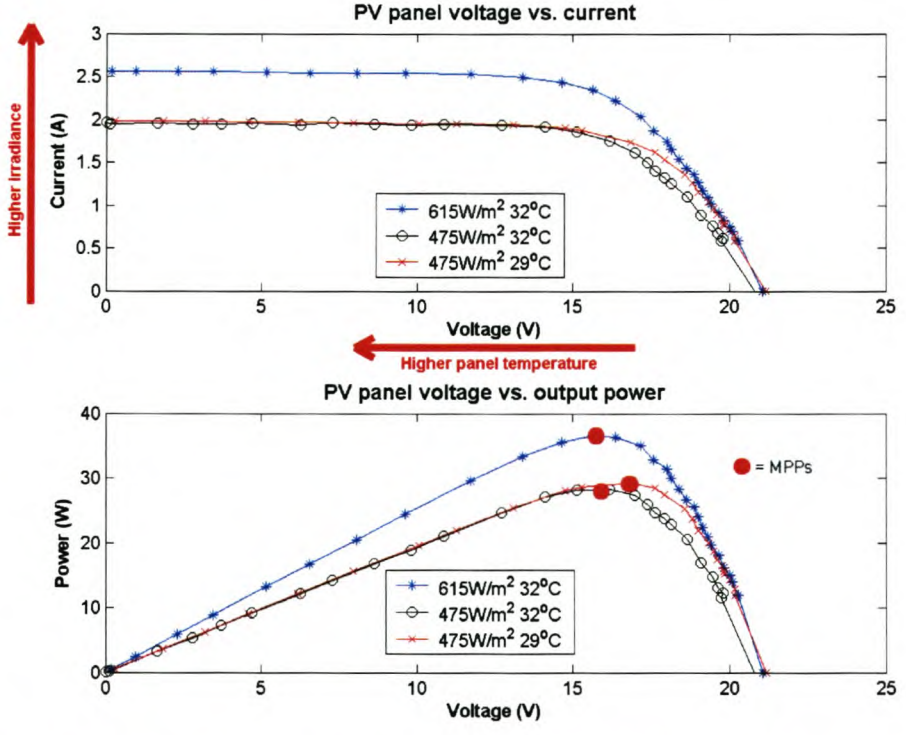

Figure 4-1:Measurements showing the effects of global irradiance and panel temperature on PV panel voltage, current, and power output

4.2.2 The effects of shading on panels

Due to the fact that a PV panel is constructed out of groups of series-connected PV cells in parallel, a reduction in current in one PV cell will force down the current output of the entire string of series-connected PV cells, changing the output characteristics of the PV panel. This reduction in current in one PV cell can be due to e.g. bird droppings, or partial shading of the panel by the branch of a tree.

Two measured power vs. voltage curves are presented in Figure 4-2: that of a panel with no shade, and that of a shaded panel with a shade pattern as shown in Figure 4-3, where an object was placed between the PV panel and the sun.

The need for a MPPT in this scenario is clearly illustrated: connected directly to a battery, the PV panel would operate at the battery voltage (around 12 V to 13.5 V), giving 60% less power than if a MPPT keeping the panel at 7 V is inserted between the PV panel and the battery.

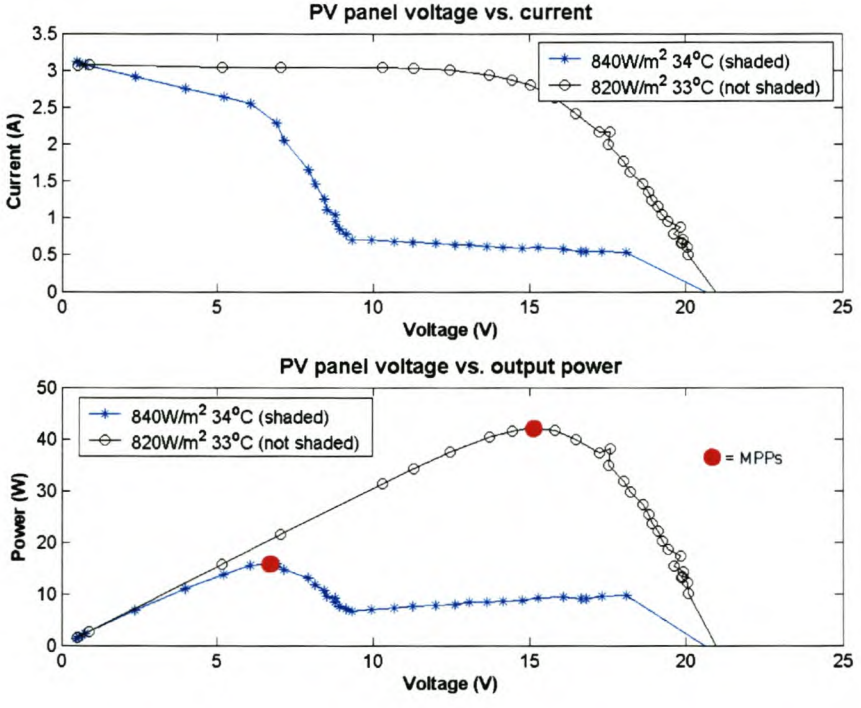

Figure 4-2: The effect of PV panel shading on power output. V-I and V-P curves are shown for two measured scenarios: PV panel shaded as shown in Figure 4-3, and PV panel not shaded.

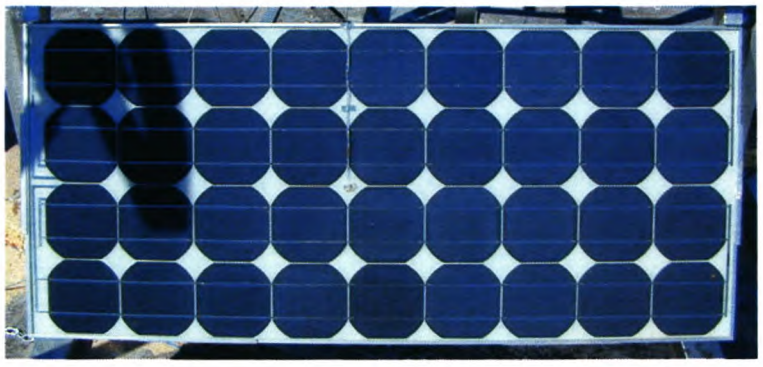

Figure 4-3: Shade pattern on PV panel, resulting in the V-I characteristics shown in Figure 4-2

4.3 Analysis of MPPT algorithms

4.3.1 The relationship between PV panel I_{SC} and I_{MPP}, and V_{OC} and V_{MPP}

A variety of algorithms exist to find the MPP of a PV panel, as will be discussed later in this section. First, however, some background will be given on the relationship between the PV panel's short-circuit current (I_{SC}) and maximum power point current (I_{MPP}), and open-circuit voltage (V_{OC}) and maximum power point voltage (V_{MPP}).

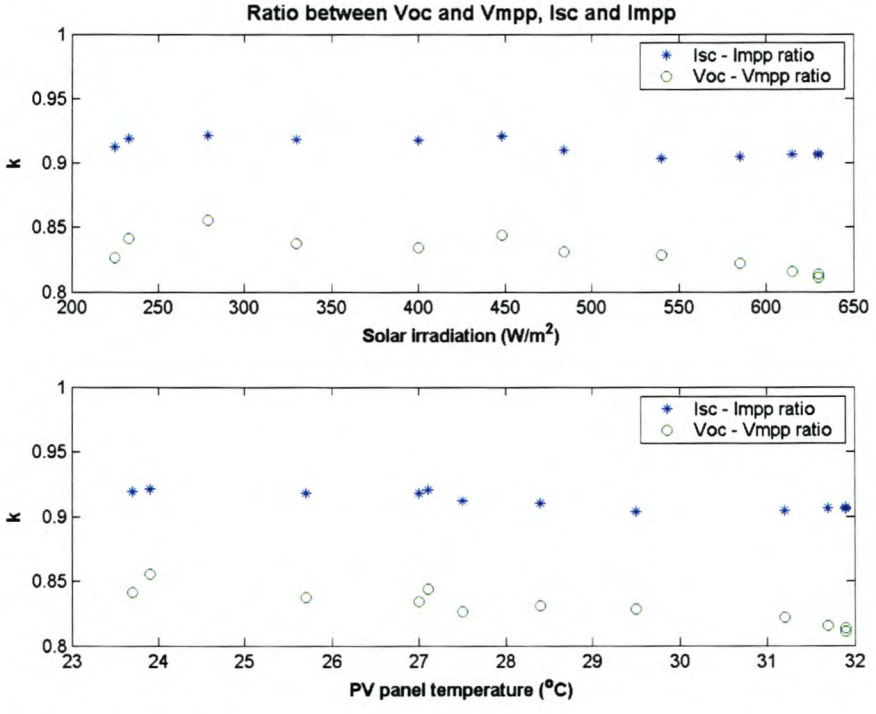

Figure 4-4: The relationship between the PV panel I_{SC} and I_{MPP}, and V_{OC} and V_{MPP}, for a variety of measurements done with irradiance values between 200 and 650 W/m^2 and panel temperatures between 23 and 32 °C

The data shown in Figure 4-4 was found by measuring the voltage-current curves for a PV panel operating at various solar irradiation and panel temperature values. From this data it is clear that there is a relationship (represented by k for the rest of this chapter) between the PV panel's I_{SC} and I_{MPP}, and V_{OC} and V_{MPP}, which can be described as follows:

$$I_{MPP} = k_{current} \times I_{SC} \quad 4\text{-}1$$

and

$$V_{MPP} = k_{voltage} \times V_{OC} \quad 4\text{-}2$$

The measured data presented in Figure 4-4 shows that $k_{current}$ does not vary by more than 2%, and $k_{voltage}$ by no more than 4%, for irradiance values between 200 and 650 W/m^2 and panel temperatures between 23 and 32 °C. Comprehensive measurements presented in [31], across a wider range of irradiance values and temperatures (0 to 60 °C) found a variation of less than 5% for $k_{current}$ and 10% for $k_{voltage}$.

These relationships form the foundation of a family of MPPT algorithms, as is explained next.

4.3.2 Overview of MPPT algorithms

4.3.2.1 The hill-climbing MPPT algorithm

The hill-climbing algorithm seeks the MPP by measuring and trying to minimize the gradient of the PV panel output power to the PV panel output voltage. Although this algorithm gives good results when tracking in fluctuating illumination and temperature conditions, the main problems include the slow response speed of the MPPT to swiftly changing conditions, and the problems associated with multiple-peak power-voltage curves, as shown in Figure 4-5.

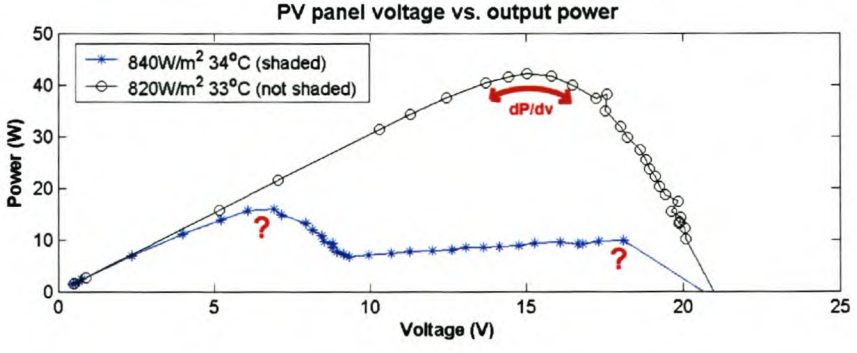

Figure 4-5: The operation and problems associated with the hill-climbing MPPT algorithm.

4.3.2.2 Database and sensor MPPT algorithm

Another family of MPPT algorithms uses database tables and temperature and irradiation sensors to predict the maximum power point. These algorithms require additional sensors, with the associated financial and reliability costs. Effects like partial shading of the PV array, which has not been foreseen in the database, further limits the accuracy of these algorithms.

4.3.2.3 Constant voltage ratio MPPT algorithm

As the open-circuit voltage of the PV panel can easily be measured, the relatively constant ratio k between V_{OC} and V_{MPP}, described in section 4.3.1, can be used to operate the PV panel at the MPP voltage. The simplest algorithm based on this ratio principle assumes that the ratio k will always be constant at, for example, 78%. The open-circuit voltage of the PV panel is measured periodically, and the operating voltage adjusted to 78% of this measured voltage. This algorithm is very easy to implement, but does not take panel shading into account, leading to inaccurate operation when connected to shaded panels.

4.3.2.4 The k-sweep, current ratio MPPT algorithm

The solution to this problem of variations in k due to panel shading, proposed in [31], is to sweep the PV panel voltage from open-circuit to short-circuit every few minutes while measuring the PV panel current. From these measurements the new k, the ratio between the measured I_{SC} and I_{MPP} or V_{OC} and V_{MPP} can be calculated.

[31] implements this k-sweep MPPT algorithm by using the circuit as shown in Figure 4-6. The PV panel is momentarily short-circuited for 80 µs every 80 ms (using mosfet S2) to measure I_{SC}, while k is re-calculated every few minutes by varying mosfet S2 from open to short. With knowledge of I_{SC} and k, the MPP current can be calculated and implemented using Equation 4-1.

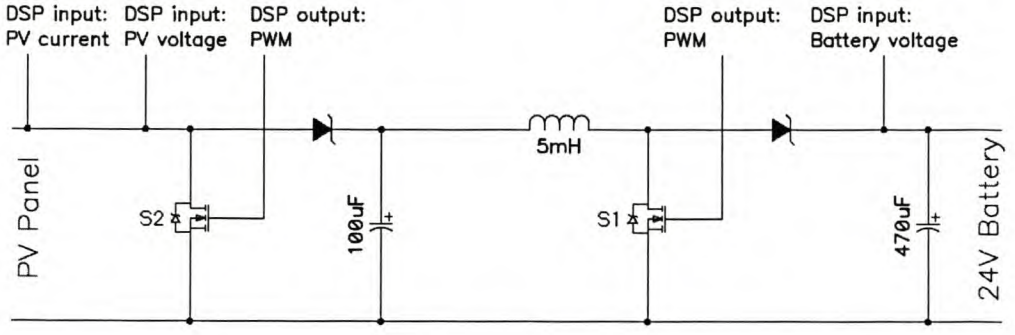

Figure 4-6: Circuit used to implement the k-sweep, current ratio MPPT algorithm

4.3.2.5 Problems associated with the k-sweep, current ratio MPPT circuit

The implementation of a current ratio MPPT presents some problems, however, compared to voltage ratio MPPTs.

These problems mostly relate to the need to periodically short-circuit the PV panel to find I_{SC}. As I_{SC} varies with irradiance, fast cloud movements can for example cause I_{SC} to change very quickly, necessitating frequent short-circuits (every 80 ms was suggested in [31]). To accurately measure I_{SC} within a short period (80 µs in [31]), the boost-converter mosfet (mosfet S1 in Figure 4-6) cannot be used, as the 100 µF capacitance across the PV panel, needed for stable switching, will cause a too slow response. Mosfet S2 and an additional diode are therefore added to the circuit.

The problem with adding the mosfet and diode is that the circuit now has more components, thereby increasing system cost, lowering reliability and decreasing efficiency. In addition an extra PWM control channel from the DSP for mosfet S2 is required, thereby lowering the amount of MPPTs that can be controlled with one DSP, once again increasing system cost.

DSP control for a current ratio MPPT is relatively complicated, as k and I_{MPP} need to be calculated, and I_{MPP} implemented by changing the duty cycle of mosfet S1 (i.e. current control by means of voltage control, implying some form of feedback system).

4.4 Development and implementation of the k-sweep, voltage ratio MPPT

4.4.1 Development of the k-sweep, voltage ratio MPPT algorithm

4.4.1.1 Voltage ratio versus current ratio

The biggest problem associated with the k-sweep, current ratio MPPT algorithm is the fact that I_{SC} have to be measured accurately and often, leading to a complicated implementation. If the voltage ratio V_{OC} : V_{MPP} is used instead of the current ratio I_{SC} : I_{MPP}, a much simpler implementation results, as V_{OC}, based on the PV panel temperature, changes much slower than I_{SC}, based on the irradiance on the panel, and can be measured more easily.

The k-sweep, voltage ratio MPPT algorithm proposed in this chapter finds the voltage ratio k by sweeping the PV panel voltage from open-circuit to short-circuit periodically, and then using k to implement V_{MPP}. Measurement of I_{SC} is no longer required, therefore mosfet S2 in Figure 4-6 and the associated diode and DSP control channel can be removed, resulting in the circuit shown in Figure 4-7, with higher efficiency and reliability, and lower cost.

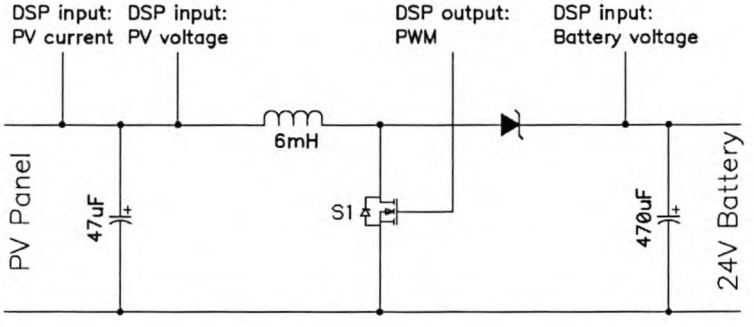

Figure 4-7: Circuit used to implement the k-sweep, voltage ratio MPPT algorithm

The accuracy of k represents the main problem for MPPT algorithms based on the voltage ratio. However, as Figure 4-4 has shown in addition to the results found in [31], the accuracy of k is a function of the range of change in irradiance and PV panel temperature, and varies at worst by around 10%. If this irradiance and temperature range can be limited, e.g. by making the period between consecutive measurements of k short enough, the accuracy of k can be improved considerably.

4.4.1.2 Choosing the period between consecutive k-sweeps

The main factor that limits the shortness of the period between consecutive k-sweeps is that optimal energy is not extracted during a PV panel voltage sweep. If k-sweeps were therefore done too often, the efficiency of the system would decrease.

As can be seen from Figure 4-15, a k-sweep takes around 25 ms, during which time only around half the maximum amount of available PV energy is transferred to the battery. In order to make the losses associated with the k-sweep less than 0.1% of the total energy, the sweep period must therefore be chosen as greater than 12.5 s. A k-sweep period of 12.5 s was chosen to ensure the highest possible accuracy of k.

Panel temperature stays relatively stable during the 12.5 s between k-sweeps, due to the thermal time constant of the PV panel materials. The biggest influence on the accuracy of k is therefore rapid changes in irradiation during the 12.5 s before the next k-sweep occurs. These rapid irradiance changes only occur on days with fast-moving clouds.

4.4.1.3 The relationship between the voltage ratio and the duty cycle

As the PV panel temperature stays relatively stable during the 12.5 s period between k-sweeps, the assumption is made that the PV panel open-circuit voltage will also stay stable during this period (refer to section 4.2.1).

Instead of calculating k and measuring V_{OC}, and then using Equation 4-2 to calculate V_{MPP} and implementing this new voltage, this stable PV panel open-circuit voltage allows the MPPT algorithm to only measure the duty cycle at which the MPP occurs during the k-sweep, and immediately implementing this duty cycle as soon as the sweep completes. For the rest of the period between k-sweeps, mosfet S1 will operate at this duty cycle. This simplifies the DSP code required to control the MPPT, freeing processing power for other functions, at the cost of a loss in accuracy that is negligible, given the short period between k-sweeps.

The flowchart in Figure 4-8 illustrates the k-sweep, voltage ratio MPPT algorithm operation.

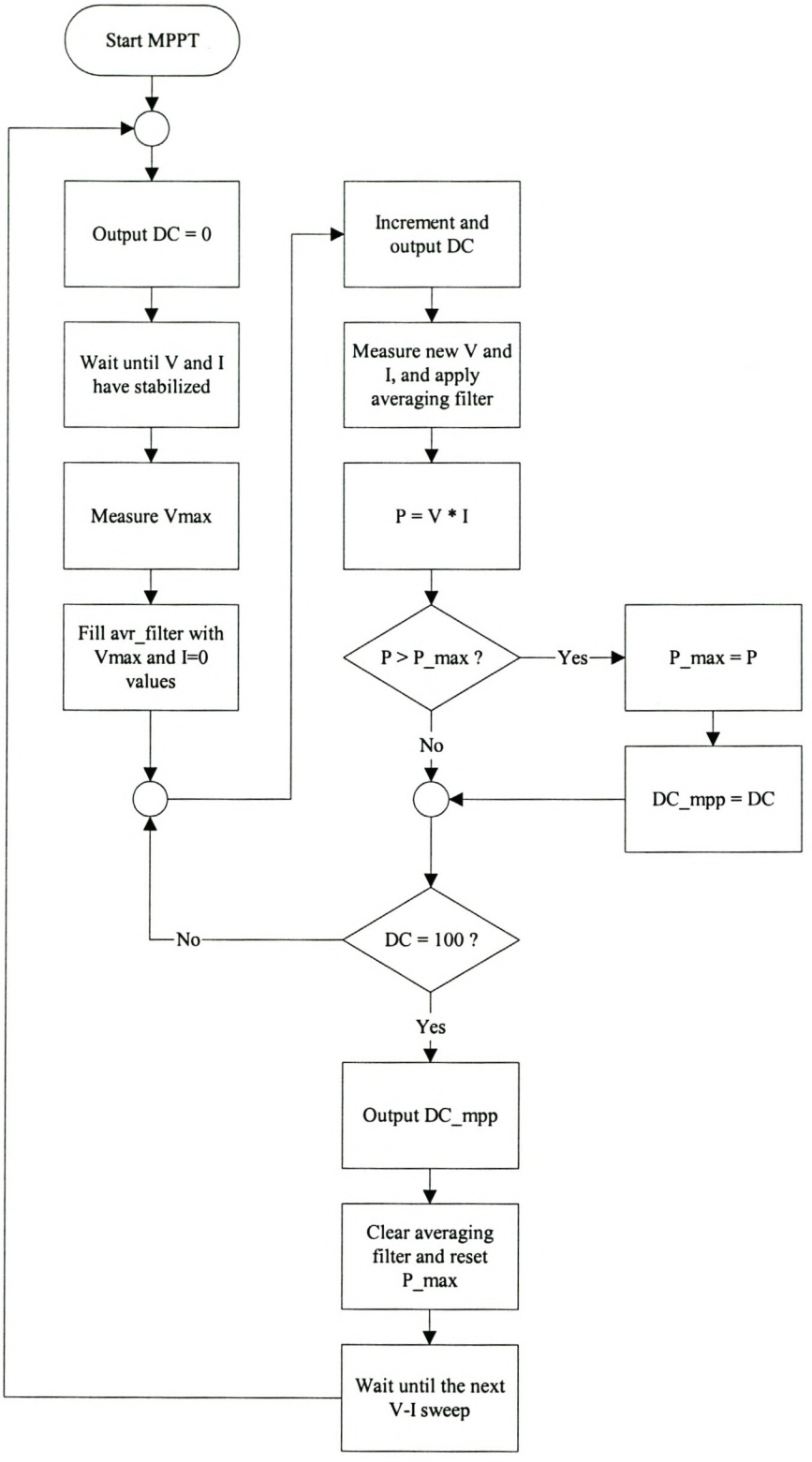

Figure 4-8: Flowchart showing the control algorithm of a k-sweep, voltage ratio MPPT.

4.4.2 Implementation of the k-sweep, voltage ratio MPPT

The boost-converter configuration shown in Figure 4-6 was used as base for the design presented in this chapter, with a PV panel with a V_{OC} of around 20 V on the left, and a 24 V lead-acid battery on the right. Mosfet S2 and the additional diode were removed from the original circuit, resulting in the circuit shown in Figure 4-7.

A Texas Instruments TMS320LF2407 DSP was used to measure the PV panel current and voltage, and control mosfet S1. This DSP offers 16 analog-to-digital input channels, and 8 PWM output channels, allowing control of five separate MPPTs if one ADC channel per MPPT is used for battery-charging purposes.

4.4.2.1 Choosing a suitable transistor

The process of choosing a suitable switching device for S1 is described in this section. A switching frequency higher than 20 kHz is required in this design to operate outside the audible frequency spectrum. At this high switching frequency, mosfet transistors offer better performance than the other available high-current transistor option, IGBTs. The higher reverse-voltage blocking capabilities of IGBTs are not of much use in this design, as the operating voltage for this system would be around 20 to 30 V.

A switching ripple of 1% is chosen for this design to allow the use of cheap electrolytic capacitors instead of the more expensive polypropylene capacitors required for high ripple current.

International Rectifier's range of mosfets is used due to previous positive experience with the brand. Within this range the chosen device must satisfy the following criteria:

- a low R_{ds} (drain-to-source resistance), for high efficiency,
- the capability of conducting 6 A current continuously (the tracker will be connected to a 75 W PV panel, with operating current at STC given as 4.8 A, and 25% added for higher radiation values or cooler operation),
- a forward voltage limited to a maximum constant voltage of 27 V (21.7 V at STC plus 25%),
- fast t_{on}, t_{off}, t_{rise} and t_{fall} times, for high efficiency,
- reasonable cost.

In order to make an accurate choice, the total power dissipation for each potential mosfet must be calculated, using the following equation,

$$P_{total} = P_c + P_s \quad \text{4-3}$$

where P_c represents the conductive losses, and P_s switching losses.

The worst-case conductive losses can be calculated as follows,

$$P_c = R_{ds} * I_{max}^2 * 0.75 \quad \text{4-4}$$

with the maximum current I_{max} taken as 6A, at a duty factor taken as 75% (typically V_{in} / V_{out} = 18V / 24V = 75%), and R_{ds} read from the mosfet specifications at a junction temperature of 80°C.

The switching losses are difficult to calculate as it depends on many difficult to quantify and often unspecified parameters. Assuming a perfect diode, the switching losses in the mosfet can be approximated by the following equation,

$$P_s = 0.5 * I_{max} * V_{max} * t_{rise+fall} * f_s \quad \text{4-5}$$

where t_{rise} and t_{fall} are the periods taken by the current to fall or rise in response to a change in voltage, V_{max} is the maximum forward voltage, and f_s is the switching frequency .

The total power dissipated in the mosfet S1 is a function of the switching frequency as described by equation 4-5, and shown in Figure 4-9. Before a suitable mosfet can therefore be chosen, the switching frequency first has to be chosen. This choice cannot be made until all switching frequency dependent losses within the circuit have been described.

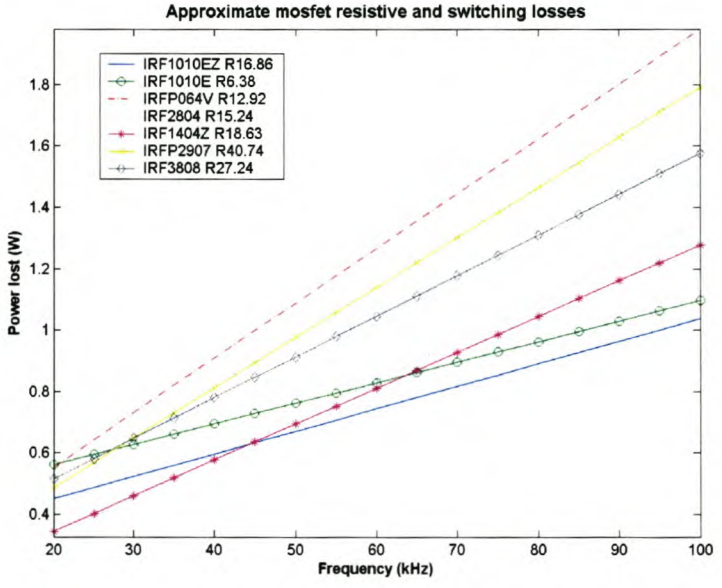

Figure 4-9: Approximate mosfet resistive and switching losses for a variety of IRF mosfets.

4.4.2.2 Choosing a suitable inductor

The other component representing a significant switching-frequency dependant power loss in the boost converter configuration is the inductor. The process of inductor design will now be described briefly. The required inductance value can be calculated as follows:

$$L = V_{in} \times \frac{dt}{di} \tag{4-6}$$

where

$$dt = \frac{V_{in}}{V_{out} \times f_s} \tag{4-7}$$

and

$$di = \frac{I_{in} \times R}{100} \tag{4-8}$$

therefore

$$L = \frac{V_{in}^{\ 2} \times 100}{V_{out} \times f_s \times I_{in} \times R} \tag{4-9}$$

where V_{in} represents the PV panel voltage and V_{out} the battery voltage, I_{in} the current through the inductor and R the ripple percentage. Figure 4-10 shows the choice of inductor values as a function of switching frequency, based on the equations presented above.

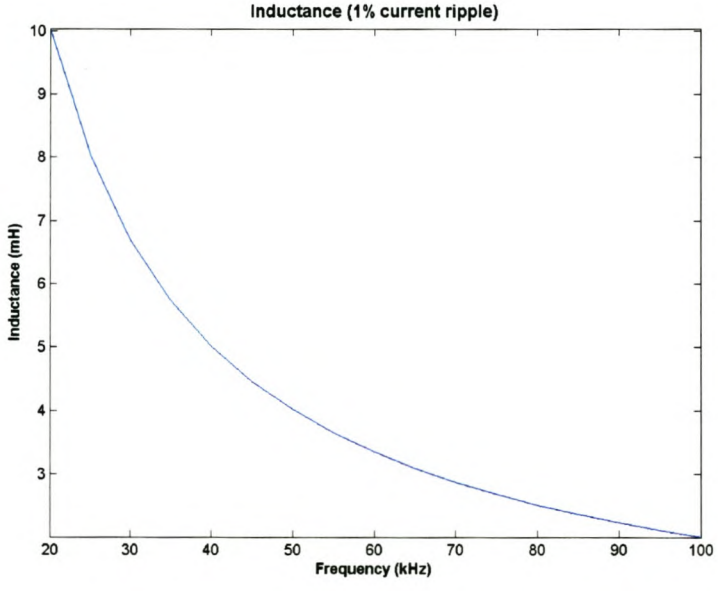

Figure 4-10: Inductor value as a function of switching frequency for the circuit shown in Figure 4-7

To calculate the power lost in the inductor L, the following equation can be used to first find the amount of windings on the inductor,

$$n = \sqrt{\frac{L}{A_l}} \qquad 4\text{-}10$$

where A_l represents the inductance factor specified in the data sheet of the inductor.

The length of copper wire needed to wind the inductor can now be calculated:

$$l_c = n \times 2\pi \times r_i \qquad 4\text{-}11$$

where r_i represents the average radius of the inductor core.

Copper wire resistance is given by the following equation,

$$R_c = \frac{17.2414 \times l_c}{A_c} \qquad 4\text{-}12$$

where A_c represents the area of the copper wire.

The power lost in the inductor can now be calculated as

$$P_i = I_{in}^2 \times R_c \qquad 4\text{-}13$$

1 mm thick wire was used to wind the inductor. The resulting inductor resistive power losses as a function of switching frequency are shown in Figure 4-11.

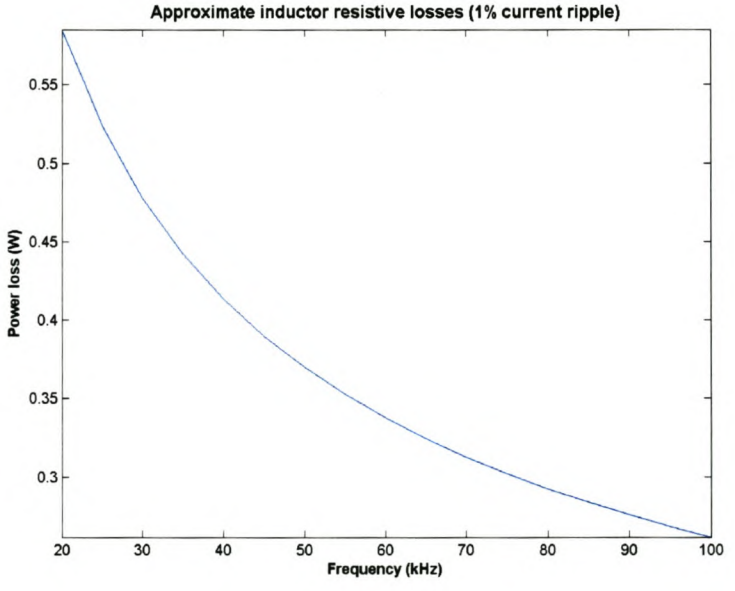

Figure 4-11: Approximate inductor resistive losses as a function of the switching frequency.

4.4.2.3 Choosing a switching frequency

The total power dissipated by the inductor and the mosfet can now be plotted as a function of switching frequency, as shown in Figure 4-12. The IRF1010E mosfet was chosen, as its cost is almost three times less than the two mosfets that offered higher efficiencies. From this figure the optimal switching frequency was read as 35kHz, with an inductor value of 6 mH (Figure 4-10).

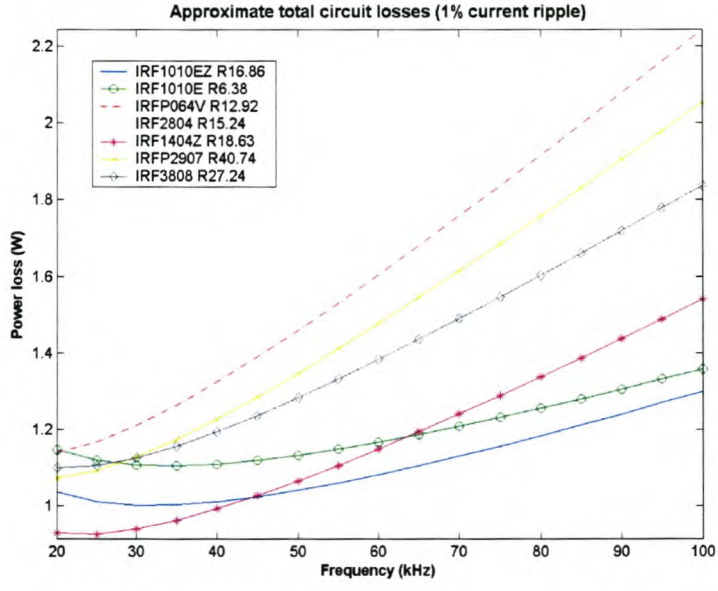

Figure 4-12: The total power dissipated by the inductor and mosfet in the circuit shown in Figure 4-7, as a function of switching frequency

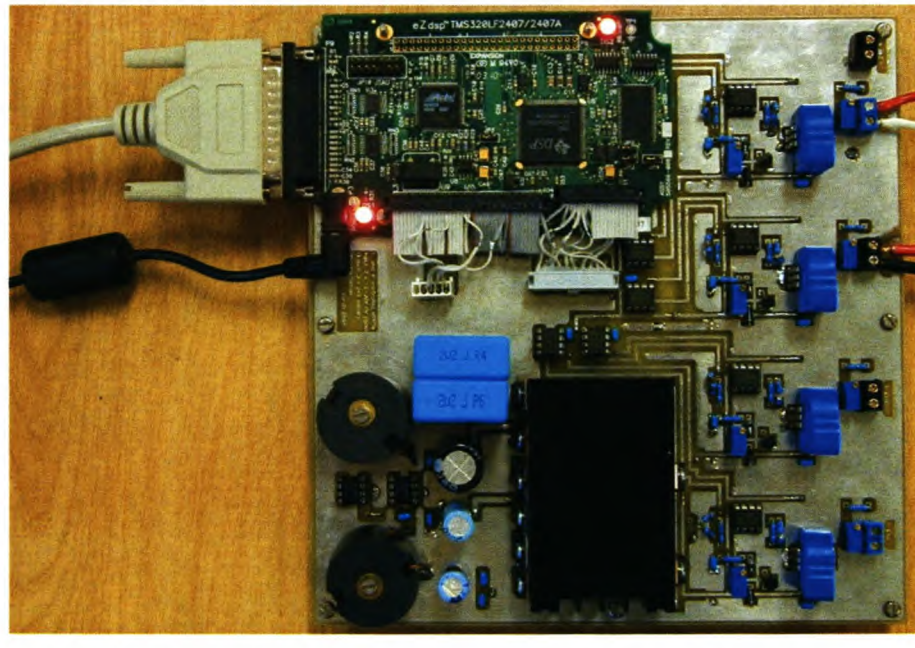

Figure 4-13: A photo showing the setup build to investigate different MPPT algorithms. The TI DSP is located at the top left corner of the board. Two boost converter circuits and four blue LEM current sensors are also visible.

4.4.3 Problems experienced

The capacitor across the PV panel in Figure 4-7 was chosen as small as possible to allow fast response of the PV panel to new duty cycle commands. A disadvantage of a small PV panel capacitor, however, is that mosfet S1 switching noise has a greater influence on the measurements of the PV panel voltage and current.

This problem was addressed by adding a digital averaging filter within the DSP, to clean the measured PV panel voltage and current values. Figure 4-14 explains the operation of this filter, which uses the same amount of DSP processing time irrespective of the filter size. This is made possible by using a variable that always points to the oldest value in the filter array.

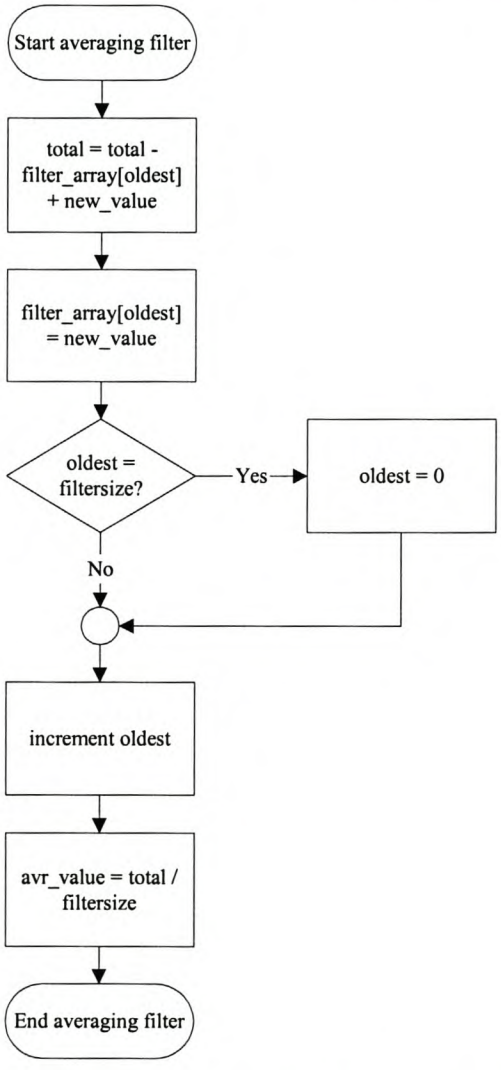

Figure 4-14: Flowchart showing the DSP-based averaging filter used to clean PV panel voltage and current measurements

4.5 Measurement results

4.5.1 Normal operation of the k-sweep, voltage ratio MPPT

Figure 4-15 and Figure 4-16 demonstrates the operation of the k-sweep, voltage ratio MPPT during the two scenarios shown in Figure 4-2: a shaded PV panel and a PV panel with no shade. The top oscilloscope signal is the PV panel voltage, the middle signal is the PV panel output power, and the bottom signal is the PV panel current. As can be seen the MPP is implemented as soon as the k-sweep to find k is completed.

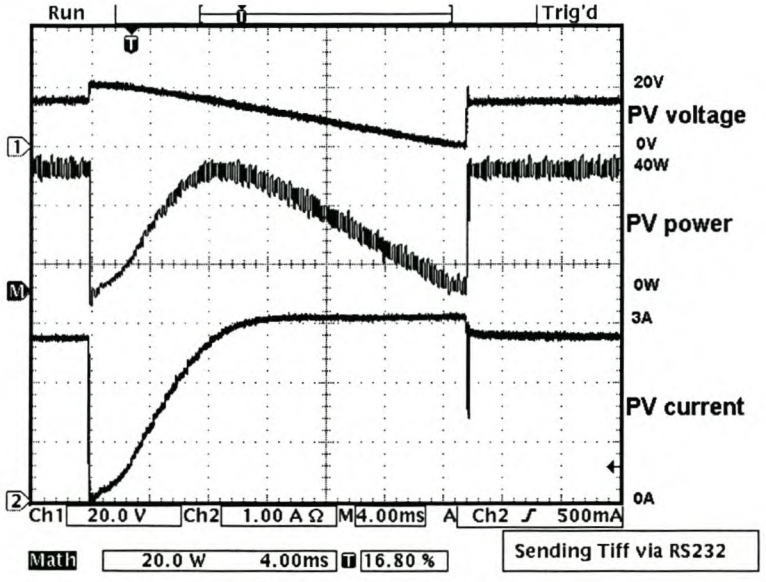

Figure 4-15: Measurements of the operation of the k-sweep, voltage ratio MPPT for a PV panel with no shade

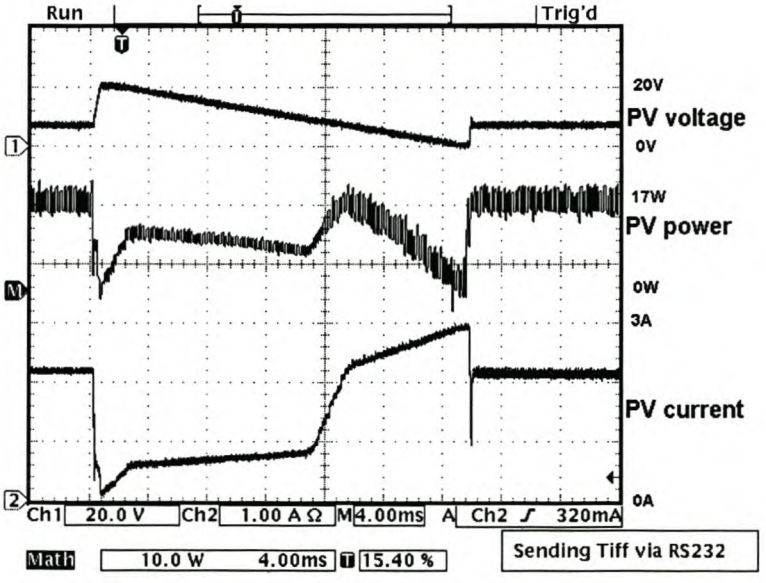

Figure 4-16: Measurements of the operation of the k-sweep, voltage ratio MPPT for a PV panel with a shade-pattern as shown in Figure 4-3

4.5.2 Low-irradiation operation of the k-sweep, voltage ratio MPPT

The measurements presented in Figure 4-15 and Figure 4-16 demonstrate the accurate operation of the MPPT circuit at high irradiance levels. Measurements were also done on cloudy days with very low irradiance values to demonstrate that the MPPT still operates accurately in such conditions. The results are shown in Figure 4-17.

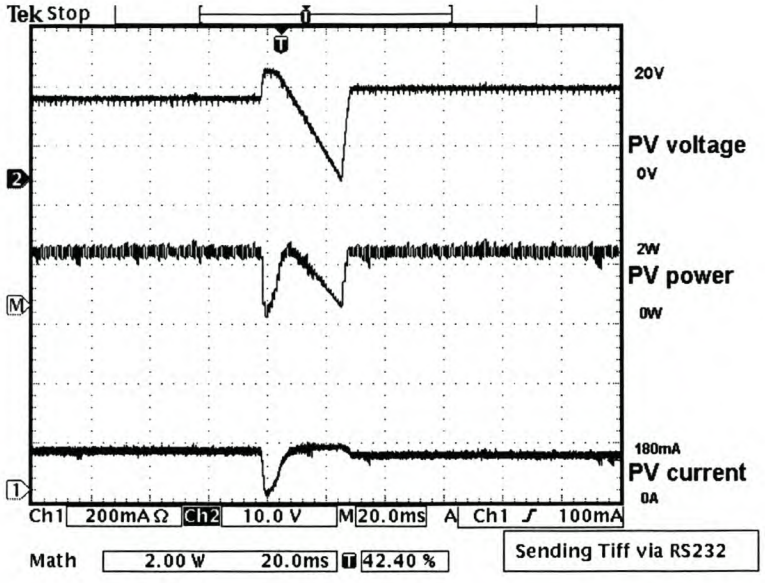

Figure 4-17: Measurements of the operation of the k-sweep, voltage ratio MPPT for a PV panel with low irradiance values

4.5.3 Efficiency of system

The efficiency of the MPPT circuit was found by measuring the PV panel power input and battery power output of the MPPT, using current and voltage probes and Seriallog. The efficiency of the system, shown in Figure 4-18, is at present disappointing, with a maximum efficiency of around 82%.

Further study of optimal circuit configurations and a detailed design of all circuit components are outside the scope of this thesis – the reader is referred to [33], a thesis focussing on the optimal design of a boost converter, for more details on this topic. In [33], MPPT circuit efficiencies of up to 96% were achieved.

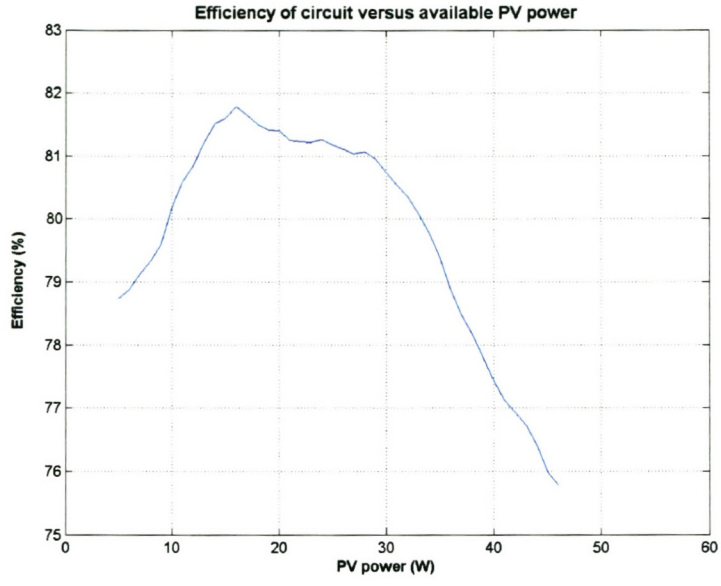

Figure 4-18: Efficiency of the k-sweep, voltage ratio MPPT circuit shown in Figure 4-7, as measured at the input and output of the MPPT, as a function of available PV power.

4.6 Conclusion

This chapter discussed the important role MPPT plays in optimally transferring power from the PV panel. A variety of MPPT algorithms were presented, after which the optimal MPPT algorithm was developed, where the benefits of a PV panel voltage sweep to obtain k was combined with the advantages of voltage ratio instead of current ratio MPPT.

Measurements confirmed that this MPPT algorithm operated very effectively in a variety of irradiance conditions. Although low circuit efficiency values were measured, these can be solved by optimal design of switching components and circuit configurations.

A great advantage of the DSP controlled MPPT circuit designed in this chapter is the ease with which efficient battery charging strategies can be implemented using exactly the same circuit design. The next chapter will explain this implementation in detail.

4.7 Future work

The MPPT algorithm explained in this chapter offered very promising results. Future work on this topic can include the following:

- A practical comparison can be done between the k-sweep voltage vs. current ratio MPPT algorithms, focussing on measurements during times of fast-changing irradiance. This comparison will answer the uncertainty that still exists on whether voltage ratio MPPTs offer worse performance during these conditions than current ratio MPPTs.
- The use of a boost converter limits the application of the MPPT to batteries of 24V and higher. A buck-boost converter design will make operation with a 12V battery possible, broadening the field of application of the MPPT.
- A MPPT will only be used in a PV system if it offers a financial benefit to do so. At the moment the k-sweep voltage controlled MPPT design is expensive to implement due to especially the cost of the LEM current sensors and the DSP controller. Now that the algorithm has been proven, a detailed circuit design can focus on reducing the manufacturing costs of the MPPT, and increasing the efficiency of the circuit.

Chapter 5 - Optimal energy storage

5.1 Introduction

Energy storage (ES) is the final PV system element discussed with a view towards optimising the total energy available from the PV system. Efficient storage of energy is necessary, as much of the irradiance converted by the PV panel is usually stored for later use during periods when little or no irradiance are available.

Storing energy efficiently starts with choosing a suitable ES technology. A variety of technologies exist, with widely ranging characteristics. The first section of this chapter introduces and compares these ES technologies. The objective of this comparison is to find an ES technology most suitable for use in a rural, off-grid application, the most likely type of PV system installation in South Africa (refer to Chapter 2).

Once a suitable ES technology has been identified, strategies are investigated on how to optimally transfer PV energy to this technology. The characteristics of the chosen ES technology are firstly presented, after which a variety of charging strategies relating to this technology are discussed.

The final section of this chapter explains how elements of these charging strategies can be combined into an ES charging algorithm specifically suited for PV energy. This algorithm is implemented using the MPPT circuit described in Chapter 4.

5.2 *Choosing an optimal ES technology*

5.2.1 Comparison criteria

Chapter 2 concluded that PV energy is most suited to rural, off-grid applications in South Africa, mostly due to its comparatively high generation cost, and the reliability and ease of installation of PV arrays. The focus of this comparison is therefore to find the most suitable ES technology for PV arrays in rural settlements and villages.

The following criteria are used to compare the different ES technologies:

5.2.1.1 Charge/discharge efficiency

The charge/discharge (round-trip) efficiency of an ES system is defined as the ratio of energy available for discharge compared to the energy required for full recharge. For example, an efficiency of 50% means that for every 1 kWh of energy used to charge the energy store, only 0.5 kWh of energy is available during discharge.

5.2.1.2 Power transfer period

The power transfer period is defined as the period over which the ES technology can continuously supply power (i.e. its energy storage capacity). This period varies widely between different ES technologies, as can be seen in Figure 5-1.

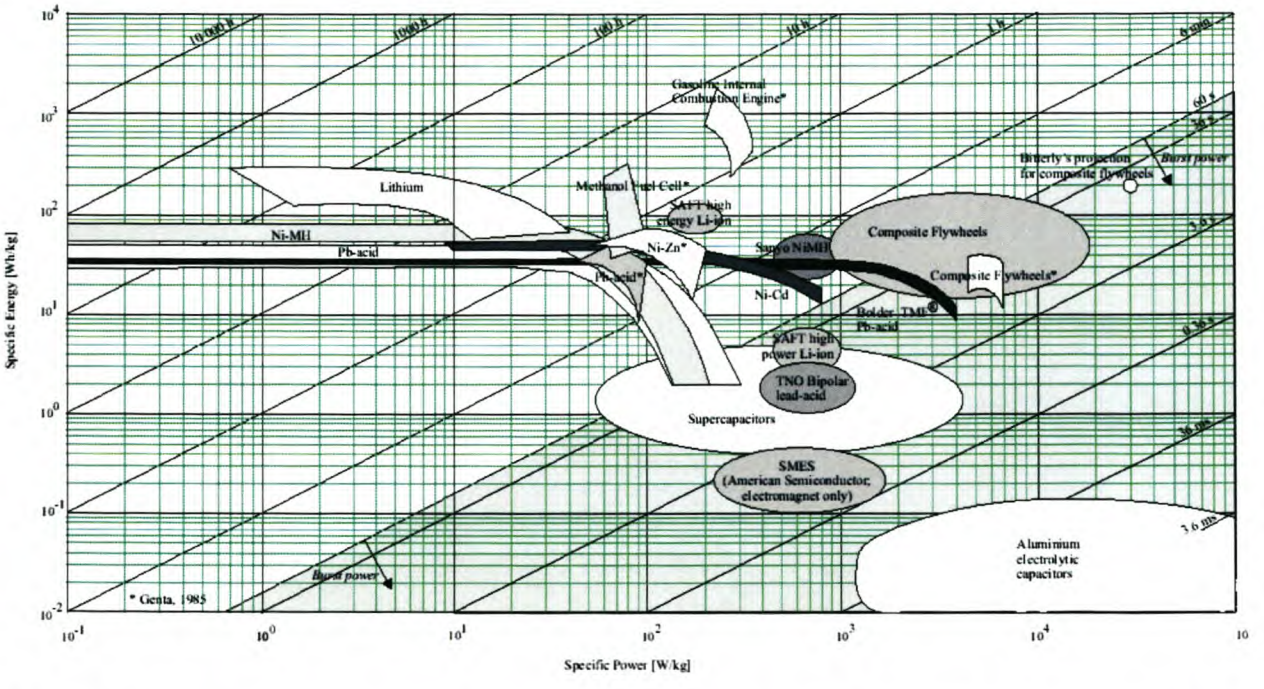

Figure 5-1: Specific energy vs. specific power, including the power transfer period, of a selection of ES technologies [36].

As PV energy is directly related to the amount of available irradiation, ES technology must be able to continue to supply energy during periods of low or no irradiance, for example during the night or overcast days. PV ES designs for domestic use usually aims to ensure availability of energy for at least three consecutive days of no irradiation [18], which leads to a power transfer period requirement in the order of tens of hours.

5.2.1.3 Power rating

The design load parameters for rural communities in South Africa, as given in [44], indicate that these loads have average daily mean demand values of between 0.4 kVA and 0.7 kVA per domestic consumer. Assuming a maximum of 50 consumers per rural settlement / village, the power rating of a suitable ES technology can be estimated as below 50 kW.

5.2.1.4 Lifespan and cycle life

The lifespan of an ES system is defined as the length of time before a major part of the system needs to be replaced. Operating temperature, the amount of charge and discharge cycles (cycle life), in some cases the depth of discharge and the state-of-charge of the system when not in use for a long time can all influence the lifespan of the system.

5.2.1.5 Financial cost

The financial cost necessary to create and operate an ES system is usually measured as cost per unit energy, per unit power, or per charge and discharge cycle, depending on the most important design criteria of the system.

5.2.1.6 Reliability and maintenance

The reliability of an ES technology and its maintenance requirements are important factors to consider, especially when the ES system will be used in a remote location, as is typically the case with rural off-grid PV installations in South Africa.

5.2.1.7 Implementation time

Implementation time is the time required to design, install and test an ES technology before the technology is ready for use.

5.2.1.8 Environmental impact

This criteria looks at the impact that installing, operating and decommissioning the specific ES technology has on the environment.

The ES technologies included in this comparison are described according to the four types of temporary energy forms in which the generated electrical energy is stored: electrochemical, electric field, magnetic field and kinetic ES technologies.

5.2.2 Electrochemical energy storage

Electrochemical energy storage is based on the conversion of electrical energy into chemical energy and vice versa. Consequently each electrochemical ES system is characterised by a chemical reaction, and the amount of energy stored is determined by the difference in energy content between those chemical substances existing in the charged state and those existing in the discharged state.

During a chemical reaction electrical charge is exchanged between ions. To utilize this electrical charge as electrical energy the chemical reaction is split into two reactions, occurring at two electrodes separated by electrolyte. At the one electrode electrons are released by the chemical reaction, while at the other electrode electrons are absorbed. If a conductor is connected between the two electrodes, the electrons will flow through it as electrical current.

By changing parameters like the chemical composition and construction of the battery components, batteries can be created with different characteristics to suit different applications. Two families of electrochemical ES technologies are discussed: secondary batteries and fuel cells.

5.2.2.1 Secondary batteries

Rechargeable batteries are usually called secondary batteries, compared to primary batteries that are designed for one-discharge-only applications.

The specific energy of secondary batteries is high compared to other ES technologies, but the specific power is low, mostly due to their high internal impedances (caused by the contact resistance between the electrodes and the electrolyte [36]). Secondary batteries therefore have low to medium power ratings and high power transfer periods, which are ideal for rural, off-grid applications as described in the previous section.

A wide variety of secondary batteries exist, classified according to their chemical composition. Most of these families are however not considered, due to the previously defined comparison criteria. So, for example, financial cost considerations eliminate the silver-oxide, lithium and nickel-hydrogen families of batteries. Low cycle life makes the nickel-zinc and zinc-manganese

dioxide families impractical, while high maintenance requirements disqualify the nickel-iron family.

The following paragraphs briefly discuss the three families of secondary batteries that are potentially suitable for rural off-grid PV ES applications.

Lead-acid

The most common battery today is the lead-acid secondary battery, invented in 1859 [36]. Some of the reasons why this battery is so popular include low cost, high availability, easy state of charge indication and reliability. Some disadvantages include that long-term storage in a discharged state can lead to irreversible polarization of electrodes, and the fact that it contains hazardous materials like lead, stibene and arsenic. These metals are vaporized if fed as rubbish into incinerator plants, requiring expensive filtering of the resultant gas, and toxic ashes. If it is dumped in rubbish pits, the metals can gradually be released into ground water. More than 95% of lead-acid batteries are however recycled [38].

The charge/discharge efficiency of lead-acid batteries is very low (around 45-50% [48]), with a typical cycle life of between 200 and 1500 cycles. Lead-acid batteries constructed with long cycle life as main design criteria can however offer a cycle life of up to 3500 cycles [48].

Another disadvantage of lead-acid batteries is their sensitivity to depth of discharge (D.O.D., i.e. the percentage of the total available energy in the storage system that is discharged), as shown in Figure 5-2.

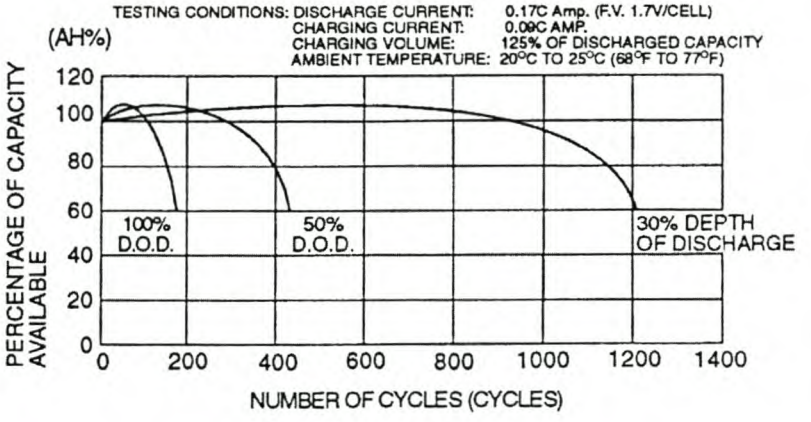

Figure 5-2: The influence of depth of discharge on the total energy available and cycle life of a lead-acid battery [37]

Nickel-cadmium

The nickel-cadmium secondary battery offers a round-trip efficiency of around 70% and a maximum cycle life of more than double that of lead-acid [48]. The battery is also reliable with excellent long-term storage properties, and is not harmed by 100% depth of discharge.

Disadvantages include the toxicity of the cadmium used in the battery, higher installation cost than lead-acid batteries, and the memory effect (discussed in detail later in this section). Over 20-year lifespan nickel-cadmium batteries tend to cost less than lead-acid batteries, due to the higher efficiency and cycle life [48].

Nickel-metal hydride

The characteristics of nickel-metal hydride batteries are very similar to that of nickel-cadmium, with the charging and discharging performance so alike that either battery system can replace the other in normal application. In comparison, though, nickel-metal hydride stores up to 100% more energy, and are much easier to dispose of at the end of service-life due to the lack of toxic cadmium.

Disadvantages include a moderate memory effect, poor charge retention, higher cost and lower high-current rate performance than nickel-cadmium.

The memory effect

The memory effect is experienced with nickel-cadmium batteries, and to a lesser extend with nickel-metal hydride batteries. Low-current rate recharging and repeated partial discharge and charge cycles causes cadmium crystals to grow on the negative electrode. This reduces the voltage level of the whole discharge curve, which means that the end-of-discharge voltage is reached faster (see Figure 5-3). Complete discharge and subsequent recharge at high current densities sometimes eliminate this problem.

Low-current rate recharging and repeated partial discharge and charge cycles characterises PV systems in rural areas, due to the relationship between the PV array charging current and irradiance, and the usage profiles of rural communities [44]. For this reason the memory effect will be pronounced if nickel-cadmium or nickel-metal hydride ES technologies are used for this application. These two battery families will therefore not be considered further in this comparison.

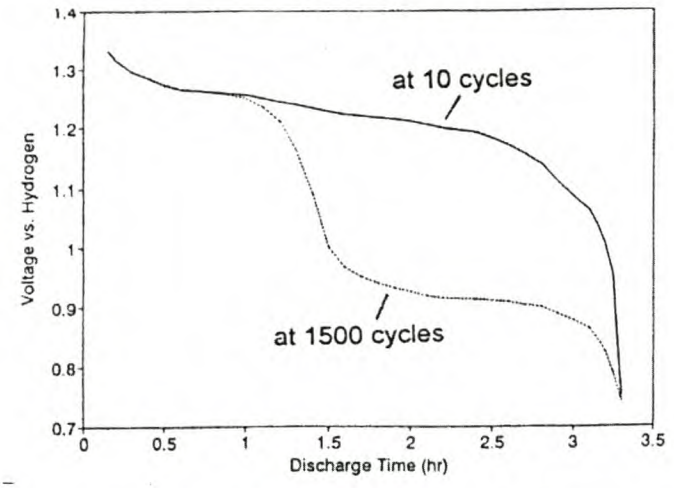

Figure 5-3: The influence of the memory effect on the discharge curve for a typical nickel-cadmium battery [38].

5.2.2.2 Fuel Cells

Per definition fuel cells are devices that convert chemical energy into electrical energy, and therefore can be defined as electrochemical batteries. In practice the fuel cell label is only used for devices where the free-energy containing substance flows into the cell, for example flow batteries or hydrogen fuel cells (compared to secondary batteries, which stores the free-energy containing substance within the cell).

Hydrogen fuel cells are still being developed at present, leading to very high costs. For this reason, only flow batteries are considered.

Flow batteries

Flow batteries provide a reversible electrochemical reaction between two salt solution electrolytes, which are brought close together in battery cells where they are separated by a polymer membrane. This membrane allows only certain ions to travel through, thereby producing a voltage across the membrane. In all flow batteries the power and energy ratings are independent of each other, i.e. if more energy is needed, more electrolytes are added, while more membranes are added for extra power.

Zinc-Bromide

Zinc-bromide flow batteries are made from low-cost and easily available materials, are capable of rapid recharging, and operate at ambient temperature. These characteristics make it an attractive technology for both utility-energy storage and electric vehicle applications. Disadvantages include the use of bromide, an environmentally hazardous element.

Zinc-bromide batteries operate at around 70% round-trip efficiency, and have a cycle life of around 2500 cycles before major maintenance is required [48].

Vanadium-redox

The vanadium-redox flow battery operates on the same principle as the zinc-bromide battery. The main advantage of vanadium-redox above zinc-bromide is that it is environmentally sound, and offers higher cycle life (15000 cycles) and round-trip efficiency (80% [48]).

Sodium-beta

The advantage of this high operating temperature battery above the previously discussed flow batteries is its insensitivity to ambient conditions due to its temperature management. This is also its main disadvantage, as it requires energy-intensive thermal management, and represents a safety risk. The cycle life of this flow battery is 7000 cycle, with a round-trip efficiency of 75% [48].

The best-known implementation of the sodium-beta technology is the NaS flow battery, named from the chemical reaction that takes place in the battery between natrium and sodium.

The results of a recent study [41], done on the costs of ES technologies for a variety of power utility applications, are shown in Figure 5-4. The comparative costs of the three flow batteries are shown, as well as the study's conclusion that the lead-acid battery family is the most cost efficient technology for long duration power quality ES solutions.

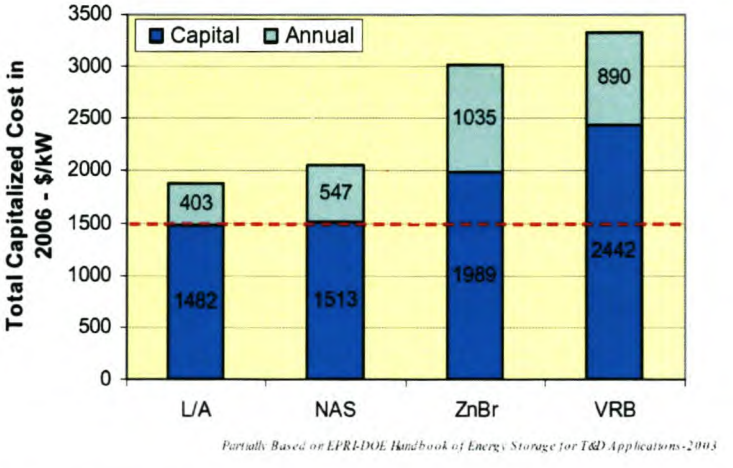

Figure 5-4: Cost of long duration power quality ES solutions (20 year lifespan, 250 cycles per year) [41]

5.2.3 Electric field energy storage

Electrical energy is stored indirectly in the electrochemical batteries discussed above, as chemical energy requiring Faradaic oxidation and reduction of the electrochemically active reagents to create electricity. Electric field ES devices (also called capacitors) on the other hand, store electrical energy directly in an electrostatic way between two plates. This energy E is given as

$$E = \frac{1}{2}CV^2 \qquad 5\text{-}1$$

where V is the voltage between the plates, and C is the capacitance, given as

$$C = \frac{\varepsilon_r \varepsilon_0 A_e}{d} \qquad 5\text{-}2$$

where $\varepsilon_r \varepsilon_0$ is the permittivity of the dielectric, A_e the equivalent area between the plates and d the distance between them.

Because charge and discharge of a capacitor involves only the addition or removal of electrons to and from the capacitor plate, compared to the chemical intro-conversions that takes place on the positive and negative electrode of electrochemical batteries during charge and discharge, much higher cycle life and efficiency are possible with capacitors.

Metal-film and electrolytic capacitors, as well as super capacitors, are however developed with short power transfer periods in mind (in the milliseconds to seconds range, as can be seen in Figure 5-1), and are therefore not suitable for the tens of hours power transfer period range required for rural PV ES applications.

5.2.4 Magnetic field energy storage

Magnetic field ES technologies operate on the principle that an inductor stores energy in the magnetic field associated with the current flowing through it, as represented in the following equation,

$$E = \frac{1}{2}LI^2 \qquad 5\text{-}3$$

where E is the stored energy, I is the current and L is the inductance of the inductor.

From Equation 5-3 it is clear that maximizing the current flowing in the inductor will maximize the amount of energy stored. Normal, non-super-conducting inductors offers too much resistance

to the flow of current for much energy to be stored. Super-conducting inductors, however, offer energy densities similar to capacitors, at very high power levels (up to 1 GW). Super-conducting magnetic energy storage (SMES) systems are however very expensive at present [36], and will therefore not be considered in this comparison.

5.2.5 Kinetic energy storage

5.2.5.1 Flywheels

A flywheel energy-storage device consists of a flywheel that can spin at a very high speed (around 22,500 rpm) and an electrical motor/generator that transfers energy to and from the flywheel. Flywheels usually spin inside a vacuum on magnetic bearings to reduce friction.

The energy stored in a flywheel can be approximated by the following equation,

$$E = \frac{1}{2}mv^2 \qquad 5\text{-}4$$

where m is the cylinder mass and v the linear rim velocity. From this equation it becomes clear that the speed of the flywheel contributes more to the energy stored that its mass. This fact led to the development of lighter but stronger composite flywheels that can achieve much higher rim velocities (600 to 1000 m/s tip speed) than the traditional steel flywheels (200 to 375 m/s tip speed).

Some of the advantages of flywheels are low maintenance, insensitivity to deep discharges, long cycle life (20 years or tens of thousands of deep cycles) and environmentally inert materials. Referring to Figure 5-1, however, it is clear that flywheels are not designed to deliver power for tens of hours. This ES technology will therefore also not be considered.

5.2.5.2 Pumped hydro

A pumped hydro ES system generally consists of two water reservoirs at different elevations. Water can be pumped to the upper reservoir, where it is stored as potential energy. On demand, the water drops down from the upper to the lower reservoir through shafts, where turbine-powered generators convert kinetic energy into electricity. If no natural elevated reservoirs are available, underground lower reservoirs can be considered, either man-made or by making use of natural non-porous caverns.

Two factors influence the power produced by these turbine-powered generators: the vertical distance through which the water falls before hitting the turbine (called the 'head'), and the flow

rate of the water. The power generated by a potential hydropower site can roughly be determined as follows:

$$P = efficiency \times flow\_rate \times head \times 9.8 \qquad 5\text{-}5$$

From Equation 5-5 it is clear that the higher the head, the less water is necessary for a given amount of power. High head turbines in general are also more efficient. Low head is commonly defined as less than 3 meter.

The most obviously impact of building large pumped hydro reservoirs is the flooding of vast areas of land, which would previously have been forested or used for agriculture. Rare ecosystems are often destroyed and native people relocated and culturally disrupted in the process of building such a reservoir. Recent studies of large hydro reservoirs suggested that decaying vegetation, submerged by flooding, might give off large quantities of greenhouse gases.

Hydropower systems are generally defined according to their maximum power rating, into large (>30 MW), small (0.1 – 30 MW) and micro (<100 kW) hydropower. The only hydropower systems suitable for rural PV ES applications, micro hydropower ES, rarely has efficiencies above 50% due to the low head [49]. Micro hydropower will not be considered further in this comparison because of its site-specific nature.

5.2.5.3 Compressed air energy storage (CAES)

CAES plants use off-peak electricity to compress and store gas (air or natural gas) in airtight underground caverns. Cavities in salt deposits, natural rock or aquifers may be used. Upon demand, the compressed air is extracted and used to power a combustion turbine to generate electricity.

The scale of a CAES project makes it impractical for the applications considered in this comparison.

5.2.6 Conclusion

From the four types of ES technologies discussed in the previous sections, it is clear that electrochemical batteries are best suited to the needs of rural PV ES applications. Especially the lead-acid secondary battery and the three flow batteries represents cost-effective long power transfer period ES solutions. Another popular ES technology, the nickel-cadmium secondary battery, was shown to be unsuitable for rural PV ES applications due to the memory effect.

Due to the modularity of lead-acid batteries, the design of the battery array is flexible, and transport and construction uncomplicated. This leads to considerably shorter implementation times than for flow batteries, the only other potentially viable rural PV ES technology. Further benefits of the lead-acid battery above flow batteries include its lower cost (refer to the study done in [41]), as well as its proven reliability compared to the relatively new and unproven flow battery technologies.

The main disadvantage of lead-acid compared to flow batteries is its low efficiency. Another disadvantage of lead-acid batteries, the relatively low cycle life, can be partly overcome by limiting the D.O.D. to less than 30%.

In the view of the above conclusions, the following section will look in more detail at the application of the lead-acid ES technology within a PV system.

5.3 *Optimal energy transfer using lead-acid batteries*

5.3.1 Lead-acid battery characteristics

Before a battery charging strategy can be designed, the characteristics of the lead-acid battery to be charged need to be examined. This will now be done, focussing on the change in battery parameters as the battery is charged and discharged.

Most of the current values in this section will be defined according to the 1C rate, which is defined as the current rate at which a fully charged secondary battery will be discharged in one hour at 25°C ambient temperature. The Willard Solar 105 Ah lead-acid battery, used in the practical system described in this thesis, has a stated capacity of 105 Ah, and therefore a 1C rate of 105 A. A C/20 discharge rate will mean that the battery was discharged at 5.25 A in 20 hours.

The chemical characteristics of secondary batteries cause the battery voltage to vary as a function of the state of charge of the battery, as shown in Figure 5-5 for a variety of secondary batteries. As can be seen from the charge and discharge curves shown in this figure, the voltage of lead-acid batteries can be used to offer a battery state-of-charge indication.

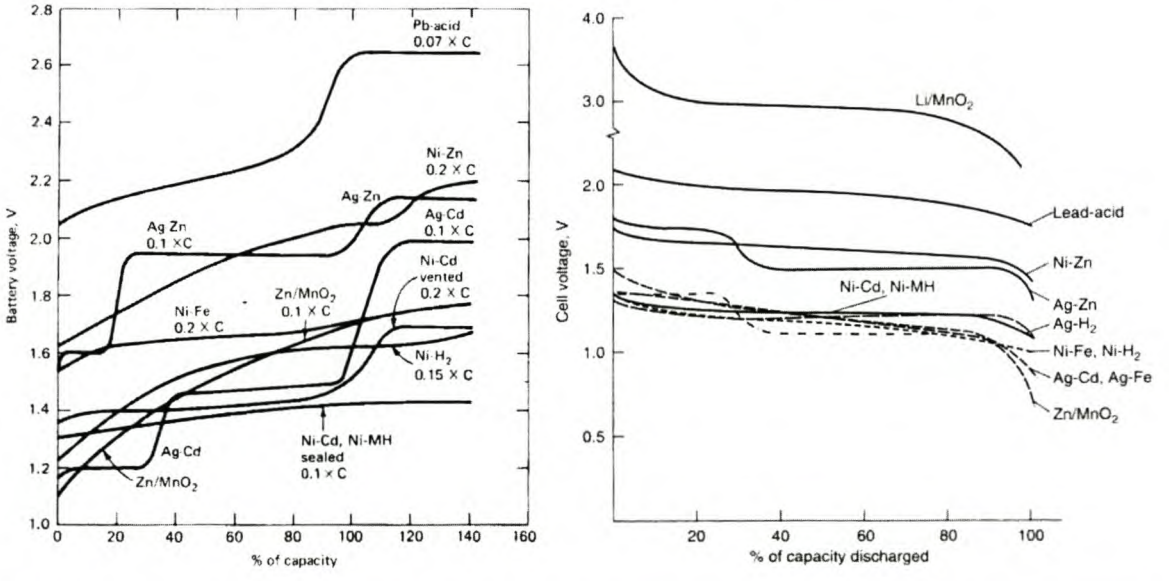

Figure 5-5: Typical charge and discharge curves for secondary batteries, constant current charged at 20°C, and discharged at C/5 discharge current [38]

This battery voltage, due to the internal impedance of the battery, is a function of the amount of current flowing through the battery, as shown in Figure 5-6 for a typical lead-acid battery.

Furthermore, the internal resistance of a battery increases as the battery's temperature decreases, leading to a fall in the charge voltage, and a rise in the discharge voltage, of around 30 mV per °C rise in temperature.

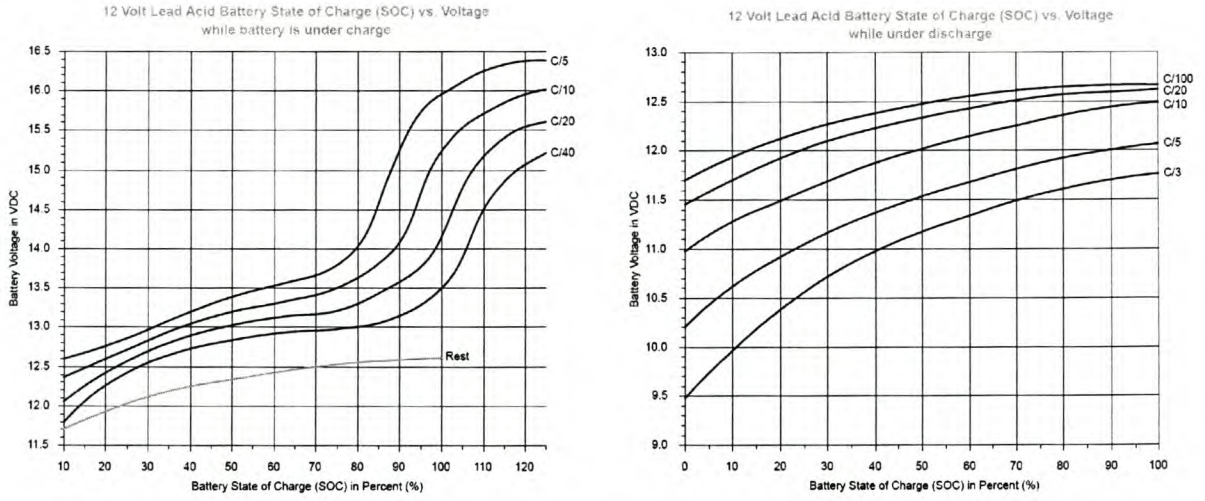

Figure 5-6: Charge and discharge curves for a variety of current rates, for a typical 12 V lead-acid battery [42]

The transient response of the lead-acid battery voltage to a sudden drop in charging / discharging current will be of interest later in this section, and is shown in Figure 5-7 and Figure 5-8. From these figures it is clear that with an interrupted battery charging current of 1 A / 3 A, a minimum period of around 10 s / 30 s need to elapse before an open-circuit voltage can be measured with an accuracy of higher than 1%.

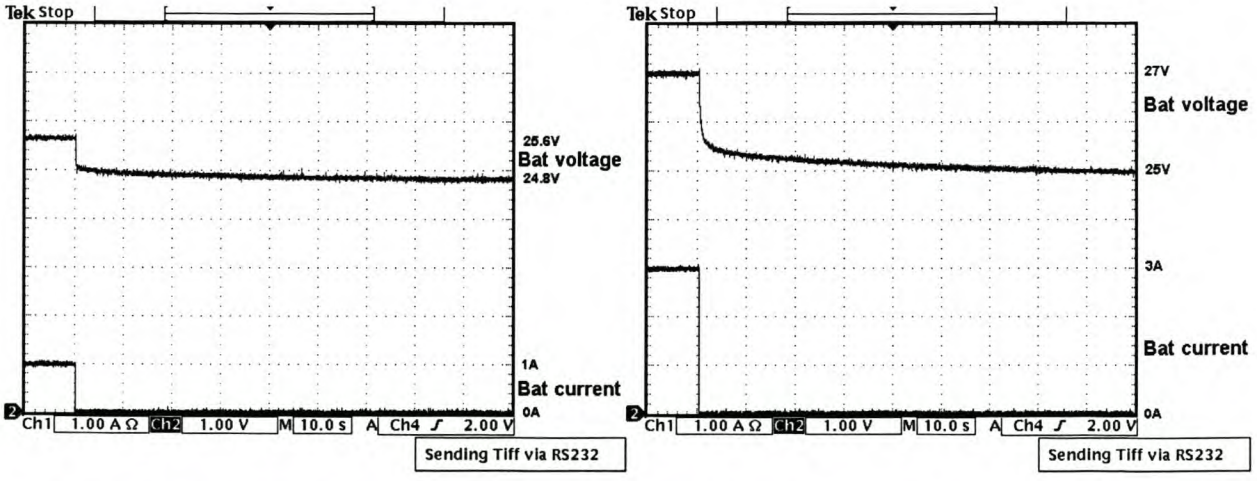

Figure 5-7: Battery voltage transient response for a change in battery charging current from 1 A / 3 A to 0 A, for two Willard Solar 105 Ah 12 V lead-acid batteries connected in series.

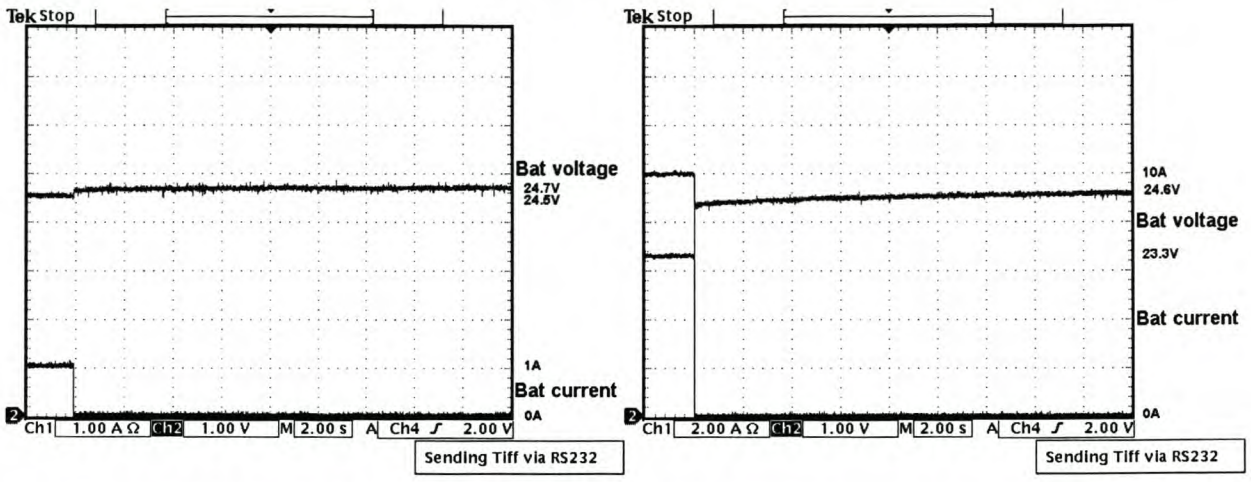

Figure 5-8: Battery voltage transient response for a change in battery discharging current from 1 A / 10 A to 0 A, for two Willard Solar 105 Ah 12 V lead-acid batteries connected in series.

Research done in [39] deduced that at up to around 80% of capacity, the charging of lead-acid batteries occurs at high efficiency, where the battery is able to sink high charge currents, in the order of 1C. Between 80% and 100% of capacity the charging efficiency is less, partly because of less electrode surface being available for chemical reactions, requiring special charging strategies. The next section will look at these charging strategies in detail.

5.3.2 Lead-acid charging strategies background

5.3.2.1 Constant current trickle charging

This "overnight charging" method is common in consumer products, where a very low, constant current rate is fed to the battery.

These chargers are very economical to manufacture, but the low charge rate causes chemical reactions to be localized on the electrode surface, leading to potential dendrite growth [40]. Overcharging and associated battery damage can also occur, as user-intervention is required to stop the charge once full capacity is reached. Overcharging occurs when the battery is unable to absorb additional energy chemically – this energy is instead converted into heat, which causes the electrolyte to evaporate and can permanently damage the battery.

5.3.2.2 Constant current fast charging

An advance from trickle charging is to add termination-of-charge circuitry that stops the charging process when a certain battery voltage is reached. The charging current can now also be increased, as some form of overcharging protection exists.

This high current charging strategy results in much shorter charging times, but does not take the electrochemical processes within the battery into account. For example, the high charging current can force chemical reactions to occur faster than the ion concentration available at the electrodes can support, generating heat and stimulating dendrite formation. This causes reduced battery capacity and cycle life.

5.3.2.3 Constant voltage charging

This strategy is implemented by keeping the battery voltage constant at its end-of-charge voltage. The charging current will be very high to begin with, but will decrease as the battery's state-of-charge increases. This strategy is very easy to implement, although some circuitry must be included to protect the battery from too high initial currents.

5.3.2.4 Constant current / constant voltage charging

This charging strategy applies constant current to the battery until a certain battery voltage is reached, after which the battery voltage is kept constant, with the charging current diminishing until the battery is fully charged. As the current drops during the final inefficient 20% of the charging stage, slightly less damage occurs to the battery than with the constant current fast charging strategy.

5.3.2.5 Pulse charging

One of the biggest problems with the constant current strategies discussed above is that an ion concentration gradient builds up in the battery. This gradient occurs because all the ions generated at one electrode during the charging process cannot move simultaneously to the other electrode. This gradient leads to poor charge efficiency, which results in the generation of heat, the growth of dendrites, and loss of cycle life and battery capacity.

Pulse charging operates on the principle of periodically interrupting the charge current, allowing ions to diffuse more evenly through the battery during the rest periods. This strategy minimizes the negative effects of constant current charging, while still offering the shorter charging period advantage of high current charging.

5.3.2.6 Pulse charging / discharging

As with the pulse charging method, the constant current is interrupted periodically to allow the ion concentration within the battery to return to normal levels. Pulse charging / discharging goes

one step further, adding a very short discharge pulse to the charging method, accelerating the balancing of the ion concentration [40].

5.3.3 Designing an optimal lead-acid battery charger

The MPPT circuit developed in Chapter 4, and duplicated in Figure 5-9 for convenience, will be used to implement a battery charging strategy. The only addition to this system will be an extra DSP input to measure the battery temperature.

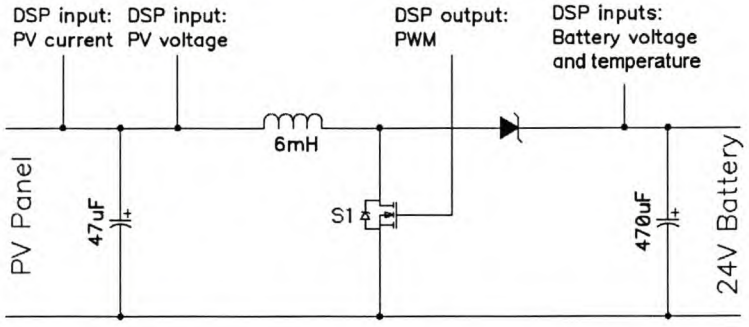

Figure 5-9: Circuit used to implement the k-sweep and voltage-control MPPT method, with lead-acid battery charging capability

As the topology of this MPPT circuit does not function in two quadrants, the most advanced battery charging strategy, pulse charging /discharging, will not be considered in this design.

The lead-acid pulse charging strategy researched in [39] will instead be used as foundation for the battery charging design in this thesis. [39] divides the charging process into three stages. In the first stage, from 0% to around 80% of battery capacity, the battery is charged at 1C constant current. The second stage of the battery charging process, between 80% and 100%, utilizes pulse charging, applying a 0.5C current for 12 s, followed by a rest period of no current for 1 s. During the third stage, once the battery is fully charged, no further charging current flows through the battery.

Before the implementation of this battery charging strategy is explained, the maximum potential battery charging current for the practical system described in this thesis will be calculated. The rated short-circuit PV current of the Shell SP75 PV panels used in this practical system, at an irradiance of 1000 W/m^2 is 4.8 A at 17 V. From the measurements done in section 4.5.3, the efficiency of the MPPT circuit was found to be around 80%. The current flowing through the battery can now be calculated as follows,

$$I_{bat} = 80\% \times I_{PV} \times \frac{V_{PV}}{V_{bat}} \qquad 5\text{-}6$$

where V_{bat} and I_{bat} is the battery voltage and current, and V_{PV} and I_{PV} is the PV panel voltage and current. Using Equation 5-6, the maximum potential current rate through the battery will therefore be around 3 A.

5.3.3.1 Finding the lead-acid battery state-of-charge

Temperature and electrolyte density measurements

In order to implement the design in [39], a way first needs to be found to accurately measure the state of charge of the battery. In [39], this is done by measuring the temperature and electrolyte density of the battery. A sharp rise in the value of these two parameters during 1C constant charging will for example indicate that the transition period has been reached where the charging efficiency starts to drop (i.e. the 80% of capacity moment).

This method of monitoring the battery temperature and electrolyte density has at least two disadvantages in a PV system. Firstly the charging current up to the 80% of capacity moment will not necessarily have been at 1C rate, as variations in irradiance on the panel will cause the charging current rate to vary. Changes in especially battery temperature will therefore not be predictable to the same extend as when a charging history at 1C rate was certain. Secondly electrolyte density sensors are required, adding to the price and complexity of the system, and lowering reliability.

Using battery voltage for state-of-charge indication

The state-of-charge can also be found, although less accurately, by monitoring the battery voltage. The main problem with using the battery voltage as a state-of-charge indication is that this voltage is influenced by the battery temperature, as well as by the current flowing through the battery.

Battery temperature can easily be measured and compensated for by using an inexpensive LM335 temperature sensor. The influence of battery current on the battery voltage is however difficult to compensate for, as the charging current in PV systems varies with irradiance, and the discharge current is not measured and therefore unknown. For this reason it was decided to determine the battery state-of-charge by measuring the open-circuit battery voltage. The open-circuit battery voltage ranges, measured for the two 12 V lead-acid batteries in series used in this thesis, for the three charging stages identified earlier, are shown in Table 5-1.

Charging stage	Selection criteria	Charging strategy
High efficiency stage	*0 – 25 V*	*Constant 1C max current*
Low efficiency stage	*25 – 25.4 V*	*Pulsed 0.5C max current*
Fully charged	*25.4 V and above, 50°C and higher*	*No current*

Table 5-1: The three charging stages used, with selection criteria, and the charging strategies used

The influence of discharge current

Open-circuiting the battery implies discontinuing all current through the battery. The discharge current from the battery to the load can however not be controlled. The higher the discharge current is, the more inaccurate the measured open-circuit voltage will be, as shown in Figure 5-8. As an example, a discharge current of C/10 will result in a measured open-circuit battery voltage of 5% lower than the accurate open-circuit voltage (read from Figure 5-8).

What influence will this inaccuracy have? Firstly, a battery operating in the low efficiency stage can incorrectly be charged as if it was operating in the high efficiency stage. In the low efficiency stage the battery will be damaged by currents above 0.5C, or 51 A. The maximum charging current that will potentially flow through the battery has however been calculated at not even 10% of this value. At worst the charging process might be less efficient, as the pulse-charging strategy is not implemented.

Secondly, the fully charged stage can potentially be incorrectly reported as the low efficiency stage, increasing the risk of overcharging. Continuous overcharging will however increase the battery temperature above the limit of 50°C, discontinuing all current to the battery.

Allowing for battery voltage transient responses

A period of time needs to pass between interrupting the charging current and measuring the open-circuit battery voltage, to allow for the transient response of the battery voltage to the change in battery current, as measured in Figure 5-7. From this figure it is clear that the higher the charging current, the longer the delay before the open-circuit voltage can be accurately read.

The maximum charging current through the battery was calculated earlier as around 3.2 A. From Figure 5-7 it can be seen that for a charge current of 3 A a delay of 30 s will ensure an open-circuit battery voltage reading of more than 1% accuracy. During this delay no power is however delivered to the battery, lowering efficiency. If this delay should cause no more than 0.1% loss in efficiency, the open-circuit voltage measurement can only be repeated once every 8 hours – obviously unacceptably long. If a measurement accuracy of less than 3% is acceptable, the delay

period reduces to 2 s. Measurements can now be done every 15 minutes and still keep the losses from the delay below around 0.2%.

Except for the fully charged stage, during which the open-circuit battery voltage will be measured continuously as no current is flowing, open circuit battery voltage measurements will therefore be done every 15 minutes, with an delay of 2 s between the moments of open-circuit and measurement.

5.3.3.2 Implementing 1C, 0.5C and 0C current rates in a PV system

The next obstacle to overcome in implementing the pulse charging strategy described in [39] is to ensure that the constant current during the high and low efficiency stages never exceeds the required values of 1C and 0.5C. The batteries used in this thesis' practical system has a 1C rating of 105 A. The battery is therefore already sized so that the maximum current from the PV panel (3 A) will never exceed 0.5C or 1C. No current-limiting strategy is therefore required during the high and low efficiency stages.

To stop all charge current from flowing through the battery is simple to implement, as no PV current flows if the S1 mosfet in Figure 5-9 operates at a PWM value of 0% (the PV panel is open-circuited). This method is used to stop the flow of current during the 1 s rest period required every 12 s in the low-efficiency stage, during the 2 s battery voltage measurement period every 15 minutes, as well as when the battery is fully charged.

Even though no current-limiting strategy is required for the batteries used in this thesis's practical system, for completeness the theory behind current-limiting using the described MPPT circuit and algorithm will be explained.

Firstly the current through the battery must be measured. As no current sensor is available on the battery side of the S1 mosfet, the PV current will be monitored, from which the battery current can be calculated using 5-6.

Current-limiting can be implemented by only considering PV voltage values during the k-sweep, done every 12.5 s, which corresponds to PV current values below the equivalent maximum battery current. This can be accomplished by just adding a few additional conditions to the current MPPT algorithm. These additional conditions are shown in red in Figure 5-10.

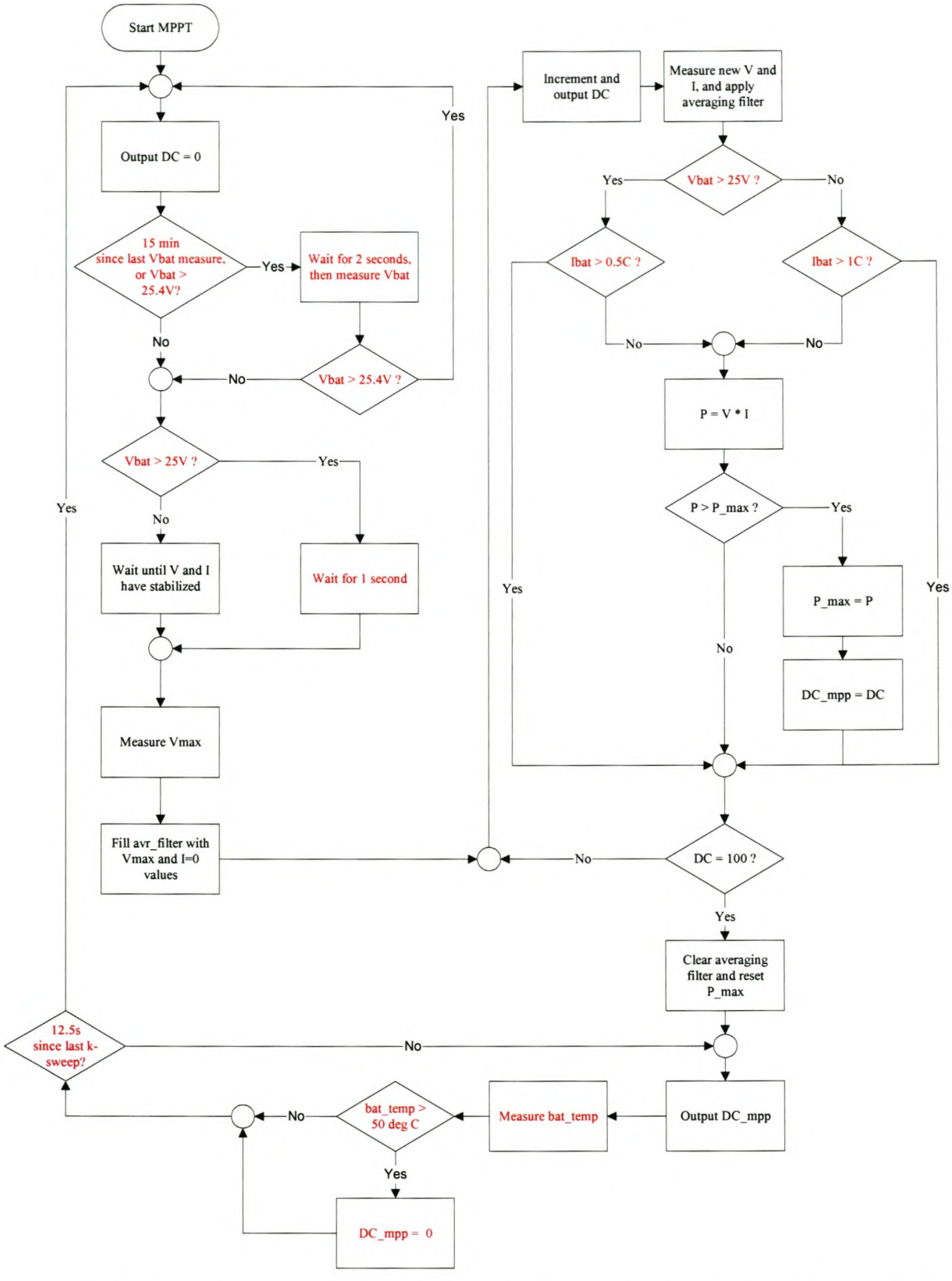

Figure 5-10: Flowchart showing the DSP control of a k-sweep voltage ratio MPPT. The blocks in red indicate additions made to the algorithm to enable charging of a lead-acid battery.

Cloudless days with high irradiance will deliver a high, relatively constant current to the battery. Testing only every 12.5 s for the maximum battery current is acceptable on these cloudless days, as the PV current, which is a function of irradiance, does not change very fast. On days with high irradiance and fast-moving clouds, this current-limiting strategy will perform less well, as the PWM of S1 can be calculated during a cloudy moment, while the rest of the 12.5 s can possibly be cloudless, delivering currents higher than the maximum value to the battery.

A way to get around this problem would be to monitor the PV current (and therefore indirectly the battery current) at shorter intervals of say 0.5 s, redoing the k-sweep every time a battery current higher than 0.5C is detected. Testing the battery current every 0.5 s has the disadvantage during days of fast-moving clouds that the k-sweep might occur more frequently than once every 12.5 s, lowering the efficiency of the system.

As the maximum temperature of the battery is limited, damage to the battery through overheating, caused by too high charging currents, does not present too big a risk. Because of this temperature protection, the battery-charging strategy shown in Figure 5-10, without additional testing of the battery current every 0.5 s, is the recommended current-limiting implementation.

5.4 Measurements and conclusion

5.4.1 Operation of the MPPT with discharged battery

The first measurement that will be presented confirms that the MPPT circuit and algorithm performs well even when connected to a fully discharged battery.

The operation of the MPPT described in Chapter 4 is based on the assumption that the battery voltage, and therefore the PV voltage, stays constant during the 12.5 s before the next k-sweep occurs. This assumption is not necessarily true in the case of a fully discharged battery. A discharged 12 V battery can have any open-circuit voltage between 0 V and 11.6 V depending on its state of discharge. Initial high internal impedance is also likely if the battery has been stored in a discharged state for a long period, due to dendrite growth on the electrodes of the battery.

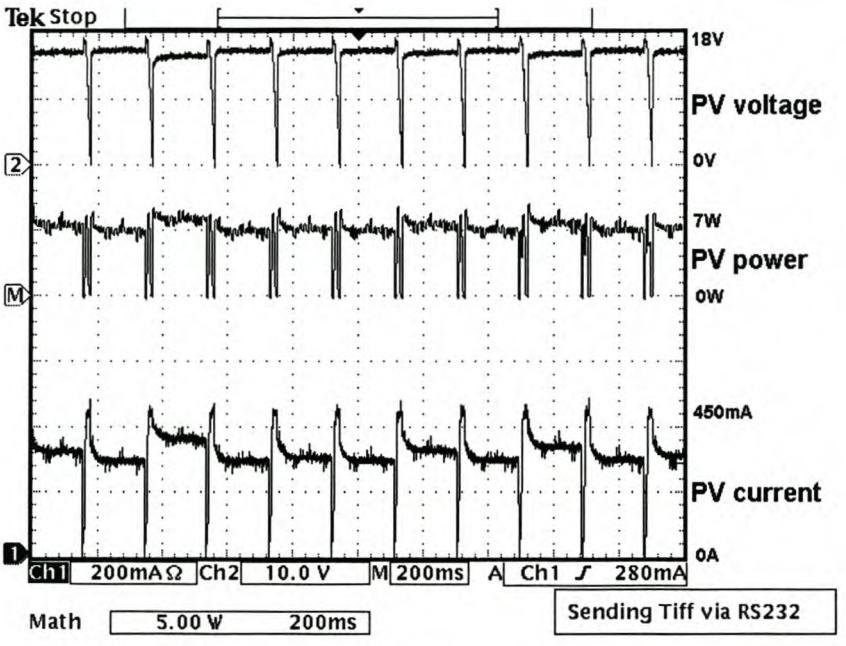

Figure 5-11: Measurements of the operation of the voltage ratio MPPT when connected to a normal PV panel and a fully discharged lead-acid battery, on a day with low irradiance. The k-sweep was executed every 170 ms.

There is, therefore, a risk that if the described MPPT method is used during this discharged state, inaccurate PV voltages will deliver minimum or no power to the battery, which will keep it in a discharged state.

No problems were, however, experienced with the accuracy of the MPPT when connected to a totally discharged lead-acid battery, as can be seen from the measurement shown in Figure 5-11. For this measurement a k-sweep was executed every 170 ms to illustrate the accuracy of the resulting MPP measurement.

5.4.2 Operation of the lead-acid battery charging strategy

Figure 5-12 shows the battery voltage, current and the power transferred to the battery during the low-efficiency charging stage. As can be seen from the figure, the current is interrupted every 12.5 s to implement a rest period of 1 s. Once the rest period is completed, a k-sweep is done, and the new MPP implemented for the next 12.5 s.

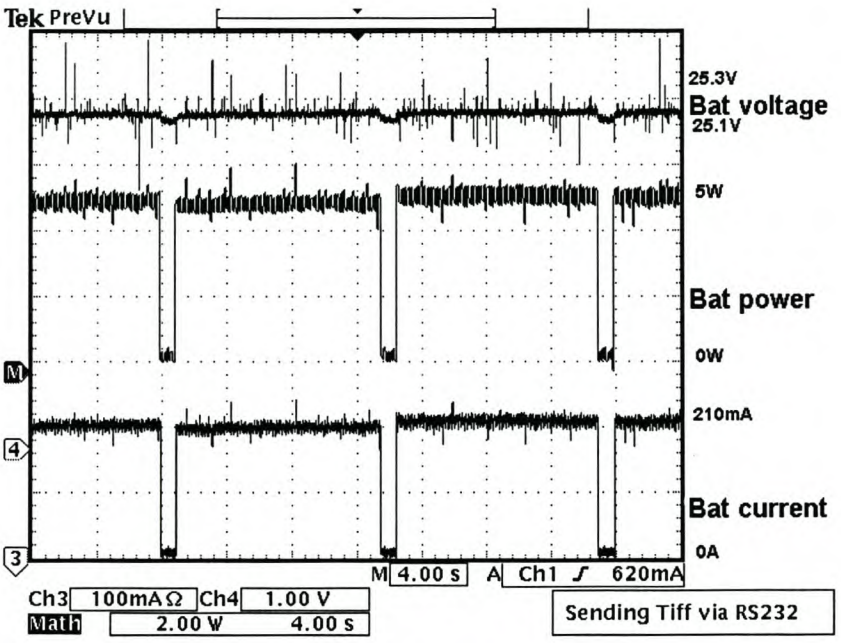

Figure 5-12: Battery voltage and current during the low efficiency charging stage, on a day with low irradiance.

The next measurement, shown in Figure 5-13, shows the operation of the battery charging strategy in the high efficiency stage, where only a short k-sweep interrupts the transfer of maximum power to the battery. Once every 15 minutes the battery current is discontinued for 2 s, after which the battery voltage is measured, a k-sweep done, and the new MPP implemented. This two-second interruption is also shown in this figure.

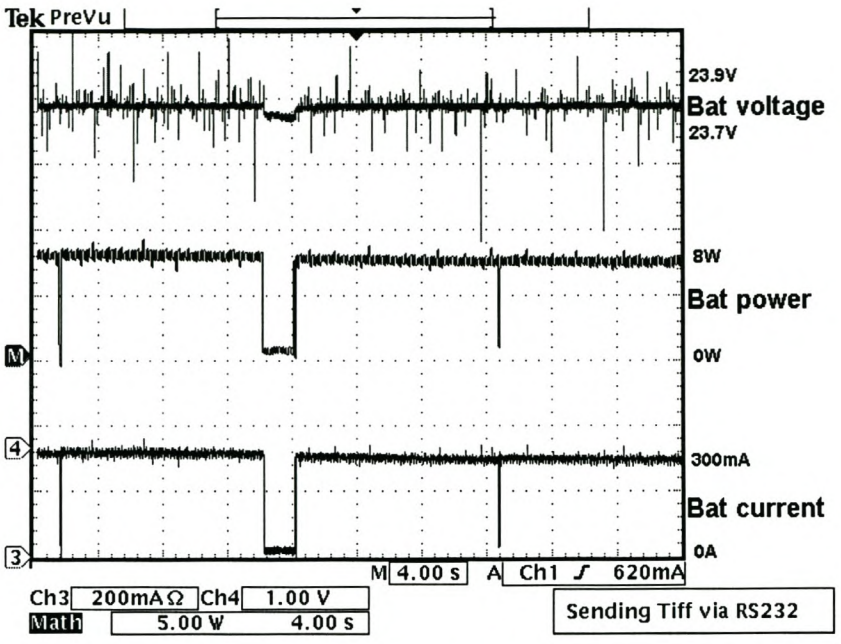

Figure 5-13: Battery voltage and current during the high efficiency stage, on a day with low irradiance. The 2 s interruptions for current measurement are also shown.

5.5 *Conclusion*

This chapter started by identifying the optimal ES technology for application in rural, off-grid PV installations. This technology was found to be the lead-acid secondary battery family, due to advantages such as cost, reliability and energy capacity. Flow batteries were found to be the most efficient ES solution for the required application, but offered disadvantages like cost and reliability.

A lead-acid battery charging strategy was then developed. This strategy takes the unique characteristics of PV energy generation, like varying charging current, into account. It furthermore takes the chemical characteristics of the lead-acid battery into account, like the benefit of pulse charging during the last 20% of battery capacity, and thereby represents an efficient strategy to charge lead-acid batteries with minimum damage to the battery.

The measurements in the previous section confirm the successful implementation of this lead-acid battery charger based on the MPPT circuit designed in Chapter 4.

Chapter 6 – Conclusion

This thesis investigated ways in which to extract maximum electrical energy from PV panels on the earth's surface. A variety of methods were discussed, ranging from positioning the PV panels optimally, to optimal MPPT algorithms and efficient charging of the battery used to store the generated energy. The result of these investigations offered substantial potential increases in the amount of available PV energy from PV panels.

These results will be briefly summarized according to the four chapters of this thesis:

6.1 The future contribution of PV energy

An energy generation cost comparison was done between different generation technologies, which showed that, over a 20-year life cycle, a well-positioned PV array generates energy that is around ten times more expensive than coal-fired energy, and almost three times as expensive as wind energy. Technological developments in the near future were predicted, however, to almost half the PV energy generation cost.

It was further shown that PV energy will be utilized mostly for rural, off-grid applications in South Africa's future energy scenario, due to the high cost of PV energy generation. Factors that positively influence the future role of PV energy include its modularity, reliability and ease of installation, along with the excellent solar resource in South Africa, governmental legislation encouraging renewable energy generation and predicted increases in coal/nuclear generation costs.

6.2 Optimal positioning of the PV panel

The SunSim computer model developed in this chapter can potentially contribute significantly to more efficient PV energy generation in South Africa, by making it possible to calculate the optimal positioning of a PV panel anywhere in South Africa, based on historic irradiation data.

SunSim can furthermore assist in finding locations within South Africa where PV energy can be produced most cost-effectively.

With additional sets of historic atmosphere data, which can easily be imported, SunSim can accurately predict irradiation and calculate optimal PV panel positioning on any other location

on earth. A typical application would be irradiation calculations for the SANAE base in Antarctica.

Results from simulations by SunSim include that full solar tracking PV panels offer the cheapest PV energy generation costs, that solar declination tracking through the year given almost the same benefits as just adjusting the slope angle of the PV panel twice yearly, and that facing PV panels in any direction other than North does not offer much additional total yearly energy benefits. Cooling PV panels are shown to be beneficial, delivering around 20% more energy per year.

6.3 Optimal MPPT methods

This chapter illustrated that MPPT algorithms, capable of taking shading of PV panels into account, can increase PV power output by up to 60%.

A study of existing MPPT algorithms showed that the hill-climbing and constant voltage ratio MPPT algorithms perform well, except with shaded panels, and that current ratio algorithms offers slightly higher accuracy than voltage ratio algorithms, but adds a lot of complications to the MPPT implementation.

An easy to implement, yet very effective voltage ratio MPPT algorithm was then developed capable of optimising power from shaded PV panels.

6.4 Optimal energy storage

In this chapter, lead-acid secondary batteries were identified as the optimal ES technology for rural, off-grid PV installations, even though flow batteries offered higher efficiency. The reasons for this included, amongst others, the reliability and ease of implementation of the lead-acid batteries, and their cost advantages above flow batteries.

A lead-acid battery charging strategy was then developed, taking the unique characteristics of PV energy generation, like varying charging current, into account, and offering an efficient way to charge lead-acid batteries with minimum damage to the battery.

The above conclusions are the results of a detailed study into methods to extract maximum electrical energy from PV panels on the earth's surface. What becomes clear through this study is that careful thought when designing a PV generation system can lead to a much more economically viable end product, offering personal satisfaction for the engineer designing the system, and contributing to a future society with abundant, clean energy.

References

1 *Climate change information kit*, UNEP and UNFCCC, July 2002, www.unfccc.int/resource/iuckit

2 *Understanding climate change: a beginner's guide to the UN Framework Convention and its Kyoto protocol,* UNEP and UNFCCC, revised July 2002, www.unfccc.int

3 *United Nations Framework Convention on Climate Change*, www.unfccc.int

4 *Kyoto protocol to the United Nations Framework Convention on Climate Change*, www.unfccc.int

5 Deutsches Klimarechenzentrum, www.dkrz.de

6 T. Markvart, *Solar Electricity*, John Willy & Sons, 1994

7 S.W.White and G.L.Kulcinski, *Net Energy Payback and CO_2 Emissions from Wind-Generated Electricity in the Midwest*, Fusion Technology Institute, Department of Engineering Physics, University of Wisconsin, December 1998

8 Ian Smith, Private discussion, Eskom Klipheuwel wind turbine test facility

9 Department of Minerals and Energy, *Baseline study on wind energy in South Africa*, 2003

10 Andries Gouws, '*Goedkoop sonkrag sterk op dreef*', Landbou Weekblad, Friday 2 Julie 2004

11 '*Energie-deurbraak!*', Die Burger, Vrydag 9 Januarie 2004, p9

12 H.C. de Coninck and N.H. van der Linden, *An Overview of Carbon Transactions, General Characteristics and Specific Peculiarities*, ECN-C—03-022, March 2003

13 Gunnar Boye Olesen, *The Danish CO_2 Emission Cap and Trade System*, International Network for Sustainable Energy, January 2003

14 Conningarth Economists in association with COW1, *Economic and Financial Calculations Modelling for the Renewable Energy White Paper and Strategy Formulation*, 2003

15 Department of Minerals and Energy, *White paper on the promotion of renewable energy and clean energy development in South Africa*, August 2002

16 American Wind Energy Association, *Wind Energy Fact Sheet*, 2001, www.awea.org/pubs/factsheets/Cost2001.PDF

17 Gordon Bell, '*Electricity production costs set to rise, warns Eskom*', Business Report, 2004/02/03, page 4, www.ner.org.za/0202_0203.htm

18 Roger Messenger and Jerry Ventre, *Photovoltaic Systems Engineering*, CRC Press LLC, 1999 ISBN 0-8493-2017-8, 621.31'244

19 http://www.kippzonen.com/

20 Wehrli, C. 'Extraterrestrial Solar Spectrum', Publication no. 615, Physikalisch-Meteorologisches Observatorium + World Radiation Center (PMO/WRC) Davos Dorf, Switzerland, July 1985.

21 http://personal.cityu.edu.hk/~bsapplec/solar1.htm

22 Bent Sorensen, *Renewable Energy*, 2nd edition, 2000, ISBN 0-12-656152-4

23 Raymond A. Serway, *Physics for Scientists and Engineers*, 3rd edition, 1992, ISBN 0-03-096027-4

24 K.YA. Kondratyev, *Radiation in the Atmosphere*, Academic Press,1969

25 Kinsell L. Coulson, *Solar and Terrestrial Radiation, Methods and measurements*, Academic Press, 1975, ISBN 0-12-192950-7

26 B. Grimmig and Detlef Mencke, *Vergleichsmessung an unterschiedlichen Solarstrahlungssensoren und –integratoren*, 1996

27 H. Field, *Solar cell spectral response measurement errors related to spectral band width and chopped light waveform*, 1997, National Renewable Energy Laboratory

28 R.Gasch and J. Twele, *Wind Power Plants*, 2002

29 Mukund R. Patel, *Wind and Solar Power Systems*, 1999, ISBN 0-8493-1605-7, 621.31'2136

30 *Renewable energies: success stories*, European Environmental Agency, 2001

31 Tohihiko Noguchi, Shigenori Togashi, Ryo Nakamoto, *Short-current pulse-based MPPT method for multiple PV-and-converter module system*, IEEE trans. Industrial Electronics, vol. 49, no. 1, Feb. 2002.

32 C. Hua and C. Shen, *Comparative study of Peak Power Tracking Techniques for Solar Storage System*, IEEE, 1998

33 S.M.M. Wolf, *Development of a maximum power point tracker, optimising cost and efficiency*, October 1993

34 Shell Solar product information sheet, Shell SP75 Photovoltaic solar module.

35 Mike Keagy, Electronic design, October 14, 2002

36 S.R. Holm, H. Polinder, J.A. Ferreira, P. van Gelder and R. Dill, *A comparison of energy storage technologies as energy buffer in renewable energy sources with respect to power capability*, IEEE

37 D. Berndt, *Maintenance-free Batteries*

38 David Linden, *Handbook of batteries*, second edition

39 J.Alvarez, J.Marcos, A.Lago, A.A.Nogueiras,J.Doval and C.M.Penalver, *A fully digital Smart and fast lead-acid battery charge system*, IEEE, 2003

40 R.C.Cope and Yury Podrazhansky, *The art of battery charging*, IEEE, 1999

41 Ali Nourai, *Comparison of the costs of energy storage technologies for T & D applications*, American Electric Power, Energy Storage Association, www.electricitystorage.com, July 2004.

42 Richard Perez, *Lead-acid battery state of charge vs. voltage*, Home Power #36, August / September 1993, http://www.homepower.com/files/battvoltandsoc.pdf

43 Christian Gueymard, *SMARTS2 – A simple model of the atmospheric radiative transfer of sunshine – algorithms and performance assessment*, Florida solar energy centre, December 1995

44 *Electricity distribution – Guidelines for the provision of electrical distribution networks in residential areas – Part 1: Planning and design of distribution systems*, Draft 1b of 034-1:1999, NRS project, South African Bureau of Standards

45 J.H. Krenz, *Energy conversion and utilization*, second edition,

46 Nancy Mackman-Hunt, *Small hydropower systems*, US Department of energy

47 www.electricitystorage.org

48 VRB Power Systems Inc., *Executive summary*

49 Intermediate technology development group, *Micro-hydro power*, technical brief, www.itdg.org

Appendix A – SunSim explained

SunSim Explained

Version 1.2

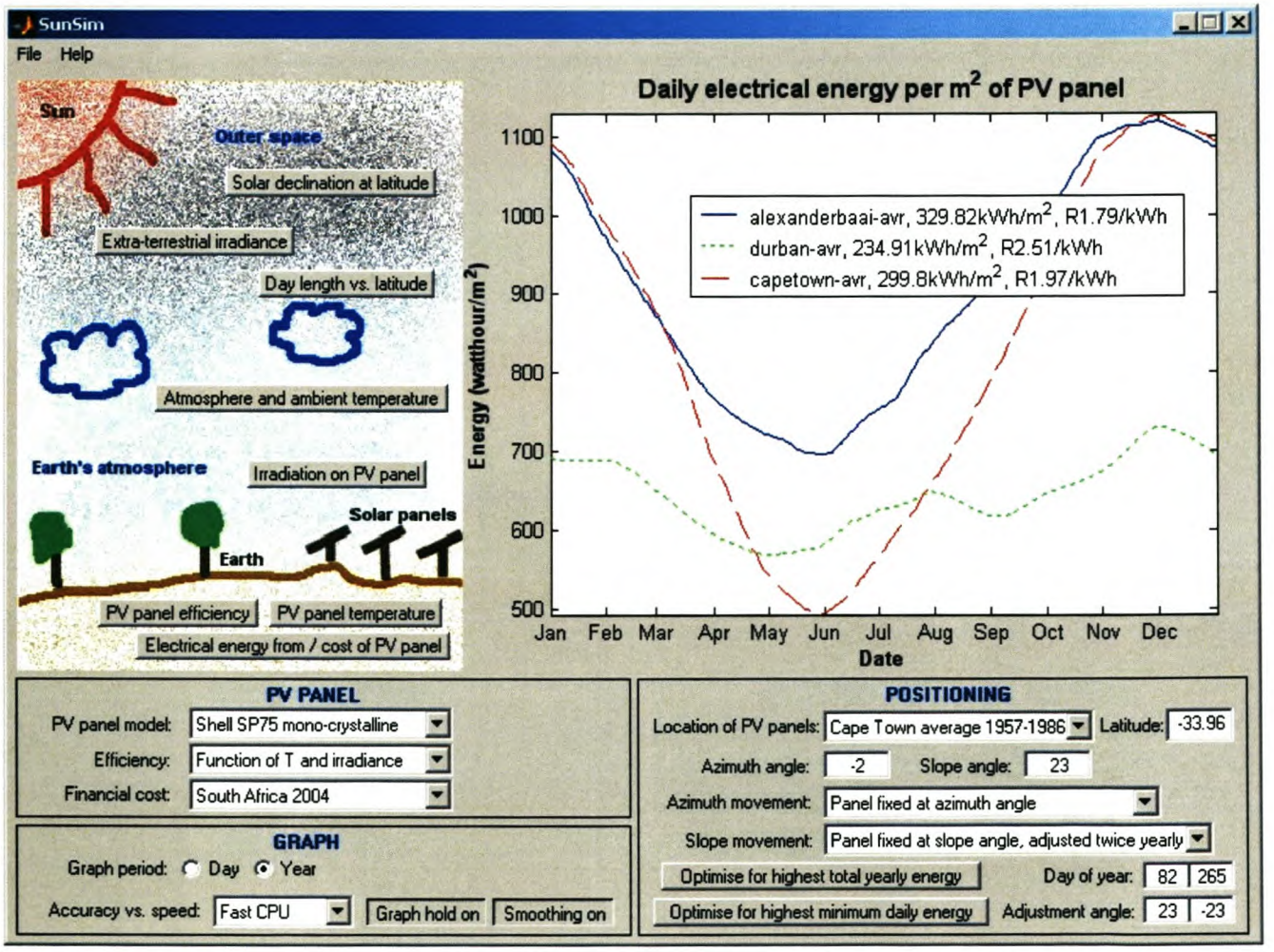

Table of Content

?

Introduction

The SunSim computer model simulates the conversion of solar energy into electrical energy by a photovoltaic (PV) panel. The model takes the influence of the atmosphere, the positioning of the PV panel, and PV panel characteristics into account. SunSim offers the following functionality:

- Predicts a PV panel's energy output through the year, given a nearby site's historic atmosphere data, info on the PV panel's position relative to the sun and the PV panel characteristics.
- Calculates the PV panel's optimal position relative to the sun for highest total energy output through the year, or for highest minimum daily energy through the year.
- Displays how different factors like the atmosphere and PV panel positioning and characteristics can influence the generation of PV electricity.
- Calculates the PV energy cost over a 20-year life cycle, given current PV system component prices.

The following important assumptions are made in the model:

- All data presented in SunSim are in Local Apparent Solar Time (LST), which differs slightly from Standard Time as displayed on our watches.
- Albedo radiation is not taken into account in SunSim calculations, as it is assumed that the PV panel are not bifacial (i.e. only the front of the panel is sensitive to solar irradiance), and the contribution from the albedo component is therefore minimal.
- The PV panel modelled in SunSim operates at its maximum power point (MPP) at all times, and is not shaded or defective in any manner.
- Array mismatch losses, caused by mismatches in PV panel operating voltages when connected together in a PV array, are not taken into account in SunSim.
- Energy storage losses during the charge/discharge cycle of the energy storage device are also not taken into account.
- During leap years, data from the 29th of February is ignored, i.e. SunSim always works with a 365-day year.

The different areas of the program will now be described in detail.

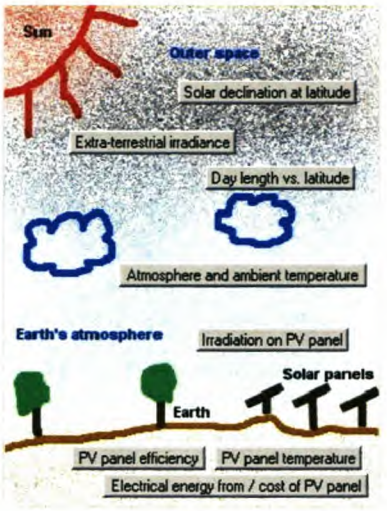

Command area

Click on the buttons in this area to draw different graphs in the graph window, based on the information you selected in the PV panel, Graph and Positioning areas.

Solar declination at latitude

Draws a graph of the solar declination observed on earth through the year, at the latitude specified by the user. The angle between the direction of the solar rays and straight up at noon, is called the solar declination angle. The angle is caused by the rotation axis of the earth being tilted 23.45 degrees with respect to its orbit plane around the sun. Because of this tilt, the position of the sun observed from the earth moves north or south depending on the time of year. This declination causes the seasons on earth.

Extra-terrestrial irradiance

Draws a graph of the solar irradiance falling on a plane just outside the earth's atmosphere, normal to the sun, positioned at the latitude specified by the user. The slightly elliptical yearly orbit of the earth around the sun causes the small variation in intensity.

Day length vs. latitude

Draws a graph indicating the amount of daylight hours as a function of latitude and day of year. The closer you get to the poles, the bigger the difference gets between the amount of daylight hours in summer and winter. From around 67 degrees North and South of the equator 24-hour daylight/night periods start occurring.

Atmosphere and ambient temperature

Draws graphs of the clearness of the atmosphere of the earth, and the ambient temperature, for a location selected by the user. The clearness of the atmosphere is defined as the ratio between the amount of direct irradiance measured on a horizontal plane at latitude, compared to the amount of extra-terrestrial irradiance that would have fallen on the same plane if no atmosphere existed, expressed as a percentage.

Irradiance on PV panel

Draws graphs of the direct, diffuse and total irradiance falling on a PV panel positioned as defined in the Positioning area. The legend of the graph indicates the total daily or yearly irradiation falling on the panel for the two types of irradiance and their sum.

PV panel efficiency

Graphs the conversion efficiency from solar energy to electrical energy of the PV panel described in the PV panel area. Among other factors, efficiency is a function of the irradiance on the panel and its temperature. By changing input parameters in SunSim and redrawing the efficiency graph, these dependencies are clearly demonstrated, e.g. the effect of cooling on PV panel efficiency. The Graph hold off/on button can be used to plot up to four different graphs on the same axis, for comparison purposes.

PV panel temperature

Graphs the temperature of the cells of the PV panel. The Graph hold off/on button can be used to plot up to four different graphs on the same axis, for comparison purposes.

Electrical power from / cost of PV panel

Draws a graph of the predicted power or energy that will be available from a PV panel with panel characteristics, positioning and location as described by the user. The legend of the graph indicates the total daily or yearly amount of electrical energy available. The Graph hold off/on button can be used to plot up to four different graphs on the same axis, for comparison purposes. The 20-year life cycle PV energy cost, calculated using PV system cost data supplied by the user, will also be displayed if yearly graphs are plotted.

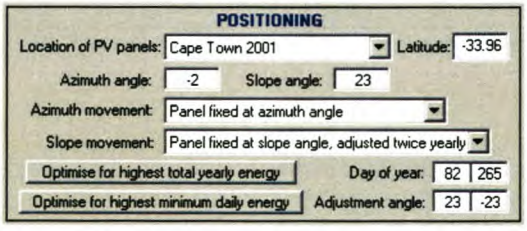

Positioning area

The user can adjust the parameters in this area to reflect different atmospheric conditions, as well as different ways in which the PV panel faces/tracks the sun through the year.

Location of PV panel:

This popup menu allows the user to load one of a variety of atmospheric data sets.

Atmosphere has no influence

This menu option loads a 100% clearness atmosphere (i.e. all direct irradiance is allowed through, therefore reducing diffuse irradiance to zero) and a constant 25°C ambient temperature.

Display map with data locations

A map of Southern Africa is displayed (see below), with towns indicated for which global, diffuse and temperature data are available. This data is available either averaged over a number of years, or measured over a one-year period, or both.

Cape Town 2001

Loads atmosphere and temperature data measured at Cape Town in 2001. The data was converted from daily 5-minute data sets made available by the South African Weather Bureau.

Cape Town average 1957-1986

Loads atmosphere and temperature data for Cape Town, averaged over the period 1957 to 1986. The data was converted from monthly 1-hour data sets made available by the South African Weather Bureau.

Load atmosphere from file...

Loads atmosphere and ambient temperature data from file. The file format is described later in this document. Three files, for ambient temperature, global and diffuse irradiance, represent one data set. When the file open dialog box (see below) appears, select and open any one of the three files in the data set. The remaining two will automatically be loaded.

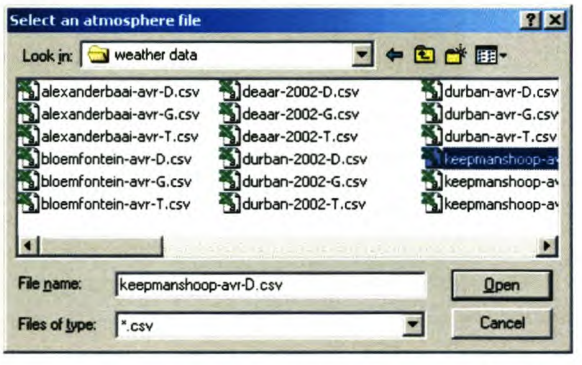

A time format prompt will now appear (see below), requesting information on the time format. All calculations and data displayed within SunSim uses Local Apparent Solar Time (LST), which in essence defines 12h00 as the time when the sun is directly overhead. Standard Time is the time displayed on our watches, and is not suitable for models like SunSim, as time at a certain location is, for example, calculated within time zones, instead of using longitude. If the data sets to be loaded are in Standard Time, it first needs to be converted to LST by SunSim. All the data sets supplied with SunSim are already in LST format.

Latitude:

The latitude where the PV panel are located is entered here. When an atmosphere is loaded from file, the latitude value is automatically updated to the location's latitude. A negative value implies south of the equator.

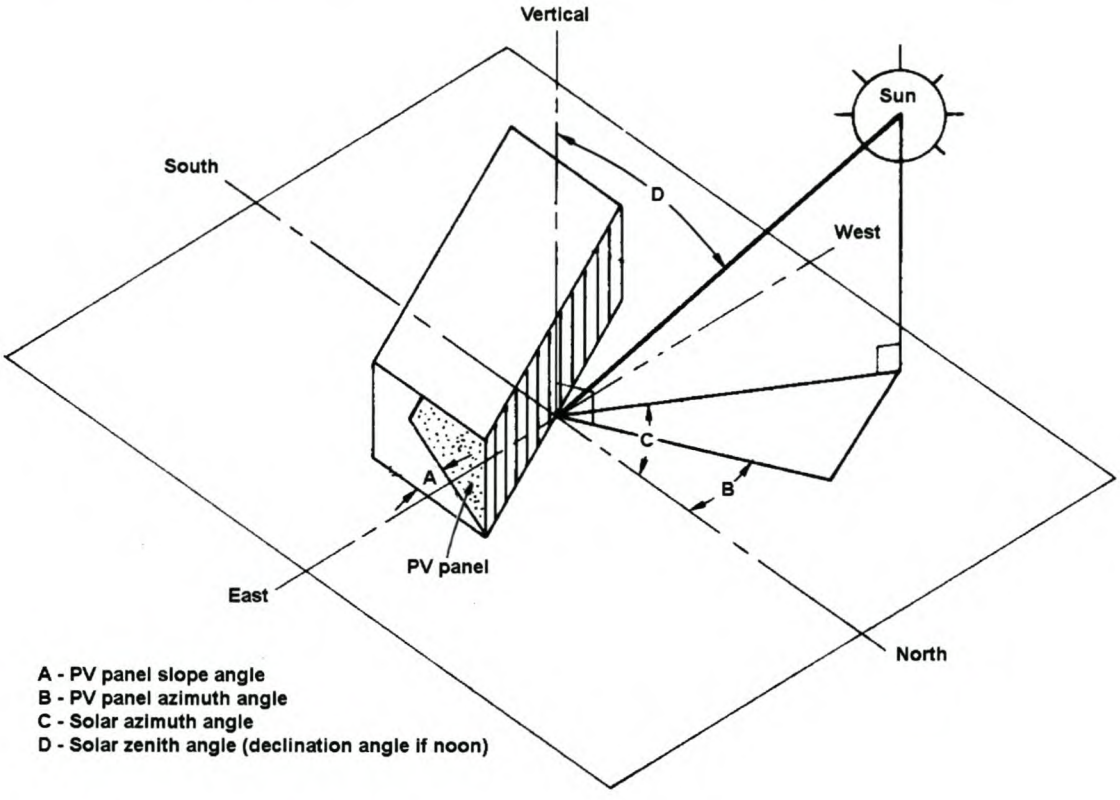

Azimuth angle:

The figure above explains the tilt angles used in SunSim. The angle (B in the above figure) at which the PV panel positioned relative to the north-south plane, i.e. towards sunrise or sunset, is called the azimuth angle. Positioned towards west/sunset is defined as positive. The azimuth angle is not applicable if the PV panel track the azimuth angle of the sun (C in the above figure) throughout the day.

Slope angle:

The slope angle is defined as the angle at which the PV panel are tilted relative to the horizontal plane (A in the above figure). A negative value represents a southward adjustment. When the PV panel tracks the solar declination (D at noon in the above figure) through the year, this slope angle is automatically set to the negative of latitude, for maximum irradiance. The slope angle is not applicable if the PV panel track the zenith angle of the sun (D in the above figure) throughout the day.

Azimuth movement:

This popup menu defines how the PV panel azimuth angle tracks the sun through the day and year.

Panel fixed at azimuth angle

PV panel does not track the sun, but is fixed at the azimuth angle.

Tracks the azimuth angle of the sun

The PV panel tracks the sun throughout the day from sunrise to sunset, i.e. the azimuth angle of the PV panel is always equal to the azimuth angle of the sun.

Slope movement:

This popup menu defines how the PV panel slope angle tracks the sun through the day and year.

Panel fixed at slope angle

PV panel does not track the sun, but is fixed at the slope angle.

Panel fixed at slope angle, adjusted twice yearly

The PV panel is fixed at the slope angle, but twice a year, on the days defined in the 'Day of year:' boxes, the slope angle is adjusted by the amount of degrees indicated in the 'Adjustment angle:' boxes. This tracking option is cheaper to implement than to continuously track the solar declination through the year, and gives higher electrical energy through the year than keeping the PV panel fixed at only one slope angle through the year.

Latitude slope angle, tracks declination of sun

When this menu option is selected, the PV panel track the solar declination (i.e. the zenith angle of the sun at noon) through the year. This means that the PV panel's surface is always normal to the solar irradiance at noon, as long as the PV panel azimuth angle is also 0° at noon.

Tracks the zenith angle of the sun

When this menu option is selected, the PV panel track the zenith angle of the sun through the day and year, i.e. the PV panel's surface is always normal to the solar irradiance, as long as the PV panel azimuth angle is always equal to the sun's azimuth angle.

Day of year:

The days of the year (between 1 and 365) on which the slope angle is adjusted by the amount of degrees in the 'Adjustment angle:' boxes.

Adjustment angle:

The amount of degrees by which the slope angle is adjusted on the days defined in the 'Day of year:' boxes. A negative value represents a southward adjustment.

Optimise for highest total yearly energy

When selected, calculates the azimuth and slope angles that will ensure the highest total amount of electrical energy from the PV panel through the year, taking parameters like the atmosphere and panel efficiency into account. The 'Accuracy vs. speed:' popup menu determines the accuracy of this calculation. If the PV panel tracks the sun through the year, no optimisation is required, as the PV panel will always be positioned at the optimal angles.

Optimise for highest minimum daily energy

When selected, calculates the azimuth and slope angles that will ensure that the day with the least electrical energy in the year gets the most irradiation possible, taking parameters like the atmosphere and panel efficiency into account. The 'Accuracy vs. speed:' popup menu determines the accuracy of this calculation.

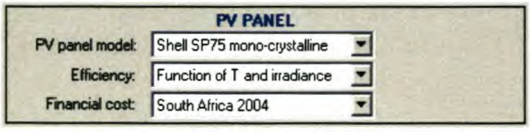

PV panel area

In this area the characteristics of the PV panel used by SunSim during simulations are defined.

PV panel model:

A popup menu used to load five parameters that govern the efficiency of energy conversion of the PV panel. The five parameters are described in the Data file layout section of this document.

Shell SP75 mono-crystalline

Load the characteristics of the Shell SP75 mono-crystalline PV panel.

BP SX 75TU multi-crystalline

Load the characteristics of the BP SX 75TU multi-crystalline PV panel.

Load parameters from file:

Load PV panel characteristics from a file. The format of the file is described in the Data file layout section.

Efficiency:

This popup menu allows the user to select different methods with which the efficiency of the PV panel used in SunSim is calculated.

Constant at STC efficiency

The efficiency of the PV panel is kept constant at Standard Test Conditions (STC), which is defined as an irradiance of 1000W/m², an atmospheric clearness of AM 1.5, and an ambient temperature of 25°C. The sensitivity of the PV panel efficiency to irradiance and temperature variations is not taken into account.

Function of T and radiation

The efficiency of the PV panel is calculated taking all available influences into account, including variations in irradiance and ambient temperature.

Panel is cooled to 15°C

The efficiency of the PV panel is calculated taking all available influences into account, but keeping the PV panel temperature constant at 15°C, thereby simulating a cooled PV panel.

Financial cost:

A popup menu used to load nineteen parameters that govern the energy production cost of the PV panel. The nineteen parameters are described in the Data file layout section of this document.

South Africa 2004

Load typical PV system costs for South Africa in 2004.

Load costs from file

Load PV system costs from a file. The format of the file is described in the Data file layout section.

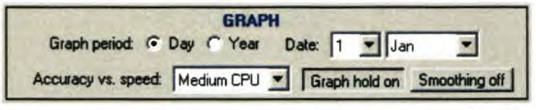

Graph area

The user can adjust parameters relating to the way graphs are drawn, as well as the accuracy at which calculations are done, in this area of SunSim.

Graph period:

Sets the period of time represented by the x-axis of graph been drawn. To show information for all 365 days of the year, select 'Year', or select 'Day' and a date to show data from 0H00 to 23H55 of the day selected. SunSim ignores the 29th of February, and does all calculations using six values per hour (i.e. 10-minute intervals).

Accuracy vs. speed:

Sets the accuracy of the calculations done when finding the optimal azimuth and slope angles (when one of the 'Optimise for highest ... energy' buttons are pressed). These optimisations do a number of iterations, which can take a long time on slower computers. For computers with slow CPUs, the optimisation angle results will be within three degrees of the correct angle, medium CPUs two degree, and with fast CPUs the correct angle within one degree will be calculated.

Graph hold off/on

Allows multiple graphs to be plotted on the same axis when the 'Electrical power/energy from PV panel', 'PV panel temperature' or 'PV panel efficiency' buttons are selected. A maximum of four graphs can be plotted on one axis.

Smoothing off/on

If smoothing is selected, an averaging filter with a width of five is applied to the yearly data displayed, i.e. the energy value of each day is given as an average of the four days surrounding it and itself. This button does not influence daily data.

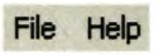

Menu bar area

The area at the top left corner of SunSim offers the user information about SunSim, and allows graphs to be saved and the program to be closed.

File

Save Graph

Saves the currently displayed graph to disk as a Tagged Image File Format (.tif) file.

Quit

Close and exit SunSim.

1	28	16.35	16.45
1	29	22.1	22.05
1	30	19.45	19.45
1	31	18.25	18.15
2	32	15.65	15.25
2	33	18.7	18.45
2	34	21.6	21.15
2	35	23.25	22.85
2	36	21.6	21.4

Data file layout

The format of the two types of data files that can be imported into SunSim is explained in this section.

PV panel parameters

The PV parameter data file is imported into SunSim using the 'PV panel model:' popup menu, and allows the user to specify detailed characteristics of the PV panel to be modelled by SunSim.

The file must have a .txt extension, and must contain only numbers (no text). The easiest way to create the file is by using Notepad, entering the six values one to a line with no commas, and saving the file as an ANSI text file.

The five values represent the following:

1) The peak power at Standard Test Conditions (STC), i.e. P_{mmp} (watt)
2) The panel size, i.e. height x width (square meters)
3) The panel temperature at Nominal Operating Cell Temperature (NOCT), i.e. T_{noct} (°C)
4) The temperature coefficient, i.e. change in power per degree Celsius temperature rise (% per °C)
5) The relative reduction in module efficiency at irradiance of 200W/sq meter in relation to 1000W/sq meter both at 25°C cell temperature and AM 1.5 spectrum (%)

Financial cost parameters

The PV parameter data file is imported into SunSim using the 'Financial costs:' popup menu, and allows the user to specify detailed costs of the PV system to be modelled by SunSim.

The file must have a .txt extension, and must contain only numbers (no text). The easiest way to create the file is by using Notepad, entering the six values one to a line with no commas, and saving the file as an ANSI text file.

The nineteen values represent the following:

1) The excess inflation, i.e. the rate of price increase of the resource in question above general inflation, usually chosen as 5% (number between 0 and 1, 1=100%)
2) The discount rate, i.e. the rate, relative to inflation, at which money would increase in value if invested, usually chosen as 8% (between 0 and 1)
3) PV panel cost (R per kW peak)
4) Structural support and wiring cost - no solar tracking (R per kW peak)
5) Operation and maintenance costs - no solar tracking (R per kW peak per year)
6) Structural support and wiring cost - slope angle twice yearly adjustable (R per kW peak)
7) Operation and maintenance costs - slope angle twice yearly adjustable (R per kW peak per year)
8) Structural support and wiring cost - zenith solar tracking (R per kW peak)
9) Operation and maintenance costs - zenith solar tracking (R per kW peak per year)
10) Structural support and wiring cost - azimuth solar tracking (R per kW peak)
11) Operation and maintenance costs - azimuth solar tracking (R per kW peak per year)
12) Structural support and wiring cost - azimuth solar tracking and slope angle twice yearly adjustable (R per kW peak)
13) Operation and maintenance costs - azimuth solar tracking and slope angle twice yearly adjustable (R per kW peak per year)
14) Structural support and wiring cost - azimuth and zenith solar tracking (R per kW peak)
15) Operation and maintenance costs - azimuth and zenith solar tracking (R per kW peak per year)
16) Installation cost: design, labour, transport etc. cost (R per kW peak)
17) DC to AC converter cost. Replaced every 10 years (R per kW peak)
18) MPPT cost. Replaced every 10 years (R per kW peak)
19) Government subsidies (R per kW peak)

The following assumptions are made during PV array life cycle costs calculations:

- The generated electricity will be fed into the national grid, i.e. 220 V, 50 Hz AC power.
- No energy storage costs will be taken into account.
- A MPPT will be connected to every PV panel.
- A period of 20 years will be taken as the life cycle. This is the average period for which PV panel output power is guaranteed (Shell and BP guarantees their PV panel for between 20 and 25 years).
- The cost is calculated for a PV array of 10 kW_{peak}, to ensure a reasonable economy-of-scale benefit.

Atmosphere data

The atmosphere data files is imported into SunSim using the 'Location of PV panel:' popup menu, and allows the user to specify the ambient temperature and the global and diffuse irradiance at or near the location of the PV panel.

Three files are required to fully specify the atmosphere, and need to be located in the same directory. The three files must each have a .csv extension, and must contain only numbers (no text). The file must not contain a new line character at the end of the file.

The filename containing the global radiation on a horizontal surface at the specified location must end with '-G', and should contain the name of the location, e.g. 'upington-2003-G.csv'. The file consists of 366 rows: row 1, column 1 contains the latitude (negative if South of the equator), column 2 the longitude (0 to 360 degrees), and column 3 the Local Standard Time Meridian of the location. Row 2 to 366 contains the data per day, with column 1 containing the month (1 to 12), column 2 the day of the year (1 to 365) and column 3 to 146 the data in 10-minute intervals (i.e. column 3 will contain the mean measured data for the period 00H00 to 00H10).

The filename containing the diffuse radiation on a horizontal surface at the specified location must end with '-D', and the ambient temperature at the location with '-T', and should contain the name of the location, e.g. 'upington-2003-D.csv' and 'upington-2003-T.csv'. The file consists of 365 rows for the data per day, with column 1 containing the month (1 to 12), column 2 the day of the year (1 to 365) and column 3 to 146 the data in 10-minute intervals.

Appendix B – Shell SP75 PV panel specifications

Shell Solar

Product Information Sheet

Shell SP75 Photovoltaic Solar Module

General

The Shell SP75 module contains 36 series connected 125 x 125 mm PowerMax® mono-crystalline silicon solar cells.

The Shell SP75 can generate a peak power of 75 watt at 17 volt.

The Shell SP75 solar module has been designed for grid connected and industrial applications.

Qualifications and Certificates

The Shell SP75 solar module meets the following requirements:

- **IEC 61215**
- **UL - Listing 1703**
- **FM approved**
- **TÜV Isolation Class II**

All Shell Solar modules are produced in EN-ISO 9001 certified factories.

Limited Warranties

- **Peak Power for 25 years***

*See Shell Solar Limited Warranty for PV-Modules 2003-01-UK.

Shell SP75 Module

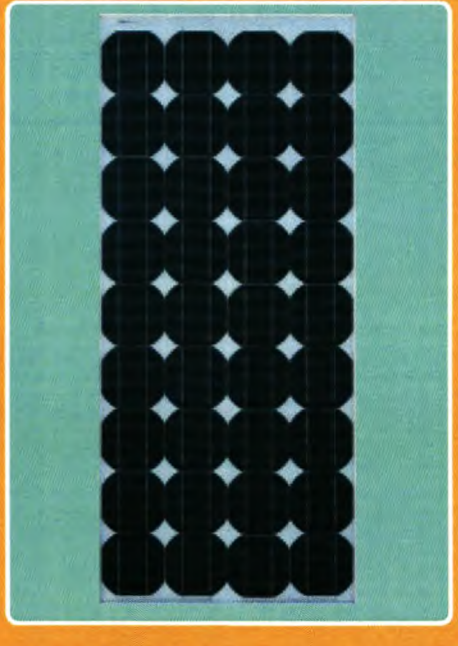

Junction Box

The junction box provides a high quality, dust protected and splash proof IP44-rated housing. The housing contains a rigid connection block with screw terminals and by-pass diodes providing "hot spot" protection for the solar cells.

ProCharger™-CR Junction Box

Maximum conductor cross-section: 4 mm²

Type of protection: IP44

Number of by-pass diodes: 2

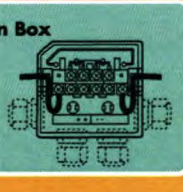

Benefits

- **PowerMax® mono-crystalline solar cells deliver maximum power output even under reduced light conditions providing more power where space is a limitation.**
- **The surface of the PowerMax® cell has a pyramidal textured surface to enable more light absorption and deliver exceptional efficiency.**
- **Highly transparent tempered glass delivers more power and ensures high impact resistance and protection against hail, snow, ice and storms.**
- **Nearly 300MW of cumulative installed experience has been applied to the evolution of our mono-crystalline range to ensure that our products have a long and reliable service life backed by a 25 year warranty.**

ELECTRICAL EQUIPMENT, CHECK WITH YOUR INSTALLER

Due to continuous research and product improvement the specifications in this Product Information Sheet are subject to change without notice. Specifications can vary slightly. For installation and operation instructions, see the applicable manuals. No rights can be derived from this Product Information Sheet and Shell Solar assumes no liability whatsoever connected to or resulting from the use of any information contained herein.

Shell SP75 Photovoltaic Solar Module

Mechanical Specifications Module

A torsion and corrosion-resistant anodised aluminium frame ensures dependable performance, even under harsh weather conditions. Pre-drilled mounting holes are provided for ease of installation.

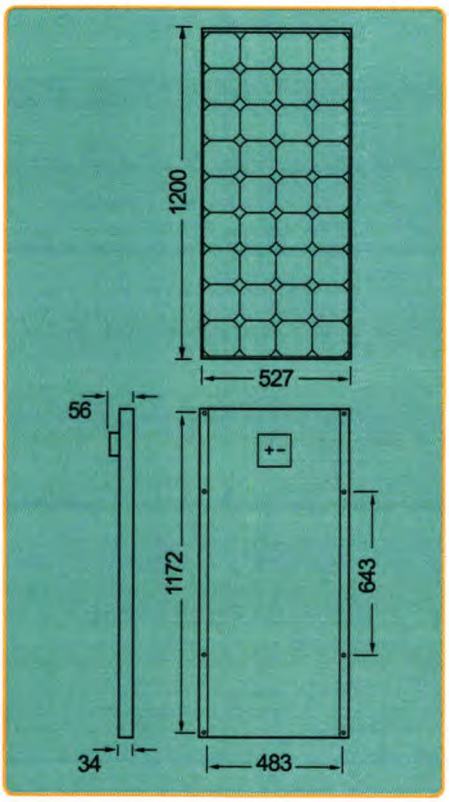

Outside dimensions (mm)	1200 x 527
Thickness (inc. junction box) (mm)	56
Thickness (exc. junction box) (mm)	34
Weight (kg)	7.6

For installation instructions, please refer to the **Installation Manual** which is available from Shell Solar.

Electrical Characteristics

Data at Standard Test Conditions (STC)

STC: irradiance level 1000W/m², spectrum AM 1.5 and cell temperature 25°C

Rated power	P_r	75W
Peak power	P_{mpp}	75W
Peak power voltage	V_{mpp}	17V
Open circuit voltage	V_{oc}	21.7V
Short circuit current	I_{sc}	4.8A
Minimum peak power	$P_{mpp\ min}$	70W

The abbreviation 'mpp' stands for Maximum Power Point.

Typical data at Nominal Operating Cell Temperature (NOCT) conditions

NOCT: 800W/m² irradiance level, AM 1.5 spectrum, wind velocity 1m/s, T_{amb} 20°C

Temperature	T_{NOCT}	45°C
Mpp power	P_{mpp}	54W
Mpp voltage	V_{mpp}	15.6V
Open circuit voltage	V_{oc}	19.9V
Short circuit current	I_{sc}	3.9A

Typical data at low irradiance

The relative reduction of module efficiency at an irradiance of 200W/m² in relation to 1000W/m² both at 25°C cell temperature and AM 1.5 spectrum is 7%.

Temperature coefficients

$\alpha\ P_{mpp}$	−0.45 %/°C
$\alpha\ V_{mpp}$	−76 mV/°C
$\alpha\ I_{sc}$	+2 mA/°C
$\alpha\ V_{oc}$	−76 mV/°C

Maximum system voltage: 715 Vdc

Typical I/V Characteristics

The I/V graph below shows the typical performance of the solar module at various levels of irradiance.

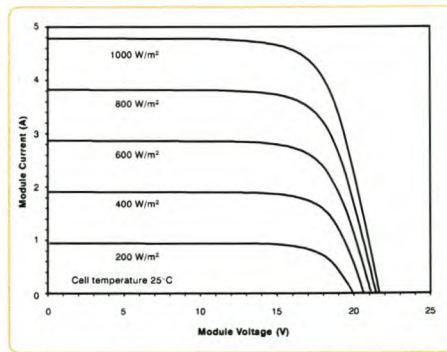

The I/V graph below shows the typical performance of the solar module at various cell temperatures.

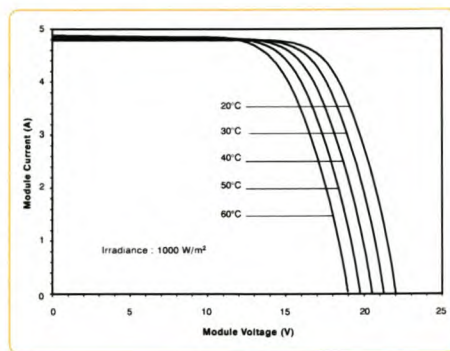

References in this Product Information Sheet to 'Shell Solar' are to companies and other organisational entities within the Royal Dutch/Shell Group of Companies that are engaged in the photovoltaic solar energy business. Shell Solar was set up in 1999 and has its principal office in Amsterdam, the Netherlands.

For further information on all Shell Solar products contact:

Shell Solar
Customer Service Centre
P.O.Box 460705 80915 Munich Germany
E-mail solarinfo@si.shell.com
Web www.shell.com/solar
Tel +49 89 636 50620
Fax +49 89 636 50622

V4/SP75/06/03 SAP ref: 400357